

Wavelets and Filter Banks: Novel design and applications

Submitted by
Selvaraaju Murugesan
M.E., La Trobe University, 2009

A thesis submitted in total fulfillment
of the requirements for the degree of
Doctor of Philosophy

Department of Electronic Engineering
School of Engineering and Mathematical Sciences
Faculty of Science, Technology and Engineering

La Trobe University
Bundoora, Victoria 3086
Australia

January, 2014

Dedicated to my parents, my sister and my supervisor

Contents

List of Figures	v
List of Tables	ix
List of Abbreviations	x
Summary	xi
Statement of Authorship	xii
Acknowledgements	xiii
1 Introduction	1
1.1 Motivation	1
1.2 Problem Statement	3
1.3 Thesis outline	4
1.4 Contributions and Publications	6
2 New Techniques for Rationalizing Orthogonal and Biorthogonal Wavelet Filter Coefficients	7
2.1 Introduction	7
2.2 Preliminaries	9
2.2.1 Filter Banks Fundamentals	9
2.2.2 Filter bank Design	10
2.2.3 Sobolev Regularity	13
2.2.4 Filter Normalisation	14
2.2.5 Canonical Signed Digit	15
2.2.6 Performance Measures	15
2.3 Rationalizing Orthogonal Filters	17
2.3.1 Ensuring One Vanishing Moment	17

2.3.2	Two Vanishing Moments	21
2.3.3	Efficient Implementation	24
2.3.4	Rationalizing Dual-Tree Orthogonal Filters	25
2.4	Rationalizing Biorthogonal Filters	26
2.4.1	Choice of parameter values	28
2.4.2	The 9/11 Filter Pair	29
2.4.3	The 13/11 Filter Pair	30
2.4.4	The 17/11 Filter Pair	32
2.4.5	Selesnick 8/12 Dual-Tree Filter Pair	33
2.5	Discussion and Comparisons	35
2.6	Conclusion	37
3	Design of Almost Symmetric Orthogonal Wavelet Filter Bank via Direct Optimisation	38
3.1	Introduction	38
3.2	Wavelet Discrete Moments and Coiflets	40
3.3	Symmlets	41
3.4	Asymmetry Minimization	43
3.4.1	Asymmetry Measure	43
3.4.2	Optimisation algorithm	45
3.5	Design Examples	47
3.6	Application in image compression	55
3.6.1	SPIHT	55
3.6.2	Performance measures	57
3.6.3	Image Compression Experiment 1	58
3.6.4	Image Compression Experiment 2	60
3.6.5	Image Compression Experiment 3	61
3.7	Conclusion	63
4	Design of Almost Symmetric Orthonormal Hilbert Pair of Wavelets	65
4.1	Introduction	65
4.2	Preliminaries	67
4.3	Hilbert pair based on Almost Symmetric Filters	71
4.3.1	Optimisation Algorithm	74
4.3.2	Design Examples	74
4.4	Improved Analyticity Design	78

4.5	Hilbert pair of wavelet with different VMs	86
4.6	Discussion and Comparison	88
4.7	Conclusion	92
5	Application of Hilbert pair of wavelets in denoising	93
5.1	Introduction	93
5.2	Mass Spectroscopy	94
5.2.1	MS preprocessing	97
5.2.2	MS postprocessing	98
5.3	MS/MS denoising	99
5.4	Image denoising	102
5.5	Conclusion	106
6	On the Aliasing effect of the Finer Directional Wavelet Transform	107
6.1	Introduction	107
6.2	Review of directional filter banks	109
6.2.1	Dual Tree Complex Wavelet Transform	109
6.2.2	Directional filter banks	110
6.2.3	Contourlets	111
6.2.4	Multiresolution Directional Filter Banks	111
6.3	Finer directional wavelet transform	112
6.4	Quadrant filter design	114
6.4.1	Quadrant filter mapping kernel	116
6.5	Aliasing effect in the subband	116
6.6	Directional Information	120
6.7	Applications	121
6.8	Conclusion	124
7	Conclusion and Future Directions	126
7.1	Main contributions	126
7.2	Further Improvements and Future Directions	127
7.2.1	Rationalising Orthogonal Wavelet Filters	127
7.2.2	Almost Symmetric Orthogonal Wavelet Filters	127
7.2.3	Almost Symmetric Orthogonal Hilbert Pair of Wavelet Filters	128
7.2.4	Applications	128

List of Figures

2.1	Lattice structure	13
2.2	Frequency response of original and rationalized Daubechies length 6 filter	22
2.3	Frequency response of original and rationalized Daubechies length 8 filter	23
2.4	Lattice structure implementation	24
2.5	Spectrum of complex wavelet in example IV. Solid line : original filter. Dotted line: rational filter	26
2.6	Plot of frequency response of the “9/11” filter pair, solid line: original filters. Dotted line: rational coefficients filter with $a_1 = -31/8$ and $a_2 = 8$	30
2.7	Plot of frequency response of the “13/11” filter pair, solid line: original filters. Dotted line: rational coefficients filter with $a_1 = -11/2$ and $a_2 =$ $21/2$	31
2.8	Plot of frequency response of the “17/11” filter pair, solid line: original filters. Dotted line: rational coefficients filter with $a_1 = -11/2$ and $a_2 =$ $21/2$	33
2.9	Spectrum of complex wavelet. Solid line: original filter. Dotted line: rational filter	34
3.1	Scaling and wavelet function of the length-6 Coiflet filter with two VMs .	42
3.2	Scaling and wavelet function of the length-6 Coiflet filter with two VMs .	43
3.3	Scaling and wavelet function of length 10 filter with 3 VMs. Solid line: Almost symmetric filter. Dotted line: Symmlets	48
3.4	Impulse response and group delay response of length 10 filter with 3 VMs.	49
3.5	Zero plot of length 10 filter having 3 VMs.	50
3.6	Scaling and wavelet function of length 12 filter having 3 VMs. Solid line: Almost symmetric filter. Dotted line: Symmlets	51
3.7	Impulse response and group delay response of length 12 filter with 4 VMs.	52
3.8	Zero plot of length 12 filter having 4 VMs.	52

3.9	Scaling and wavelet function of length 20 filter having 5 VMs. Solid line: Almost symmetric filter. Dotted line: Symmlets	53
3.10	Scaling and wavelet function of length 40 filter having 5 VMs. Solid line: Almost symmetric filter. Dotted line: Symmlets	54
3.11	Impulse response and group delay response of length 40 filter with 5 VMs.	54
3.12	(a) Original Image. (b) zoomed in image.	58
3.13	SPIHT compressed image at 0.5 bpp using length 10 filters. (a) Using almost symmetric filter. (b) Using Symmlets. (c) Using Daubechies minimum phase. (d) Using Daubechies 9/7 filter.	59
3.14	Zoomed in image. (a) Using almost symmetric filter. (b) Using Symmlets. (c) Using Daubechies minimum phase. (d) Using Daubechies 9/7 filter.	60
3.15	Zoomed in image. (a) Using AS12. (b) Using W12	61
3.16	(a) Original Image. SPIHT compressed image at 0.5 bpp using length 12 filters. (b) Using Daubechies minimum phase.(c) Using Symmlets. (d) Using almost symmetric filter.	62
3.17	Zoomed in image. (a) Original Image. (b) Using Daubechies minimum phase. (c) Using Symmlets. (d) Using almost symmetric filter.	63
4.1	Impulse Response of Length 12 filters with 2 VMs Top: AES filter Bottom: AOS filter	70
4.2	Impulse Response of Length 12 filters with 2 VMs Top: AES filter Bottom: AOS filter	71
4.3	Impulse Response of Length 12 filters with 2 VMs Top: AES filter Bottom: AOS filter	75
4.4	Top: Magnitude response of the length 12 filters having 2 VMs. Solid line: AES filter. Dotted line: AOS filter. Bottom: Phase difference between filters	75
4.5	Top: Wavelet functions $\psi^h(t)$, $\psi^g(t)$ and $ \psi^C(t) $. Bottom: Spectrum of complex wavelet	76
4.6	Impulse Response of Length 16 filters with 4 VMs Top: AES filter Bottom: AOS filter	76
4.7	Top: Magnitude response of the length 16 filters having 4 VMs. Solid line: AES filter. Dotted line: AOS filter. Bottom: Phase difference between filters	77
4.8	Top: Wavelet functions $\psi^h(t)$, $\psi^g(t)$ and $ \psi^C(t) $. Bottom: Spectrum of complex wavelet	78

4.9	Top: Plot of G Vs E_{tol} . Bottom: Plot of E_1 Vs E_{tol}	81
4.10	Top: Impulse response of the designed AOS filter. Bottom: Magnitude response of the filters. Solid line: AES filter. Dotted line: Designed AOS filter.	82
4.11	Top: Plot of G Vs E_{tol} . Bottom: Plot of E_1 Vs E_{tol}	83
4.12	Top: Impulse response of the designed AOS filter. Bottom: Magnitude response of the filters. Solid line: AES filter. Dotted line: Designed AOS filter.	84
4.13	Top: Wavelet functions $\psi^h(t)$, $\psi^g(t)$ and $ \psi^C(t) $. Bottom: Spectrum of complex wavelet	85
4.14	Top: Wavelet functions $\psi^h(t)$, $\psi^g(t)$ and $ \psi^C(t) $. Bottom: Spectrum of complex wavelet	85
4.15	Top: Wavelet functions $\psi^h(t)$, $\psi^g(t)$ and $ \psi^C(t) $. Bottom: Spectrum of complex wavelet	87
4.16	Top: Wavelet functions $\psi^h(t)$, $\psi^g(t)$ and $ \psi^C(t) $. Bottom: Spectrum of complex wavelet	88
4.17	Impulse Responses of Length 14 filters having 2 VMs. Top: Q-shift filter. Middle: AES filter Bottom: AOS filter	89
4.18	Wavelet Function. Top: Q-shift filter. Middle: AES filter. Bottom: AOS filter	90
4.19	Impulse Responses of Length 16 filters having 4 VMs	91
4.20	Wavelet functions $\psi^h(t)$, $\psi^g(t)$ and $ \psi^C(t) $. Top: Filters designed using common factor technique. Bottom: filters designed using the optimisation O_2	92
5.1	Plot of a m/z versus retention time	95
5.2	Plot of a MS scan	96
5.3	Total Ion Chromatogram	97
5.4	Plot of a MS/MS spectra of Dataset 3666	101
5.5	Test images: (a) Tesmos (b) Lena	102
5.6	(a) Original Home image. Image denoising using (b) Q14 (c) ASH14 (d) SSH14	103
5.7	Zoomed-in image (door grill). (a) Original (b) Q14 (c) ASH14 (d) SSH14	104
5.8	Zoomed-in image (chimney). (a) Original (b) Q14 (c) ASH14 (d) SSH14	105
5.9	(a) Original Home image. Image denoising using (b) Q14 (c) ASH14 (d) SSH14	105

6.1	Directionality of 2D wavelets: Left: Vertical band Middle: Horizontal band Right: Diagonal band	108
6.2	Directionality of 2D Dual Tree wavelets	110
6.3	Directional partitioning (a) Four band (b) Eight band	111
6.4	Frequency band partitioning of the (a) separable 2D DWT (b) Finer directional wavelet transform	113
6.5	(a) Diagonal subband of separable DWT (b) Frequency band of the HH band after downsampling	113
6.6	Analysis filter banks for the fiDWT.	114
6.7	Frequency response of $H_0^Q(z_1, z_2)$	117
6.8	Frequency response of $H_1^Q(z_1, z_2)$	118
6.9	Ideal frequency band support of (a) $H_0^Q(z_1^2, z_2^2)$ (b) $H_1^{1D}(z_1)H_1^{1D}(z_2)$. Shaded region: passband. Unshaded region: stopband	119
6.10	Magnitude response of subband 5 in the fiDWT. Aliasing components indicated by the arrows.	120
6.11	Magnitude response of subband 1 in the fiDWT. Aliasing components indicated by the arrows.	120
6.12	Magnitude response of subband 5 in the ufiDWT. Aliasing components indicated by the arrows.	121
6.13	(a) Original test image (b) zoomed in image of the HH band	121
6.14	zoomed in portion of image in band 6 using (a) fiDWT (b) ufiDWT.	122
6.15	<i>Lena</i> image denoised using fiDWT. Output PSNR: 25.11 dB	123
6.16	<i>Lena</i> image denoised using ufiDWT. Output PSNR: 28.11 dB	123
6.17	PSNR in denoising for <i>Lena</i>	124
6.18	PSNR in denoising for <i>Boat</i>	124

List of Tables

2.1	Rational lattice parameters of the Db6 and Db8 filters. Sobolev Regularity s_c also shown.	21
2.2	Original and quantized lattice parameters values of length 8 symmetric self Hilbertian filter.	26
2.3	Rational coefficient values of remainder part of biorthogonal filter pairs (origin is the leftmost coefficient, coefficient for negative indices follow by symmetry)	30
2.4	Selesnick 8/12 filter coefficients	34
3.1	Coefficients of Symmlets orthogonal filters. $2L$: Filter Length. p : Number of VMs.	42
3.2	Coefficients of almost symmetric orthogonal filters. $2L$: Filter Length. p : Number of VMs.	49
3.3	Asymmetry measures for length 12 filter. Comparison made with other methods.	50
3.4	PSNR and SSIM for various filters	60
3.5	PSNR and SSIM for various filters	61
4.1	Filter Coefficients	78
4.2	Filter Coefficients	82
4.3	Filter Coefficients (optimised w.r.t E_1)	86
5.1	Peptide count	101
5.2	Image Denoising	104
6.1	Ratio of aliasing energy to signal energy E_{AS} values.	119

List of Abbreviations

DWT	Discrete Wavelet Transform
DTCWT	Dual Tree Complex Wavelet Transform
VM	Vanishing Moments
PR	Perfect Reconstruction
SPT	Sum of Power of Two
CSD	Canonical Signed Digit
FB	Filter Banks
SPIHT	Set Partitioning In Hierarchial Trees
EZW	Embedded Zerotree Wavelet
PSNR	Peak Signal to Noise Ratio
SSIM	Structural SIMilarity
FIR	Finite Impulse Response
IIR	Infinite Impulse Response
SSH	Symmetric Self Hilbertian
CQF	Conjugate Quadrature Filter
AES	Almost Even Symmetric
AOS	Almost Odd Symmetric
MS	Mass Spectroscopy
ESI	Electrospray Ionisation
MALDI	Matrix Assisted Laser Desorption/Ionisation
LC	Liquid Chromatography
PMF	Peptide Mass Fingerprinting
TIC	Total Ion Chromatogram
SWT	Stationary Wavelet Transform
fiDWT	finer Directional Wavelet Trasform
DFB	Directional Filter Banks
HVS	Human Visual System

Summary

The Discrete Wavelet Transform (DWT) is widely used in signal processing applications to analyse non-stationary signals. The DWT is implemented using multirate filter banks (FB). This thesis presents several novel techniques for designing FB and also considers its applications. Most wavelet filters in the literature have irrational coefficients thus complicating the implementation in digital hardware. This thesis first proposes new design techniques to rationalise the filter coefficients while preserving the vanishing moments (VM) and other important filter properties. For orthogonal filters the technique is based on the lattice structure and for biorthogonal filter the technique is based on the complementary filter technique. Orthogonal FBs are energy preserving while the biorthogonal FBs offer symmetric wavelets. The next part of the thesis proposes a novel methodology for orthogonal FB design which gives almost symmetric wavelets. The designed almost symmetric orthogonal FBs show better performance in image compression applications. Hilbert-pairs of FBs are important building blocks in the dual-tree complex wavelet which is very popular in many applications. This thesis proposes novel techniques to design a new class of Hilbert-pairs which are orthogonal but also almost symmetric. The new Hilbert pairs have the advantages offered by both orthogonal and biorthogonal systems. These systems are then applied in proteomics and image processing. The directional wavelet transform is a simple improvement to the traditional DWT by the addition of a quadrant filter. This thesis studies the aliasing phenomena of these systems and proposes ways to circumvent the problem.

Statement of Authorship

Except where reference is made in the text of the thesis, this thesis contains no material published elsewhere or extracted in whole or in part from a thesis or any other degree or diploma.

No other person's work has been used without acknowledgment in the main text of the thesis.

This thesis has not been submitted for the award of any degree or diploma in any other tertiary institution.

Selvaraaaju Murugesan
January 9, 2014

Acknowledgements

I would like to thank my family for their endless love and support. I am greatly indebted to my supervisor Dr. David Tay for his guidance and motivation. I would like to thank my co-supervisor Dr. Dennis Deng for his encouragement and support. I would like to thank my colleagues in the Department of Electronic Engineering for their support and assistance in my work. I would like to thank all the LaTrobe University Librarians for their help with books and journal articles. I would like to thank all my friends for their inspiration.

1 Introduction

1.1 Motivation

Signal processing is an indispensable tool in a wide range of engineering and scientific applications [1],[2]. Since the inception of the Fourier transform, the signal processing field has progressed at a rapid pace and provided a lot of tools for the scientific community. One of the most significant signal processing tool is the wavelets. Most of the traditional signal processing tools can only be applied to stationary signal. But most of the practical signals are non-stationary in nature and the traditional tools like the Fourier transform does not perform well in analysing those non-stationary signals. Wavelets are well suited for both stationary and non-stationary signals. Wavelets produces efficient and sparse representation of the signal. After the wavelet decomposition of the signal, most of the transformed coefficients are close to zero so that the signal can be easily compressed. The recent JPEG 2000 image coding standard [3] utilises the Discrete Wavelet Transform (DWT) to compress the image. Wavelets are used for medical signal processing because of its ability to identify a specific information and particular event in the signal (spike detection, anomaly detection). One of the reason that wavelets gained so much popularity is its ability to provide multiresolution analysis. Most of the practical signals have high frequency at short durations and low frequency components for long duration. Wavelets can provide a good frequency resolution at low frequencies and good time resolution at high frequencies. The DWT is implemented efficiently using the multirate filter banks (FB).

Most of the orthogonal wavelet filters in the literature are designed in the continuum domain (infinite precision) and they have irrational filter coefficients. During the hardware implementation, there is always rounding or quantisation of the filter coefficients. If the fixed point arithmetic is implemented, then the quantisation of filter coefficient has significant effect on the filter characteristics and its performance. The perfect reconstruction (PR) property of the filter bank is destroyed. The vanishing moment (VM) of

the wavelet filter is also lost which will lead to DC leakage in the high pass filter. This motivates us to find new ways of rationalising orthogonal filters without losing the PR, VMs and degradation in the frequency response. If the rational filter coefficients can be expressed as sum of powers of two, it will lead to multiplier-less hardware implementation [4],[5],[6].

The orthogonal filters have the energy preservation property i.e. the energy of the signal is preserved in the transformed domain. The biorthogonal filters are preferred in image processing application because of the symmetric wavelets. The symmetric wavelets are vital for processing the salient features of the images such as edges. The symmetric wavelets do not produce any distortions while processing those salient image features. The biorthogonal wavelets are not energy preserving unlike orthogonal wavelets. But the dyadic wavelets cannot be symmetric and orthogonal simultaneously except for the simple two tap Haar filter [7],[8]. The Haar wavelet is not widely used in image processing application because it is not smooth. There has been many research [9],[10],[11] on designing symmetric and almost orthogonal filters but the filter lengths are too long and resulting filters do not satisfy the perfect reconstruction property. This motivates to design an almost symmetric orthogonal wavelet filter. The almost symmetric orthogonal filters can produce almost symmetric wavelet and at the same time it satisfies the perfect reconstruction property of the filter bank. If the almost symmetric filter bank is used in image processing application, it has the advantages of being orthogonal and approximately linear phase. The almost symmetric orthogonal wavelets have approximately flat group delay and approximately linear phase. The technique to design an almost symmetric orthogonal wavelet filters should be simple and can be applied to design longer length filters. This design versatility is addressed in our research.

Designing symmetric wavelets is also important in implementing the Dual Tree Complex Wavelet Transform (DTCWT). The DTCWT employs a pair of two channel PR filter bank. The wavelet function of the two filter banks $\psi^h(t)$ and $\psi^g(t)$ should satisfy the Hilbert transform relationship [12],[13]. The DTCWT offers near shift invariance and better directionality compared to the DWT. The symmetry of the Hilbert pair of wavelets is of prime importance for directional selectivity of the DTCWT. The orthogonal FB based on IIR filters can produce symmetric Hilbert pair of wavelets but it requires complex implementation. Most of the Hilbert pair filter design methodology [12],[14],[15],[16] focusses on satisfying the Hilbert relationship among wavelets and less

attention is given to symmetry of the wavelets in the design. If the constituent wavelets are symmetric, it can be deployed in many image processing applications. This motivates to design an almost symmetric Hilbert pair of wavelets.

Mass Spectroscopy (MS) is a widely used technique in molecular biology (see [17] for a review) for high throughput identification and sequencing of peptides (and proteins). The MS data is corrupted by electrical and chemical noise which can be modelled as zero mean additive white Gaussian noise. The preprocessing of the MS data will greatly improve the performance of post processing of MS data. The commonly used preprocessing methods are denoising of MS data followed by data normalisation. The post processing process involves peak picking and peak quantification [18],[19]. There have been many researches done on denoising MS data using DWT, undecimated DWT and Stationary Wavelet Transform (SWT). The DTCWT has emerged as an important redundant transform that offers near shift invariance. The elution time of peptides varies depending upon the various conditions such as temperature, interaction between molecules, etc. So, the MS data of a sample collected differs over the time. The DTCWT will perform best on this type of data. We also demonstrate the capabilities of the almost symmetric Hilbert pair of wavelet in a Proteomics application. The designed almost symmetric Hilbert pair of wavelets is applied to denoise the Mass Spectroscopy data and we will evaluate the performance of the DTCWT with other transforms.

The finer Directional Wavelet Transform (fiDWT) is proposed by Yu [20] to enhance the directionality of DWT. Even though there are many other transforms available in the literature [21],[22],[23] that offer better directionality than DWT, the fiDWT is very simple to implement. It can be used as an “add-on” if you need better directionality. The fiDWT uses DWT as the basic building block for implementation and also it deploys the pair of quadrant filters. We found out that fiDWT is prone to aliasing and it has got significant performance degradation in image processing applications. This motivates us to propose a new ways to reduce aliasing in fiDWT and enhance its performance. In the next section, we state all the problems that this thesis is going to address.

1.2 Problem Statement

This thesis will address the following problems.

Orthogonal FB with rational coefficients: How to obtain rational coefficient

orthogonal and biorthogonal filters while preserving perfect reconstruction, vanishing moments and frequency response?

Almost Symmetric Orthogonal FB: How to design an almost symmetric orthogonal wavelets that performs on par with 9/7 biorthogonal wavelets?

Almost Symmetric Orthogonal Hilbert pair of wavelets: How to design an almost symmetric Hilbert pair of wavelets such that both the constituent wavelets and the complex wavelets are symmetric?

Undecimated finer Directional Wavelet Transform: How to increase the directionality of the DWT?

1.3 Thesis outline

The main goal of this thesis is to design

- orthogonal and biorthogonal FB having rational coefficients
- almost symmetric orthogonal wavelets
- almost symmetric Hilbert pair of wavelets

In addition to designing new family of filter banks, some novel applications of the designed filter banks are also presented in this thesis to emphasis the effectiveness of the proposed filter banks.

Chapter 2 introduces the fundamentals of filter banks and also reviews the theory of designing wavelets. Then the literature review for designing the rational coefficient orthogonal filter banks is presented. The traditional way of designing rational coefficient orthogonal filter bank does not preserve the perfect reconstruction property of the filter banks. The vanishing moments which are crucial for wavelet generation are also lost during the rationalisation process. We propose a new technique to rationalise the orthogonal filter banks while preserving perfect reconstruction, vanishing moments and good frequency response. We extend the technique to rationalise the Hilbert pair of filters and show that the proposed technique also preserves the Hilbert pair relation of filters after rationalisation process. Up to two vanishing moments can be imposed on the rational filters. An efficient way to implement the rational orthogonal filters based on lattice structures is also presented. We then propose a generalised method to rationalise biorthogonal filters.

Chapter 3 presents a new technique to design almost symmetric orthogonal filter banks. The wavelet symmetry is preferred in image processing applications because the edges in the images are susceptible to non-linear distortions. An almost symmetric orthogonal filter bank can be designed with the proposed design technique. The almost symmetric orthogonal filter bank performs on par with the 9/7 biorthogonal filter banks in image coding application. Some image coding applications of the designed almost symmetric orthogonal wavelet filters is also presented.

In Chapter 4, we review the theory of designing the Hilbert pair of wavelets and the half sample delay condition required between filters to form a Hilbert pair. The Hilbert pair of filters form the backbone of the Dual Tree Complex Wavelet Transform (DTCWT). The DTCWT offers near shift invariance and higher directionality compared to the DWT. For better directional selectivity, the symmetry of the Hilbert pair is important. The orthogonal Hilbert pair of wavelets found in the literature produce symmetric complex wavelet but the constituent wavelets are not symmetric. A new technique is proposed in this chapter to design almost symmetric orthogonal Hilbert pair of wavelets. We also argue that designing a symmetric wavelet will correspond to approximately linear phase characteristics but not vice versa.

Chapter 5 shows the application of almost symmetric orthogonal Hilbert of wavelets in Proteomics. The Mass Spectroscopy data is corrupted by additive white Gaussian noise. We apply the DTCWT on the Mass Spectroscopy data to clean the noise using the soft thresholding method. After peak picking, more peptides are identified compared to other transforms such as DWT and SWT.

In Chapter 6, we propose the undecimated finer directional wavelet transform (ufiDWT) as it reduces the aliasing present in the finer directional wavelet transform (fiDWT). We also show that aliasing is inherent in the finer directional wavelet transform because of the characteristics of the quadrant filters. The proposed ufiDWT performs better than fiDWT in image denoising application. The ufiDWT is redundant but it is free from aliasing.

Finally we conclude and summarise the key contributions in Chapter 7 and also discuss about the future work.

1.4 Contributions and Publications

Most of the main results in this thesis has been published in international journals and conferences. The publications are listed below

- Selvaraaaju Murugesan, David B. H. Tay, “New Techniques for Rationalizing Orthogonal and Biorthogonal Wavelet Filter Coefficients”, IEEE Transactions on Circuits and Systems 59-I(3): 628-637 (2012)
- Selvaraaaju Murugesan, David B. H. Tay, “Design of Almost Symmetric Orthogonal Wavelet Filter Bank Via Direct Optimization”, IEEE Transactions on Image Processing 21(5): 2474-2480 (2012)
- Selvaraaaju Murugesan, David B. H. Tay, “On the aliasing effect of the finer directional wavelet transform”, ISCAS 2012: 2345-2348
- Selvaraaaju Murugesan, David B. H. Tay, ”A New Class of Almost Symmetric Orthogonal Hilbert Pair of Wavelets”, Signal Processing 95(2): 76-87 (2014)

2 New Techniques for Rationalizing Orthogonal and Biorthogonal Wavelet Filter Coefficients

Most wavelet filters reported in the literature have irrational coefficients. Hardware implementation can be simpler if the filter coefficients are rational valued. In this chapter, we present novel methods to rationalize both orthogonal and biorthogonal filter coefficients with perfect reconstruction and vanishing moments preservation. Rational orthogonal filter coefficients are obtained using lattice structures. Rational biorthogonal filter coefficients are obtained using the complementary filter technique in which one set of filter coefficients is expressed in terms of the other. The rationalized filters have characteristics that are very close to the original irrational filters. The techniques are simple yet general enough to be used for almost any filter bank unlike the techniques in previously reported works.

2.1 Introduction

The Discrete Wavelet Transform (DWT) has emerged as a powerful signal processing tool [1],[24] and it is widely used in applications requiring multiresolution signal or image analysis. Transforms based on orthogonal filter banks have the advantage of energy preservation but they are not preferred in image processing applications because of the lack of symmetry in the wavelet function. Linear phase filters and symmetric wavelet functions are preferred in image processing applications and for the FIR case this can only be achieved with biorthogonal filter banks. However orthogonal linear phase filter bank is possible with IIR filters [25],[26] and the IIR filters involve complex implementation than FIR filters. Wavelet theory stipulates that the low-pass filters should have zeros at the aliasing frequency so that the corresponding wavelet function has vanishing moments. Vanishing moments (VM) play an important role in determining

the regularity (smoothness) of the wavelets. More recently the Dual-Tree-Complex-Wavelet-Transform of Kingsbury [27],[28] has emerged as an important extension of the traditional non-redundant DWT. Compared to the traditional non-redundant DWT, the dual-tree complex wavelet transform has the advantages of being approximately shift-invariant and providing directional selectivity in multidimensions.

Most of the wavelet filters in the literature are designed in the real-number continuum domain (infinite precision) and the resulting coefficients usually have irrational values. There will be some rounding or quantization of these irrational values during hardware implementation [29],[30],[31]. If floating point arithmetic (with sufficient accuracy) is used the effect of quantization is negligible. However if fixed point arithmetic is used quantization can have a significant effect. It is therefore advantageous to have rational valued coefficient filters which (with proper normalization) can be implemented efficiently without multipliers [32],[33]. Direct independent quantization of the coefficients will generally result in the loss of perfect reconstruction (PR) and VMs. Polyphase based structures for filter banks, such as lattice or lifting, have structural PR. Therefore PR is preserved under quantization of the parameters of the lattice structure. Zeros at $z = -1$ of the filters are however generally lost and this results in DC leakage and the loss of VMs.

This chapter will present new techniques to rationalize both two-channel orthogonal and biorthogonal filter coefficients. The PR property and some of the VMs are preserved with the new techniques. Unlike previously reported techniques in the literature (many of which are ad-hoc), the techniques here are general enough to be applied to almost any two-channel filter bank and yet simple to use. A detailed comparison with previous works are presented in the Section 2.5. One of the main highlights of the proposed new technique is that it allows the rationalization of any orthogonal filters with *zero DC leakage preservation*. This is something not achievable with previously reported works. The rationalization technique is based on the use of lattice structures for orthogonal filters and the concept of complementary filters for biorthogonal filters. The techniques will be applied on several reported wavelet filters from the literature such as the well known Daubechies family [8], image compression optimized biorthogonal filters in [34] and the dual-tree filters in [15]. The results will show that coding gain, frequency response and other characteristics of the rational filters are close to the original irrational filters.

This chapter is organised as follows. Section 2.2 reviews the important concepts and principle of wavelets and filter bank fundamentals elaborately. The technique for

rationalizing the orthogonal filters is presented in Section 2.3. The Daubechies family of filters and Dual-Tree filters are rationalized based on the proposed technique and it is presented in the Section 2.3 along with the efficient implementation of filters in lattice framework. The technique to rationalize the biorthogonal wavelet filters is presented in Section 2.4. The popular biorthogonal filters such as “9/7”, “13/11” and “17/11” are rationalized based on the proposed technique and is also presented in Section 2.4. In Section 2.5 comparison with previous work is discussed extensively to showcase the efficiency of the proposed rationalization technique. The chapter is concluded in Section 2.6.

2.2 Preliminaries

2.2.1 Filter Banks Fundamentals

Let H_0 and F_0 be the analysis and synthesis low pass filters of a two channel biorthogonal filter bank system. Then the analysis and synthesis high pass filters H_1 and F_1 respectively are obtained by quadrature mirroring the low pass filters

$$\begin{aligned} H_1(z) &= z^{-1}F_0(-z) \\ F_1(z) &= zH_0(-z) \end{aligned}$$

and this achieves aliasing cancellation. The perfect reconstruction (PR) condition is then given by

$$H_0(z)F_0(z) + H_0(-z)F_0(-z) = k \quad (2.1)$$

where k is a constant. Usually $k = 2$ but in practice can also have other values (see section 2.2.4). The orthogonal filter bank is a special case of the biorthogonal filter bank in which the low pass filters are mirror images of each other $F_0(z) = H_0(z^{-1})$. The product filter is given by

$$P(z) = H_0(z)F_0(z)$$

and as per the PR condition (2.1) the product must satisfy the following condition

$$P(z) + P(-z) = 2 \quad (2.2)$$

The design of the wavelet filters is thus reduced to the design of the product filter $P(z)$ and the factorisation of $P(z)$ will yield the filters $H_0(z)$ and $F_0(z)$. For the orthogonal case, the product filter must satisfy the following *non-negativity* condition

$$P(e^{j\omega}) \geq 0 \quad \forall \omega$$

The biorthogonal filters are obtained from the family of Lagrange-Halfband-Filters (LHBF) [8],[35][36] which has a maximum number of vanishing moments (also known as the maximally flat product filter). The LHBF of order K is given by

$$P(z) = z^K \left(\frac{1 + z^{-1}}{2} \right)^{2K} R_K(z)$$

where

$$R_K(z) = \sum_{n=0}^{K-1} \binom{K+n-1}{n} \left(\frac{2 - (z + z^{-1})}{4} \right)^n$$

The wavelet $\psi(t)$ (spectrum $\Psi(\omega)$) and the scaling function $\phi(t)$ (spectrum $\Phi(\omega)$) can be generated from the infinite product formula [2] and are given by

$$\Psi(\omega) = \frac{1}{2} H_1(e^{j\omega/2}) \prod_{k=1}^{\infty} \{(1/2)H_0(e^{j\omega/2^{k+1}})\}$$

$$\Phi(\omega) = \frac{1}{2} H_0(e^{j\omega/2}) \prod_{k=1}^{\infty} \{(1/2)H_0(e^{j\omega/2^{k+1}})\}$$

To ensure the equivalent wavelet function $\psi(t)$ is smooth, zeros at $z = -1$ are imposed on the low-pass filter H_0 (F_0) and this is called the vanishing moment (VM) condition [2]. Sum rules can be applied to the filter coefficients $h_0(n)$ to ensure VMs. The general expression for the l^{th} sum rule is given by

$$H_0^{(l)}(e^{j\pi}) = \sum_n (-1)^n n^l h_0(n) = 0 \quad (2.3)$$

For p VMs p sum rules are required, i.e. (2.3) for $l = 0, 1, \dots, p - 1$. If $p \geq 1$, then $H_1(e^{j0}) (= H_0(e^{j\pi})) = 0$. i.e *no DC leakage*.

2.2.2 Filter bank Design

There are two main frameworks for the construction of two-channel filter bank

1. Factorization of product filter [7]
2. Polyphase structure which includes lifting [37] and lattice structure [38]

The factorization of LHBF was introduced by Daubechies [7],[8] and the design of wavelet filters is based on the *spectral factorization* technique. The lattice structure is utilised by Vaidyanathan *et. al* [38] to design a PR FB. Sweldens introduced the lifting structure [37] to design and implement the FB. The lifting structure is the popular way to implement the biorthogonal filters even though there are plethora of other methods [5],[39],[6],[40],[30],[41],[4] available. In this section, the review of the available framework for filter bank design is presented.

2.2.2.1 Factorization of Product Filter

Daubechies [7] used the LHBF to design the wavelet filter bank containing the maximum vanishing moments using the *spectral factorisation* technique [7],[8]. In the orthogonal filter bank the product filter $P(z)$ is given by

$$P(z) = H_0(z)H_0(z^{-1})$$

and it must satisfy the power complementary property. i.e.

$$|H_0(\omega)|^2 + |H_0(\omega + \pi)|^2 = 2$$

Daubechies used the LHBF as the product filter $P(z)$ and performed a spectral factorisation to design a family of Daubechies orthogonal filters. The z -transform of $P(z)$ is defined as

$$P(z) = \sum_n p(n) z^{-n}$$

For the PR condition (2.1) to be satisfied, we need $p(2n) = 0$ for $n \neq 0$. The product filter $P(z)$ is symmetric i.e., $p(2n) = p(-2n)$. The middle value of the product filter should be $1/2$. i.e., $p(0) = \frac{1}{2}$. Because the product filter contains symmetric coefficients, then $P(z) = P(1/z)$ i.e., if z_i is a root, then $1/z_i$ is also a root. Daubechies's [7],[8] spectral factorisation of $P(z)$ allocate the z_i and z_i^{-1} roots into $H_0(z)$ and $H_0(z^{-1})$ respectively. Daubechies allocated half the VMs (zeros at $\omega = \pi$) and all the roots inside the unit circle $z = 1$ to design a family of minimum phase filters. The maximum phase filters are obtained by choosing half the VMs roots and the roots outside the unit circle of product filter $P(z)$. When the length of the product filter $P(z)$ increases, the choice of selection

of roots increases. The algorithms used for spectral factorisation may become unreliable if the product filter length increases above 50. If the filter length is $2L$, then the PR condition (2.1) takes half of degrees of freedom in the design. The remaining degrees of freedom (L) is utilised to have zeros at aliasing frequency. There are many other works in the literature [11],[42],[43],[44] that uses the remaining degrees of freedom L to tweak the other characteristics of the filter instead of utilising all of them for VMs. It should be noted that all the Daubechies filters have irrational coefficients and rationalising the Daubechies filter coefficients will lead to losing some of the properties of the filters.

2.2.2.2 Polyphase Structure

The polyphase structure can be implemented either using lattice framework [1],[2],[45] or lifting framework [37]. The analysis filters can be represented as

$$\begin{bmatrix} H_0(z) \\ H_1(z) \end{bmatrix} = \mathbf{H}_p(z^2) \begin{bmatrix} 1 \\ z^{-1} \end{bmatrix} \quad (2.4)$$

where $\mathbf{H}_p(z)$ is the (analysis) polyphase matrix and it is given by

$$\mathbf{H}_p(z) = \begin{bmatrix} H_{00}(z) & H_{01}(z) \\ H_{10}(z) & H_{11}(z) \end{bmatrix}$$

where $H_{00}(z)$ ($H_{10}(z)$) and $H_{01}(z)$ ($H_{11}(z)$) are the odd and even coefficients of the low pass filter $H_0(z)$ (high pass filter $H_1(z)$) respectively. The filters $H_0(z)$ and $H_1(z)$ are given by

$$\begin{aligned} H_0(z) &= H_{00}(z^2) + z^{-1}H_{01}(z^2) \\ H_1(z) &= H_{10}(z^2) + z^{-1}H_{11}(z^2) \end{aligned}$$

The polyphase matrix for orthogonal filter banks has a lattice structure that is implemented using rotation matrices and delay matrices [38]. The standard rotation matrix is given by $\begin{bmatrix} \cos \theta & -\sin \theta \\ \sin \theta & \cos \theta \end{bmatrix}$ [46] and is properly normalized. However for the purpose of developing the rationalization technique (described in the Section 2.3) an un-normalized

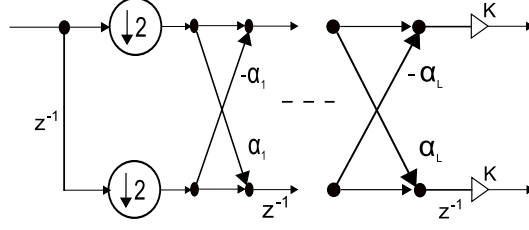


Figure 2.1: Lattice structure

version as defined by \mathbf{R}_l below will be used. The lattice polyphase matrix is given by

$$\begin{aligned} \mathbf{H}_p(z) &= K \mathbf{R}_L \mathbf{D}(z) \mathbf{R}_{L-1} \dots \mathbf{D}(z) \mathbf{R}_1 \\ &= K \mathbf{R}_L \prod_{l=1}^{L-1} [\mathbf{D}(z) \mathbf{R}_l] \end{aligned} \quad (2.5)$$

where

$$\mathbf{D}(z) = \begin{bmatrix} 1 & 0 \\ 0 & z^{-1} \end{bmatrix}, \quad \mathbf{R}_l = \begin{bmatrix} 1 & -\alpha_l \\ \alpha_l & 1 \end{bmatrix}$$

Now L is the number of stages, α_l 's are the lattice parameters which can also be expressed in terms of rotation angles as $\alpha_l = \tan \theta_l$. The normalisation constant K is given by

$$K = \prod_l \frac{1}{\sqrt{(1 + \alpha_l^2)}} \quad (2.6)$$

The lattice structure shown in Figure 2.1 is an efficient way to implement the filter banks [38]. The PR condition (2.1) is structurally imposed and is therefore preserved under lattice parameter quantization. If the lattice parameters are quantized to rational values then the filter coefficients will also have rational values.

2.2.3 Sobolev Regularity

Sobolev regularity s_c is a measure of smoothness of the wavelet. It is defined as the smallest real number s_c such that $\Phi(\omega)$ (Fourier transform of the scaling function $\phi(t)$) satisfies:

$$\int_{-\infty}^{\infty} (1 + |\omega|^2)^s |\Phi(\omega)|^2 d\omega < \infty \quad \forall s < s_c$$

The Sobolev regularity s_c can be obtained by solving an eigenvalue problem and the procedure to is given below [47]:

- Eliminate all the factors $(1 + z^{-1})$ factors (multiplicity M) from the product filter $P(z)$ to give the remainder filter $Q(z)$ with the normalization that is given by $Q(1) = 2^{(1-M)}$
- Construct a matrix R with elements given by $[Q]_{k,l} = q_{2k-1}$ for $-L_Q \leq k, l \leq L_Q$, where $q_k (-L_Q \leq k \leq L_Q)$ are the coefficients of the filter $Q(z)$. The matrix Q will be of size $(2L_Q + 1) \times (2L_Q + 1)$.
- Find the largest absolute eigenvalue, $|\lambda|_{max}$ of Q . Then $s_c = -\frac{1}{2} \log_2 |\lambda|_{max}$.

The Sobolev regularity s_c and Holder regularity r_c are related by the inequality

$$r_c \leq s_c \leq r_c + \frac{1}{2}$$

The Holder measure r_c can be obtained using the above inequality from s_c . Sobolev regularity is used as regularity measure in this thesis.

2.2.4 Filter Normalisation

Denote the DC gain of the low-pass filters by $\Delta_H \equiv H_0(1)$ and $\Delta_F \equiv F_0(1)$. The gain values are related to the k value in (2.1) as follows: $\Delta_H \Delta_F = k$. For a strict PR condition with no scaling of the output $k = \Delta_H \Delta_F = 2$. The factor 2 can be distributed between Δ_H and Δ_F in various ways but the two most common distributions are:

- (i) $\Delta_H = 1$ (unity DC) and $\Delta_F = 2$
- (ii) $\Delta_H = \Delta_F = \sqrt{2}$.

Case (ii) is an equal distribution and the one specified by wavelet theory. Case (ii) will ensure the transform using orthogonal filters are energy (or l^2 norm) preserving, i.e. orthonormal filters are obtained. However rational coefficient filters are not possible in case (ii). If one is willing to accept a more general definition of PR (output is $k/2$ times input) then k can be any arbitrary constant. In practical applications the scaling can be absorbed by the subsequent processing of the signal after the transform, eg. adjustment of the quantization step sizes in compression. It is however desirable to make Δ_H and Δ_F as close to $\sqrt{2}$ as possible.

In this chapter, the unnormalised lattice structure, i.e. (2.5) without the K factor, is used in the design stage. The normalisation constant K can be applied during the implementation. The K value in (2.6) is irrational (in general) and should be quantized to a rational value for efficient implementation. If the rational value is a dyadic integer,

no multiplier is needed. If the rationalized value is close to the original irrational value then $k \approx 2$ and $\Delta_H \approx \sqrt{2}$.

2.2.5 Canonical Signed Digit

The Canonical Signed Digit (CSD), a subset of SPT (Sum of Powers of Two) representation has proven to be useful in efficient implementation of digital filters [48],[49]. If the filter coefficients are expressed in SPT terms, then the multiplication is performed using shifts and addition. A N_D bit number D having is represented in canonical form [50] as

$$D = \sum_{i=0}^{N_D-1} s_i 2^i \quad s_i \in \{-1, 0, 1\}$$

The unique properties of CSD are

1. the number of non-zero digits is minimal
2. no two adjacent digits are nonzero.

These properties make the canonical form optimal in terms of how many nonzero digits are required to represent a given number.

If the lattice coefficient values can be expressed as a SPT (Sum of Powers of Two) value, i.e. *dyadic integer* ($\gamma/2^c$, γ and c are integers), the digital hardware required then consists of simple shifts and adders. In this chapter, we use the CSD [4],[51] to express the lattice coefficients.

2.2.6 Performance Measures

2.2.6.1 Coding gain

Coding gain is the widely used performance measure in image processing applications especially in image compression. We use the expression derived by Katto and Yasuda [52], which is valid for nonorthogonal transforms. The input is assumed to be first order Markov process with unit variance and correlation coefficient ρ . Let $h_k(i)$ ($k = 1, 2, \dots, N$) and $g_k(i)$ ($k = 1, 2, \dots, N$) denote the coefficients of the analysis and synthesis filters of an N band subband decomposition. Usually five levels of decomposition are used and the correlation coefficient value is taken to be $\rho = 0.95$. A five level decomposition has been justified experimentally as providing the best performance measure for the largest

number of images. The coding gain expression is the best indicator of performance as it measures the filter bank's coding efficiency.

There are a few assumptions made while deriving the formula for coding gain by Katto and Yasuda. They are

1. uncorrelated quantization error
2. input is assumed to be a first order Markov model

The coding gain $G(\rho)$ is given by

$$G(\rho) = \prod_{k=1}^N (A_k B_k)^{-\alpha_k} \quad (2.7)$$

where

$$A_k = \sum_i \sum_j h_k(i) h_k(j) \rho^{|i-j|},$$

$$B_k = \sum_i g_k(i)^2$$

α_k is the equivalent downsampling factor for the k th channel

2.2.6.2 Analytic Quality Measures for Hilbert pair

The dual-tree complex wavelet transform of Kingsbury is based on a pair of filter banks whose corresponding wavelet functions, denoted by $\psi^h(t)$ and $\psi^g(t)$, form a Hilbert pair

$$\Psi^g(\omega) = \begin{cases} -j\Psi^h(\omega), & \omega > 0 \\ j\Psi^h(\omega), & \omega < 0 \end{cases} \quad (2.8)$$

where $\Psi^h(\omega)$ and $\Psi^g(\omega)$ are Fourier transforms of $\psi^h(t)$ and $\psi^g(t)$ respectively. The corresponding low-pass filters of the filter bank, denoted by $H^h(z)$ and $H^g(z)$, should satisfy [12]

$$H^g(e^{j\omega}) = e^{-j\omega/2} H^h(e^{j\omega}) \quad (2.9)$$

but in practice (2.9) and therefore (2.8) can only be approximated. By defining $\Psi^C(\omega)$ as the complex wavelet spectrum given by

$$\Psi^C(\omega) = \Psi^h(\omega) + j\Psi^g(\omega)$$

The quality measures based on the level of analyticity can be defined [15] as

$$E_1 \equiv \frac{\max_{\omega < 0} |\Psi^C(\omega)|}{\max_{\omega > 0} |\Psi^C(\omega)|} \quad (2.10)$$

$$E_2 \equiv \frac{\int_{-\infty}^0 |\Psi^C(\omega)|^2 d\omega}{\int_0^{\infty} |\Psi^C(\omega)|^2 d\omega} \quad (2.11)$$

Ideally $E_1 = E_2 = 0$ if (2.8) is exact and $\Psi^C(\omega)$ is complex analytic, i.e. $\Psi^C(\omega) = 0$ for $\omega < 0$. In practice E_1 and E_2 are non-zero and the smaller the values, the better the analytic quality.

2.3 Rationalizing Orthogonal Filters

The lattice structure is utilized for rationalizing orthogonal filter coefficients. The justification of this approach is presented in section 2.5 along with comparison with other techniques. The lattice parameters α_l are first determined from the original irrational filter coefficients. If the filter length is $2L$, then the number of lattice parameters would be L . Quantizing these irrational lattice parameters will not destroy the perfect reconstruction (PR) property due to the structural PR property in lattice structures. However if the lattice parameters are quantized independently, the zeros at $z = -1$ of the low-pass filter will be perturbed in general, i.e. vanishing moments (VMs) are destroyed. There should be at least one zero at $z = -1$ (VM) to generate the wavelet function. One VM is also needed to avoid DC leakage in the equivalent band-pass and high-pass filters. A technique that ensure at least one VM is presented next.

2.3.1 Ensuring One Vanishing Moment

Imposing one vanishing moment by using the first sum rule will result in an equation relating the lattice parameters. We will show that this equation can be solved algebraically in closed form for one of the lattice parameter, e.g. α_i , in terms of other parameters $\tilde{\alpha} = [\alpha_1, \alpha_2, \dots, \alpha_L] \setminus \alpha_i$. We will also show that α_i is rational if $\tilde{\alpha}$ is rational.

Lemma 1: Suppose the first sum rule is imposed ensuring one vanishing moment, then

$$\alpha_i = \frac{f_1(\tilde{\alpha})}{f_2(\tilde{\alpha})} \quad (2.12)$$

where $i \in \{1, \dots, L\}$, $f_1(\tilde{\alpha})$ and $f_2(\tilde{\alpha})$ are multilinear functions (of $[\alpha_1, \alpha_2, \dots, \alpha_L] \setminus \alpha_i$)

with *integer* coefficients. Therefore α_i is rational if $\tilde{\alpha}$ is rational.

Proof: Using (2.5) in (2.4) we have

$$\begin{bmatrix} H_0(z) \\ H_1(z) \end{bmatrix} = \underline{\mathbf{S}} \begin{bmatrix} 1 & -\alpha_k \\ \alpha_k & 1 \end{bmatrix} \cdot \underline{\mathbf{r}} = \underline{\mathbf{S}} \underline{\mathbf{R}}_k \underline{\mathbf{r}} \quad (2.13)$$

where $\underline{\mathbf{r}}$ ($\underline{\mathbf{S}}$) is the product of all the matrices to the right (left) of the matrix $\underline{\mathbf{R}}_k$. Equation (2.13) shows the explicit linear dependence on the k^{th} lattice parameter α_k . This means that the filter coefficients of $H_0(z)$ are multilinear functions of the lattice parameters:

$$h_0(n) = \sum_l C_l^n \left(\prod_{k=1}^L \alpha_k^{i_k^n} \right)$$

where $i_k^n = 0$ or 1 . The term in brackets represents a general multilinear term, e.g. $\alpha_1\alpha_2$ or $\alpha_2\alpha_3$. Since the constant coefficients of the all matrices in (2.5) are integers, C_l^n will also be an integer. Applying the first sum rule

$$h(0) - h(1) + h(2) - h(3) + \dots - h(2L - 1) = 0$$

will result in an integer coefficient multilinear equation in the lattice parameters. Collecting all terms containing α_i together, this multilinear equation can be written in the form

$$\alpha_i f_2(\tilde{\alpha}) - f_1(\tilde{\alpha}) = 0$$

where $f_1(\tilde{\alpha})$ and $f_2(\tilde{\alpha})$ are multilinear functions of $[\alpha_1, \alpha_2, \dots, \alpha_L] \setminus \alpha_i$ with integer coefficients. The equation (2.12) readily follows. ■

It is not possible to have a general closed form explicit expression for the functions $f_1(\tilde{\alpha})$ and $f_2(\tilde{\alpha})$. Some symbolic algebraic calculations are required. Firstly the filter coefficients $h_0(n)$ in terms of α_k are obtained by expanding the matrix products in (2.5). Secondly substitute $h_0(n)$ into the first sum rule equation, collect all terms containing α_i together and factor out α_i . Then the functions $f_1(\tilde{\alpha})$ and $f_2(\tilde{\alpha})$ can be easily identified from the equation. This process is illustrated with an example below.

Example I: The Daubechies length 6 ($L = 3$) filter (Db6) has three lattice parameters:

α_1 , α_2 and α_3 . The filter functions are given by

$$\begin{bmatrix} H_0(z) \\ H_1(z) \end{bmatrix} = \begin{bmatrix} 1 & -\alpha_3 \\ \alpha_3 & 1 \end{bmatrix} \begin{bmatrix} 1 & 0 \\ 0 & z^{-2} \end{bmatrix} \begin{bmatrix} 1 & -\alpha_2 \\ \alpha_2 & 1 \end{bmatrix} \begin{bmatrix} 1 & 0 \\ 0 & z^{-2} \end{bmatrix} \begin{bmatrix} 1 & -\alpha_1 \\ \alpha_1 & 1 \end{bmatrix} \begin{bmatrix} 1 \\ z^{-1} \end{bmatrix}$$

Expand the above product and consider only $H_0(z)$. The filter coefficients $\{h_0(0), \dots, h_0(5)\}$ are given by:

$$\{1, -\alpha_1, -\alpha_1\alpha_2 - \alpha_2\alpha_3, -\alpha_2 + \alpha_1\alpha_2\alpha_3, -\alpha_1\alpha_3, -\alpha_3\} \quad (2.14)$$

Applying first sum rule on (2.14) gives

$$1 + \alpha_1 + \alpha_2 + \alpha_3 - \alpha_1\alpha_2 - \alpha_1\alpha_3 - \alpha_2\alpha_3 - \alpha_1\alpha_2\alpha_3 = 0$$

Collecting all terms containing α_3 and factoring out α_3 gives

$$(1 + \alpha_1 + \alpha_2 - \alpha_1\alpha_2) - \alpha_3(\alpha_1 + \alpha_2 + \alpha_1\alpha_2 - 1) = 0 \quad (2.15)$$

Using (2.15), α_3 can be expressed in terms of α_1 and α_2 as

$$\alpha_3 = \frac{f_1(\tilde{\alpha})}{f_2(\tilde{\alpha})} = \frac{1 + \alpha_1 + \alpha_2 - \alpha_1\alpha_2}{\alpha_1 + \alpha_2 + \alpha_1\alpha_2 - 1} \quad (2.16)$$

The irrational values of α_1 and α_2 can be quantized to rational values independently. Using these rational values in (2.16) will yield α_3 with rational value. There are many potential choices for value of the lattice parameters α_1 and α_2 . Two factors need to be taken into account when the parameters are quantized. Firstly the quantized lattice parameters values should be close to the original irrational values to ensure the characteristics (and performance) of the filters do not deviate significantly. This constraint sets the range of allowable values for the lattice parameters. The second factor is the computational complexity of implementing the un-normalized rotation matrix \mathbf{R}_l . Simple dyadic integer values for the lattice parameters α_1 and α_2 will lead to an efficient multiplierless implementation. These factors lead to the following procedure to determine the suitable value for α_1 and α_2 :

1. Determine the maximum deviation from the original irrational values for α_1 and α_2 subject to the constraint $\int |H_0(e^{j\omega}) - H_0^O(e^{j\omega})|^2 d\omega < \epsilon$ (allowable level of deviation). $H_0(e^{j\omega})$ and $H_0^O(e^{j\omega})$ are the perturbed and original filter respectively.

This gives the allowable range $(\alpha_k^{min}, \alpha_k^{max})$ ($k = 1, 2$) of values.

2. Over the allowable range determine the dyadic value that gives the lowest number of SPT terms.

The original irrational and quantized rational values of the lattice parameters are given in Table 2.1. The frequency response of the original and rational filters are shown in Figure 2.2. The Sobolev regularity measure, the quantized normalisation constant $Q(\tilde{K})$, DC gain and number of SPT terms required (using CSD representation) are also shown. If $\alpha_1 = -12/5$ and $\alpha_2 = 55/100$ (small deviation from the rational value in Table 2.1) are now chosen instead as the parameters value, the characteristics (and performance) of the filter is virtually unchanged but the computational complexity is higher as the parameter values are not dyadic integers. The value of α_3 cannot be independently chosen and will be a non-dyadic integer in general. The implementation of the corresponding rotation matrix \mathbf{R}_3 will be discussed in Section 2.3.3.

Choice of dependent parameter: In the example above α_3 is chosen as the dependent parameter (i.e. $i = 3$ in (2.12)). However the procedure could also be applied with α_1 or α_2 as the dependent parameter. If the deviation of the independent parameters (from the original irrational values) are kept small by using the bounds described above, the characteristics and performance of the filter will be approximately the same irrespective of the choice of the dependent parameter (and this has been observed in the examples). However the complexity in terms of the number of SPT will (in general) depend of the choice of the dependent parameter. Therefore the procedure should be repeated with all possible choices of dependent parameter. The choice which gives the smallest number of SPT terms will be chosen as the final solution. For the example above it turns out that the best choice is with α_3 as the dependent parameter.

Example II: The Daubechies length 8 ($L = 4$) filter (Db8) has four lattice parameters: $\alpha_1, \alpha_2, \alpha_3$ and α_4 . The irrational values of α_1, α_2 and α_3 are quantised. The value of α_4 expressed in terms of other lattice parameters is given by

$$\alpha_4 = \frac{-1 - \alpha_1 - \alpha_2 + \alpha_1\alpha_2 - \alpha_3 + \alpha_1\alpha_3 + \alpha_2\alpha_3 + \alpha_1\alpha_2\alpha_3}{1 - \alpha_1 - \alpha_2 - \alpha_1\alpha_2 - \alpha_3 - \alpha_1\alpha_3 - \alpha_2\alpha_3 + \alpha_1\alpha_2\alpha_3}$$

There are many potential choices for α_1, α_2 and α_3 but a simple dyadic value of lattice parameters (chosen close to irrational values) will lead to multiplierless implementation. The original irrational and quantized rational values of the lattice parameters for Db8 filter are given in Table 2.1. The frequency response of the original and rational filters are shown in Figure 2.3.

Table 2.1: Rational lattice parameters of the Db6 and Db8 filters. Sobolev Regularity s_c also shown.

	Db6			Db8		
	Irrational	1 VM	2VM	Irrational	1 VM	2VM
α_1	-2.4255	-9/4	-73/32	-3.1029	-3	-3
α_2	0.5461	1 / 2	1 / 2	0.8109	3/4	25/32
α_3	-0.1059	-3 / 31	-23/251	-0.2593	-1/4	-1/4
α_4	-	-	-	0.0460	3/46	1/22
d	-	4	8	-	5	5
$Q(\tilde{K})$	-	13/64	3/8	-	11/64	3/8
Δ_H	1.4142	1.5393	1.4541	1.4142	1.4267	1.5097
SPT	-	10	12	-	13	12
s_c	1.415	0.995	1.409	1.775	0.961	1.781

The generic procedure to determine the suitable values for lattice parameters (α_l) for $2L$ length filter is as follows:

1. Determine the maximum deviation from the original irrational values for $(\alpha_1, \alpha_2, \dots, \alpha_L) \setminus (\alpha_{i_1})$ subject to the constraint $\int |H_0(e^{j\omega}) - H_0^O(e^{j\omega})|^2 d\omega < \epsilon$ (allowable level of deviation). This gives the allowable range $(\alpha_k^{min}, \alpha_k^{max})$ ($k = 1, 2, \dots, L - 1$)/ α_{i_1} of each lattice values.
2. Over the allowable range determine the dyadic value that gives the lowest number of SPT terms.
3. The procedure is repeated for all possible choices of α_{i_1}

2.3.2 Two Vanishing Moments

The approach is best illustrated with a simple example and can be generalized for any filter.

Example III: The Daubechies length 6 filter coefficients in terms of the lattice parameters are given in (2.14). In order to ensure two vanishing moments, both the first and second sum rules are used. The first sum rule is given in (2.15). Applying the second sum rule on filter coefficients in (2.14) gives

$$3 + 2\alpha_1 - \alpha_1\alpha_2 - 2\alpha_3 + \alpha_1\alpha_3 - \alpha_2\alpha_3 = 0 \quad (2.17)$$

Equations (2.15) and (2.17) form an underdetermined system and therefore have many

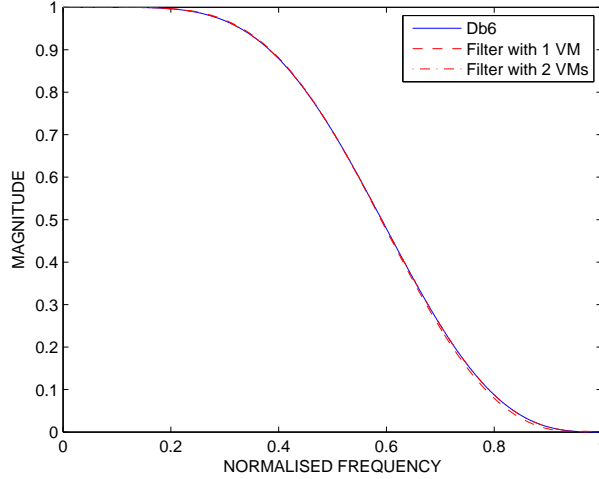


Figure 2.2: Frequency response of original and rationalized Daubechies length 6 filter

solutions. There may be rational solutions but it is hard to find these rational solutions. Furthermore these solutions may not give good quality filters anyway if their values are very different from the original irrational values. We adopt a different approach for finding a good approximate solution that is rational. Suppose the α_2 parameter is fixed at a rational value that is close to the original irrational value of 0.5461 (Refer Table 2.1). The simple value $\alpha_2 = 1/2$ (only one SPT term) is chosen here but other rational values can potentially be used. Using $\alpha_2 = 1/2$ in (2.15) and (2.17) gives

$$\alpha_1 + \alpha_3 - 3\alpha_1\alpha_3 + 3 = 0 \quad (2.18)$$

$$3\alpha_1 - 5\alpha_3 + 2\alpha_1\alpha_3 + 6 = 0 \quad (2.19)$$

Solving (2.18) and (2.19) gives two sets of irrational values for α_1 and α_3 . The solution $\alpha_1 = -2.28869$, $\alpha_3 = -0.090428$ is closest to the original values. The approach we adopt is to find a rational solution which approximates the second sum rule (eqn. (2.19)) but satisfies the first sum rule (eqn. (2.18)) exactly. The equation (2.18) can be solved for α_3 and is given as

$$\alpha_3 = \frac{3 + \alpha_1}{3\alpha_1 - 1} \quad (2.20)$$

Define the approximation error E to the second sum rule (2.19) as

$$E \equiv 3\alpha_1 - 5\alpha_3 + 2\alpha_1\alpha_3 + 6 \quad (2.21)$$

The goal then is to find the rational values α_1 and α_3 that are (i) close to the irrational

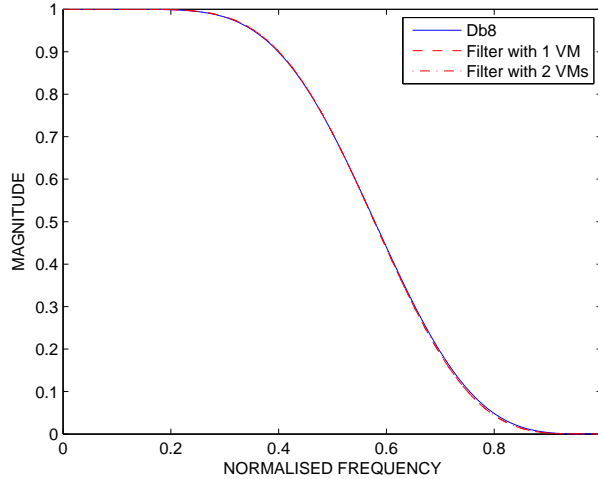


Figure 2.3: Frequency response of original and rationalized Daubechies length 8 filter

values $\alpha_1 = -2.28869$, $\alpha_3 = -0.090428$; (ii) satisfy (2.18) exactly and (iii) minimise the error E . A reasonably large set of dyadic values for α_1 that are close to the irrational value are used in the search procedure. For each α_1 value in the dyadic set, the α_3 (which will be rational) is obtained using (2.20) and the approximation error (2.21) is evaluated. The α_1 and α_3 values that give the minimum E are $\alpha_1 = -73/32$ and $\alpha_3 = -23/251$ which is chosen as the final solution. The corresponding second derivative value ($H^{(2)}(e^{j\pi})$) is 5.8×10^{-3} (close to zero). The frequency response of the modified filter with two approximate vanishing moments is close to the original irrational filter's response as shown in Figure 2.2. The choice dependent parameter shown above gives the filter with the lowest number of SPT. The Sobolev regularity of rational Db6 filter with one VM and (approximate) two VM are 0.9765 and 1.4086 respectively. Even though the second sum rule is only approximated, the Sobolev regularity has increased compared to the case with one (exact) vanishing moment.

The technique is then applied to the Daubechies length 8 filter. The quantized lattice parameters for the one and two vanishing moments cases are given in Table 2.1. The frequency response of rational Db8 filter with approximate second VMs is close to the original irrational filter's response as shown in the Figure 2.3.

For a general L stage lattice with parameters $(\alpha_1, \alpha_2, \dots, \alpha_L)$, the procedure can be summarised as follows.

1. Choose (fix) simple dyadic values for $L - 2$ parameters $(\alpha_1, \alpha_2, \dots, \alpha_L) \setminus (\alpha_{i_1}, \alpha_{i_2})$. (Note that general rational values can also be used but this would result in a more

- complex implementation).
2. Applying the first sum rule (with $(L - 2)$ parameters already chosen) will result in a multilinear equation $f_1(\alpha_{i_1}, \alpha_{i_2}) = 0$ in the remaining two parameters.
 3. Applying the second sum rule will result in another multilinear equation $f_2(\alpha_{i_1}, \alpha_{i_2}) = 0$. Now define the approximation error as $E \equiv f_2(\alpha_{i_1}, \alpha_{i_2})$.
 4. Generate a sufficiently large set of dyadic values for the lattice parameter α_{i_1} which are close to the original irrational value. For each value in the set obtain the α_{i_2} parameter value by solving the equation $f_1(\alpha_{i_1}, \alpha_{i_2}) = 0$. i.e. $\alpha_{i_2} = \hat{f}_1(\alpha_{i_1})$. (The set can be general rational values but this would result in a more complex implementation).
 5. Compute the approximation error E for each set of α_{i_1} and α_{i_2} values and choose the set which gives the least E as the final solution.

The procedure is repeated for all possible choices of $(\alpha_{i_1}, \alpha_{i_2})$.

2.3.3 Efficient Implementation

The rational orthogonal filters can be efficiently implemented using the lattice structure as shown in Figure 2.4.

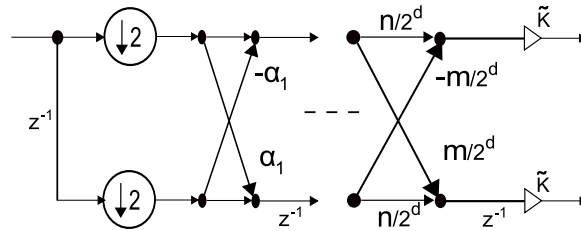


Figure 2.4: Lattice structure implementation

The un-normalized rotation matrices \mathbf{R}_l can be implemented without the use of multipliers if the corresponding lattice parameter α_l is a dyadic integer (i.e. $\gamma/2^e$). With the rationalization technique presented above there is direct control over the choice of the value of almost all the lattice parameters $(\alpha_1, \dots, \alpha_{L-1})$ except one (α_L). In all the examples presented, the lattice parameters $\alpha_1, \dots, \alpha_{L-1}$ are dyadic integers and therefore the corresponding rotation matrix can be implemented without multipliers. The last parameter $\alpha_L = m/n$ (m and n integers) in general is non-dyadic as its value cannot be

directly controlled. The corresponding un-normalized rotation matrix can be expressed as:

$$\begin{aligned} \mathbf{R}_L &= \begin{bmatrix} 1 & -m/n \\ m/n & 1 \end{bmatrix} \\ &= \frac{1}{n} \begin{bmatrix} n & -m \\ m & n \end{bmatrix} = \frac{2^d}{n} \begin{bmatrix} n/2^d & -m/2^d \\ m/2^d & n/2^d \end{bmatrix} \end{aligned}$$

where d is a suitable integer. The matrix $\begin{bmatrix} n & -m \\ m & n \end{bmatrix}$ can be multiplierlessly implemented if m and n are expressed as SPT. The scaling factor 2^d can be applied to decrease the dynamic range for larger values of m and n . Then the modified rotation matrix $\tilde{\mathbf{R}}_L \equiv \begin{bmatrix} n/2^d & -m/2^d \\ m/2^d & n/2^d \end{bmatrix}$ can be implemented without any multipliers. The scaling factor $\frac{2^d}{n}$ can be absorbed into K in (2.6) to give the modified normalisation constant

$$\tilde{K} \equiv \frac{2^d}{n} \prod_{l=1}^L \frac{1}{\sqrt{(1 + \alpha_l^2)}}$$

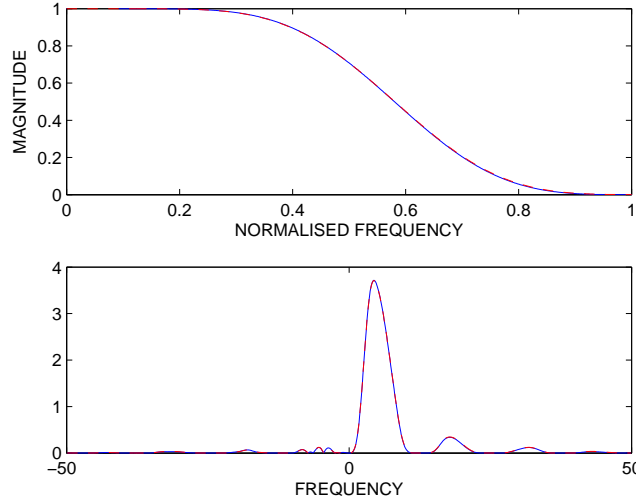
The normalisation constant \tilde{K} can be multiplierlessly implemented if it is quantized to the nearest dyadic integer ($\gamma/2^c$). The entire filter bank can therefore be implemented without any multipliers. However the DC gain of the low-pass filter Δ_H will only be approximately $\sqrt{2}$ due to the quantization of \tilde{K} .

2.3.4 Rationalizing Dual-Tree Orthogonal Filters

Example IV: The symmetric self Hilbertian filter [15] of length 8 (with three VMs) is rationalized. The unquantized and quantized lattice parameters values are shown in Table 2.2 for the one and two VMs cases. The Sobolev regularity of the rational symmetric self Hilbertian filter (length 8) with one VM and (approximate) two VMs are 1.0 and 1.7175 respectively. The frequency response of the modified filter is virtually same as the irrational filter as shown in Figure 2.5 (top). The spectra of the complex wavelet from the original irrational and rational filter (with one VM) is shown in Figure 2.5 (bottom). The analytic quality measures of the irrational filter are $E_1 = 3.2088\%$ and $E_2 = 0.0889\%$. The corresponding measures of the rational filter with one VM are $E_1 = 3.3416\%$ and $E_2 = 0.0879\%$. The corresponding measures of the rational filter with two (approximate) VMs are $E_1 = 3.4387\%$ and $E_2 = 0.0845\%$. The second derivative value of this filter ($H^{(2)}(e^{j\pi})$) is 2.9×10^{-3} (close to zero).

Table 2.2: Original and quantized lattice parameters values of length 8 symmetric self Hilbertian filter.

	α_1	α_2	α_3	α_4	d	$Q(\tilde{K})$	Δ_H	SPT
Irrational	0.0633	9.1856	0.6425	0.2656	-	-	1.4142	-
Rational 1 VM	3/64	37/4	1552/2335	17/64	10	5/128	1.4577	16
Rational 2 VMs	125/1793	561/64	41/64	17/64	10	7/128	1.4716	17


Figure 2.5: Spectrum of complex wavelet in example IV. Solid line : original filter. Dotted line: rational filter

2.4 Rationalizing Biorthogonal Filters

The rationalization method proposed here is quite general and can be applied to almost any filter pair. It is based on the idea of complementary filters: a low-pass filter $\widehat{F}_0(z)$ is said to be complementary to a given analysis low-pass filter $\widehat{H}_0(z)$ if the pair $(\widehat{H}_0(z), \widehat{F}_0(z))$ satisfy the perfect reconstruction (PR) condition (2.1). The complementary filter technique allows one set of filter coefficients to be expressed in terms of another set of filter coefficients.

Consider the case with linear phase filters which is the most common. The original irrational coefficient low-pass filters $\widehat{H}_0(z)$ whose length is L_H and $\widehat{F}_0(z)$ whose length is L_F can be expressed as

$$\begin{aligned}\widehat{H}_0(z) &= \widehat{K}_1(z+1)^n \widehat{R}_1(z) \\ \widehat{F}_0(z) &= \widehat{K}_2(z+1)^m \widehat{R}_2(z)\end{aligned}$$

where

$$\begin{aligned}\widehat{R}_1(z) &= (z^i + \widehat{a}_1 z^{i-1} + \widehat{a}_2 z^{i-2} + \dots + \widehat{a}_1 z + 1) \\ \widehat{R}_2(z) &= (z^{\widehat{j}} + \widehat{b}_1 z^{\widehat{j}-1} + \widehat{b}_2 z^{\widehat{j}-2} + \dots + \widehat{b}_1 z + 1)\end{aligned}$$

are symmetric polynomials (linear phase) with degrees i and \widehat{j} respectively. Now n and m are the number of vanishing moments of $\widehat{H}_0(z)$ and $\widehat{F}_0(z)$ respectively, $L_H = n + i + 1$ and $L_F = m + \widehat{j} + 1$, \widehat{K}_1 and \widehat{K}_2 are normalisation constants. The coefficients $\widehat{a}_1, \widehat{a}_2, \dots$ and $\widehat{b}_1, \widehat{b}_2, \dots$ are irrational in general. Without loss of generality assume $\widehat{H}_0(z)$ to be the shorter length filter and $\widehat{F}_0(z)$ to be the longer length filter, i.e. $L_F > L_H$. It is assumed that the PR condition (2.1) is satisfied for the product filter $\widehat{P}(z) = \widehat{H}_0(z)\widehat{F}_0(z)$.

Consider now the modified filters which are defined as

$$\begin{aligned}H_0(z) &= K_1(z+1)^n R_1(z) \\ F_0(z) &= K_2(z+1)^{m-\widehat{m}} R_2(z)\end{aligned}$$

where \widehat{m} ($< m$) is the number of vanishing moments that is reduced in the longer filter and

$$\begin{aligned}R_1(z) &= (z^i + a_1 z^{i-1} + a_2 z^{i-2} + \dots + a_1 z + 1) \\ R_2(z) &= (z^j + c_1 z^{j-1} + c_2 z^{j-2} + \dots + c_1 z + 1)\end{aligned}$$

are symmetric polynomials with degrees i and $j = \widehat{j} + \widehat{m}$ respectively such that H_0 (F_0) and \widehat{H}_0 (\widehat{F}_0) have the same length. The modified product filter is given by

$$P(z) = K_1 K_2 (z+1)^{n+m-\widehat{m}} R_1(z) R_2(z)$$

where K_1, K_2 are normalisation constants. The length of the product filter $P(z)$ is $L_P = L_H + L_F - 1$. For the PR condition (2.1) to be satisfied, we need $p(2n) = 0$ for $n \neq 0$. Only half of the $p(2n) = 0$ equations need to be considered because of symmetry (i.e. $p(2n) = p(-2n)$). There are then $q = (L_P - 3)/4$ number of independent equations. Now $p(2n)$ is a linear function in $\{c_1, c_2, \dots\}$ if $\{a_1, a_2, \dots\}$ is fixed. If $\{a_1, a_2, \dots\}$ has rational values, then $p(2n) = 0$ is a linear equation in $\{c_1, c_2, \dots\}$ with *rational coefficients*. If we choose the number of vanishing moments that is reduced to be $\widehat{m} = 2q - j$, then the number of unknowns $\{c_1, c_2, \dots, c_q\}$ is equal to q , which is the same as the number of linear equations. Solving this determined system of linear

equations with $\{c_1, c_2, \dots, c_q\}$ as unknowns will yield a unique rational valued solution.

Remark: It is important to point out that the key to ensuring the method is applicable to almost any biorthogonal pair is that the reduction of the VMs occurs only in one filter (F_0) and not the other (H_0). If the reduction occurs in both filters the solution to a system of nonlinear equations will be required. Not only will solving nonlinear equation be difficult in general, it is generally impossible to ensure rational valued solutions.

2.4.1 Choice of parameter values

Two factors need to be taken into account when deciding the choice of parameter values. Firstly the rationalized parameters values for $\{a_1, a_2, \dots\}$ should be close to the original irrational values to ensure the characteristics (and performance) of the filters do not deviate significantly. Secondly the choice of parameter values will effect the computational complexity of the filters in terms of the number of SPT terms. The cascade form implementation, consisting of the VM part $((1+z)^n)$ and the remainder part ($R_1(z)$), of the filters will be considered here. The coefficients of the VM part is always dyadic and can be implemented efficiently in hardware. For example if the filter has 4 VMs then the VM part will be $[1, 4, 6, 4, 1]/2^4$ which requires 6 SPT terms. Now the computational complexity of the filter $H_0(z)$ can be easily controlled by choosing simple rational numbers for $\{a_1, a_2, \dots\}$. However there is no direct control over the complexity of filter coefficients $\{c_1, c_2, \dots, c_q\}$ of the filter $F_0(z)$. The control of $\{c_1, c_2, \dots, c_q\}$ is indirect through $\{a_1, a_2, \dots\}$. The strategy adopted here is to choose rational values for $\{a_1, a_2, \dots\}$ such that the overall complexity of the filter bank (as measured by the number of SPT terms) is the lowest. The rationalization procedure for the parameters $\{a_1, a_2, \dots\}$ is then as follows:

1. Bounds for the $\{a_1, a_2, \dots\}$ values are determined by imposing the constraint $\int |\tilde{H}_0(e^{j\omega}) - H_0(e^{j\omega})|^2 d\omega < \epsilon$ where ϵ specifies the allowable level of deviation from the original irrational filter. The bounds then determine the search set.
2. Create a sufficiently large subset of rational values for $\{a_1, a_2, \dots\}$ from the search set.
3. For each $\{a_1, a_2, \dots\}$ in the subset, solve the linear equations for the $\{c_1, c_2, \dots, c_q\}$ values. Then determine the total number of SPT terms. The parameter values which give the lowest number SPT terms is chosen as final solution.

2.4.2 The 9/11 Filter Pair

The 9/11 filter pair from [34] is obtained from factorising the length 19 Lagrange-Halfband-Filter. The original filters \widehat{H}_0 and \widehat{F}_0 have four and six vanishing moments (VM) respectively. The modified filters H_0 and F_0 (without the normalisation factors) are given by

$$\begin{aligned} H_0(z) &= (z+1)^4(z^4 + a_1z^3 + a_2z^2 + a_1 + 1) \\ F_0(z) &= (z+1)^2(z^8 + c_1z^7 + c_2z^6 + c_3z^5 + c_4z^4 + \\ &\quad c_3z^3 + c_2z^2 + c_1z + 1) \end{aligned}$$

and have four and two vanishing moments (VM) respectively. Here we have reduced four vanishing moments in F_0 since imposing the PR condition on the product filter $P(z)$ yields four equations ($q = 4$). Solving the four equations for $\{c_1, \dots, c_4\}$ gives the solution:

$$\begin{aligned} c_1 &= -6 - a_1 \\ c_2 &= ((4096 + 192a_1^4 + 4a_1^3(346 + 35a_2) + 12a_1^2(340 + 48a_2 + 3a_2^2) \\ &\quad + a_1(6120 + 628a_2 + 70a_2^2 + 3a_2^3))/S \\ c_3 &= -(6656 + 480a_1^4 + a_1^3(2836 + 438a_2) + a_1^2(7364 + 1396a_2 + 149a_2^2) \\ &\quad + 6a_1(1716 + 212a_2 + 35a_2^2 + 3a_2^3))/S \\ c_4 &= 2((3840 + 320a_1^4 + 4a_1^3(434 + 83a_2) + 6a_1^2(718 + 157a_2 + 22a_2^2) \\ &\quad + a_1(5940 + 788a_2 + 163a_2^2 + 19a_2^3))/S \end{aligned}$$

where

$$S = 256 + 32a_1^3 + 6a_1^2(26 + 3a_2) + a_1(308 + 32a_2 + 3a_2^2)$$

It can be seen that if $\{a_1, a_2\}$ are rational valued, then $\{c_1, c_2, c_3, c_4\}$ and the resulting filter coefficients will also be rational valued. The original irrational values are $\widehat{a}_1 = -3.7997$ and $\widehat{a}_2 = 7.8266$. The rational values of $a_1 = -31/8$ and $a_2 = 8$ are chosen based on the criteria explained in the section 2.4.1 and their normalized (to unity DC) frequency response is shown in Figure 2.6. The response of the modified pair is very similar to the original pair's response. The rationalized coefficients of the remainder part of the filters are shown in Table 2.3. The coefficients are normalised by $1/2^c$ so that the DC gain of the remainder section is as close to unity as possible. The number of SPT terms required to implement the remainder section of H_0 and F_0 are 4 and 39

Table 2.3: Rational coefficient values of remainder part of biorthogonal filter pairs (origin is the leftmost coefficient, coefficient for negative indices follow by symmetry)

9/11	R_1	$[64, -31, 8]/2^4$
	R_2	$[9158, 3438, -2626, -697, 328]/2^{13}$
13/11	R_1	$[-7522, -2111, 2000, -271, -575, 230]/2^{13}$
	R_2	$[21, -11, 2]/2$
17/11	R_1	$[2389304, 1234566, -259427, -229548, 147522, 37448, -51613, -5666, 5666]/2^{22}$
	R_2	$[104, 57, -6, -11, 2, 2]/2^8$

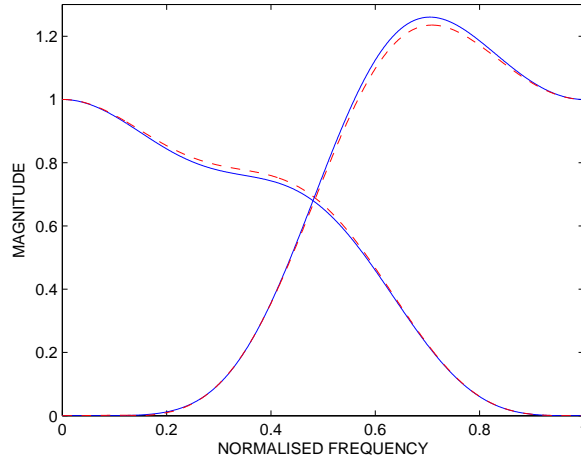


Figure 2.6: Plot of frequency response of the “9/11” filter pair, solid line: original filters. Dotted line: rational coefficients filter with $a_1 = -31/8$ and $a_2 = 8$

respectively. The DC gain of H_0 and F_0 are $\Delta_H = 1.406$ and $\Delta_F = 1.456$ if the gain factor of $5/2^2$ (2 SPT terms) and $19/2^4$ (3 SPT terms) are applied respectively.

The coding gain for the original pair and modified pair are 9.643 and 9.709 respectively. The Sobolev regularity of \widehat{H}_0 and H_0 are 1.662 and 1.642 respectively. The Sobolev regularity of \widehat{F}_0 and F_0 are 2.531 and 1.934 respectively. The decrease of regularity in F_0 (compared with \widehat{F}_0) is due mainly to the reduction in the number of VMs (from six to two).

2.4.3 The 13/11 Filter Pair

The 13/11 filter pair from [34] is obtained from factorising the length 23 Lagrange-Halfband-Filter. The original filters \widehat{H}_0 and \widehat{F}_0 have six VMs each. The modified filters

H_0 and F_0 (without the normalisation factors) are given by

$$\begin{aligned} H_0 &= (z+1)^2(z^{10} + c_1z^9 + c_2z^8 + c_3z^7 + c_4z^6 + \\ &\quad c_5z^5 + c_4z^4 + c_3z^3 + c_2z^2 + c_1z + 1) \\ F_0 &= (z+1)^6(z^4 + a_1z^3 + a_2z^2 + a_1 + 1) \end{aligned}$$

and have two and six vanishing moments (VM) respectively.

Here we have reduced four vanishing moments in \widehat{H}_0 since imposing the PR condition on the product filter $P(z)$ yields five equations ($q = 5$). The five equations can be solved for $\{c_1, \dots, c_5\}$ in terms of a_1 and a_2 . The original irrational values are $\widehat{a}_1 = -5.5563$ and $\widehat{a}_2 = 10.6707$. The rational values of $a_1 = -11/2$ and $a_2 = 21/2$ are chosen based on the criteria explained in the section 2.4.1 and their normalized (to unity DC) frequency response is shown in Figure 2.7. The response of the modified pair is very similar to the original pair's response. The rationalized coefficients of the remainder part of the filters are shown in Table 2.3. The coefficients are normalised by $1/2^c$ so that the DC gain of the remainder section is as close to unity as possible. The number of SPT terms required to implement the remainder section of H_0 and F_0 are 21 and 7 respectively. The DC gain of H_0 and F_0 are $\Delta_H = 1.369$ and $\Delta_F = 1.406$ if the gain factor of $5/2^2$ (2 SPT terms) and $15/2^4$ (2 SPT terms) are applied respectively.

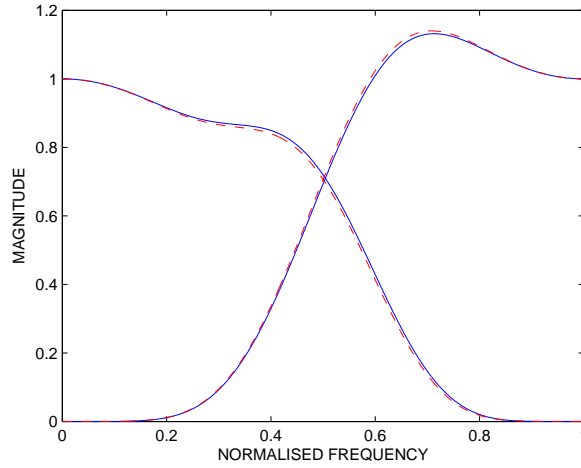


Figure 2.7: Plot of frequency response of the “13/11” filter pair, solid line: original filters. Dotted line: rational coefficients filter with $a_1 = -11/2$ and $a_2 = 21/2$

The coding gain for the original pair and modified pair are 9.818 and 9.816 respectively (almost the same). The Sobolev regularity of \widehat{H}_0 and H_0 are 2.126 and 1.991 respectively.

The Sobolev regularity of \widehat{F}_0 and F_0 are 2.638 and 2.607 respectively. The decrease of regularity in H_0 (compared with \widehat{H}_0) is due mainly to the reduction in the number of VMs (from six to two).

2.4.4 The 17/11 Filter Pair

The 17/11 filter pair from [34] is obtained from factorising the length 27 Lagrange-Halfband-Filter. The original filters \widehat{H}_0 and \widehat{F}_0 have eight and six vanishing moments (VM) respectively. The modified filters H_0 and F_0 (without the normalisation factors) are given by

$$\begin{aligned}\widehat{H}_0 &= (z+1)^4(z^{12} + c_1z^{10} + c_2z^9 + c_3z^8 + c_4z^7 + \\ &\quad c_5z^6 + c_6z^5 + c_4z^4 + c_3z^3 + c_2z^2 + c_1z + 1) \\ \widehat{F}_0 &= (z+1)^6(z^4 + \widehat{a}_1z^3 + \widehat{a}_2z^2 + \widehat{a}_1 + 1)\end{aligned}$$

and have four and six vanishing moments (VM) respectively.

Here we have reduced four vanishing moments in \widehat{H}_0 since imposing the PR condition on the product filter $P(z)$ yields six equations ($q = 6$). The six equations can be solved for $\{c_1, \dots, c_6\}$ in terms of a_1 and a_2 . The original irrational values are $\widehat{a}_1 = -4.9971$ and $\widehat{a}_2 = 9.5260$. The rational values of $a_1 = -5$ and $a_2 = 19/2$ are chosen based on the criteria explained in the section 2.4.1 and their normalized (to unity DC) frequency response is shown in Figure 2.8. The response of the modified pair is very similar to the original pair's response. The rationalized coefficients of the remainder part of the filters are shown in Table 2.3. The coefficients are normalised by $1/2^c$ so that the DC gain of the remainder section is as close to unity as possible. The number of SPT terms required to implement the remainder section of H_0 and F_0 are 57 and 13 respectively. The DC gain of H_0 and F_0 are $\Delta_H = 1.421$ and $\Delta_F = 1.406$ if the gain factor of $23/2^4$ (3 SPT terms) and $15/2^3$ (2 SPT terms) are applied respectively.

The coding gain for the original pair and modified pair are 9.922 and 9.911 respectively (almost the same). The Sobolev regularity of \widehat{H}_0 and H_0 are 2.4984 and 2.630 respectively. The Sobolev regularity of \widehat{F}_0 and F_0 are 2.794 and 2.762 respectively. The decrease of regularity in H_0 (compared with \widehat{H}_0) is due mainly to the reduction in the number of VMs (from eight to four). The frequency response of the product filter for the rationalized pair is close to the original product filter.

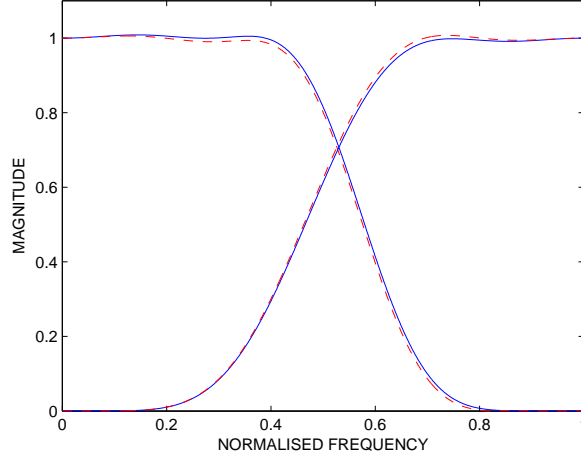


Figure 2.8: Plot of frequency response of the “17/11” filter pair, solid line: original filters. Dotted line: rational coefficients filter with $a_1 = -11/2$ and $a_2 = 21/2$

2.4.5 Selesnick 8/12 Dual-Tree Filter Pair

The Selesnick 8/12 biorthogonal filter pair [14] have approximate linear phase and is used in the DTCWT. The filters in the tree g are time reversed version of filters in the tree h . The analysis low pass filter H_0^h and synthesis low pass filter F_0^h of tree h are rationalized here. Both H_0^h (length 8) and F_0^h (length 12) have three VMs each. The modified filters \widehat{H}_0^h and \widehat{F}_0^h (without the normalization factors) are given by

$$\widehat{H}_0^h(z) = (1 + z^{-1})^3 \left(1 + \sum_{k=1}^4 \widehat{a}_k z^{-k} \right)$$

$$\widehat{F}_0^h(z) = (1 + z^{-1})^3 \left(1 + \sum_{k=1}^8 c_k z^{-k} \right)$$

For the PR condition (2.1) to be satisfied, we need $\widehat{p}(2n) = 0$ for $n \neq 0$. Since the filters have non-linear phase, $\widehat{p}(2n) \neq \widehat{p}(-2n)$ (non-symmetric), the number of equations resulting is $q = (\widehat{n} - 3)/2 = 8$ (double the number of the linear phase case). The coefficients $\{\widehat{a}_1, \dots, \widehat{a}_4\}$ are considered as knowns and the coefficients $\{c_1, c_2, \dots, c_8\}$ are considered as unknowns. Since the number of unknown coefficients is equal to the number of equations no reduction in VMs is needed. This results in a determined system of eight equations with eight unknowns $\{c_1, c_2, \dots, c_8\}$. The solution is therefore unique and has *rational* values if $\{\widehat{a}_1, \dots, \widehat{a}_4\}$ are rational valued. The original irrational values are $a_1 = -1.6025$, $a_2 = -6.0050$, $a_3 = 1.2795$ and $a_4 = 0.2$. With the rational

values of $\widehat{a}_1 = -8/5$, $\widehat{a}_2 = -6$, $\widehat{a}_3 = 5/4$ and $\widehat{a}_4 = 1/5$ the rational filter coefficients are given in Table 2.4.

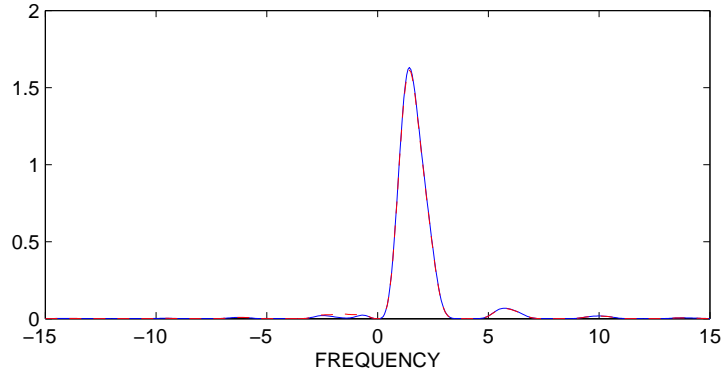


Figure 2.9: Spectrum of complex wavelet. Solid line: original filter. Dotted line: rational filter

The Sobolev regularity of H_0^h and \widehat{H}_0^h are 2.180 and 2.189 respectively. The Sobolev regularity of F_0^h and \widehat{F}_0^h are 1.041 and 1.022 respectively. Since there is no VM reduction in the original and modified filters, the Sobolev regularity remains the same for both the filters. The spectra of the complex wavelet from the original irrational and modified filters is shown in Figure 2.9. The E_1 and E_2 measures from the rational (irrational) filters are 1.8429% (1.3969%) and 0.0691% (0.0259%) respectively.

Table 2.4: Selesnick 8/12 filter coefficients

n	$\widehat{H}_0^h(n)$	$\widehat{F}_0^h(n)$
0	20	6408449151620
1	28	-8971828812268
2	-156	-530289130918556
3	-411	804118148616079
4	-313	1114311581636023
5	-33	-6315191475273163
6	37	-9230516768524775
7	4	-1711878875277323
8	-	1531732338320909
9	-	-159801949594225
10	-	-255726357322597
11	-	27646092683524

2.5 Discussion and Comparisons

The perfect reconstruction (PR) is imposed structurally in lattice and lifting structures and therefore obtaining rational coefficients is easy but imposing vanishing moment (VM) is hard. With the factorization of product filter framework imposing VM is easy, but because factorization is needed, rational coefficients are difficult to achieve. With orthogonal filters, the factorization is spectral and it is generally impossible to ensure the spectral factor has rational coefficients even though the product filter has rational coefficients. This is however not the case with biorthogonal filters as the factorization is less restrictive.

The framework based on lattice (presented in the Section 2.2.2.2) is therefore the only approach that is general for rational coefficients orthogonal filters. There are no simple constraint equations to ensure an arbitrary number of VMs with lattice structures. The constraint for one VM is [2]:

$$\sum_l \theta_l = \pi/4 \pm k\pi \quad (2.22)$$

where θ_l are the angles of the lattice parameters $\alpha_l = \tan \theta_l$ in (2.5). This constraint is augmented with another constraint on the angles for two VMs [53]. Beyond two VMs there is no reported work. Consider now the simple case of one VM. The constraint (2.22) is in terms of the angles but the coefficients however depend on the tangent of the angle, i.e. $\tan \theta_l$. For rational coefficients $\tan \theta_l$ needs to be rational valued but there is no simple way of choosing the angles that will satisfy (2.22) exactly and yield rational tangent values. Constraint (2.22) was considered by Abbas *et. al.* [40] in the construction of orthogonal filters. However (2.22) was only approximately satisfied for the filters in [40], i.e. the one VM is only approximate and the zero is only in the vicinity of (and not exactly at) $z = -1$. The orthogonal filters in [40] therefore have some DC leakage which was minimized via numerical optimization. The orthogonal filters presented here however have a zero exactly at $z = -1$ (one VM) and therefore no DC leakage. Furthermore some of the filters presented here (using the numerical procedure presented in section 2.3.2) have an approximate second VM. Our rationalization method abandons the use of the angles as the parameters and instead works directly with the tangent values. If the lifting factorization (another possible polyphase structure) is used on the orthogonal filters and the parameters of the lifting steps are quantized independently, PR is preserved but the filters are no longer orthogonal, i.e. biorthogonal in general. Orthogonality however is still preserved by independent quantization of the lattice parameters, i.e. structural orthogonality.

Regensburger [54],[55] proposed a framework that parameterize orthogonal filters based on discrete moments. Regensburger *et. al.* [54] designed the rational valued Daubechies length 4 filter having one vanishing moments and showed that it is not possible to have rational coefficient for a length 4 filter with two vanishing moments. The design framework in [54] expresses filter coefficients in terms of discrete moment but the filter coefficients have non-linear relationship with the discrete moments. For some value of discrete moments, we can get rational valued filter coefficients but the frequency response of those filters do not have the low pass characteristics. Even though Rogensburger’s framework have PR and VMs imposition, it is not viable to rationalise the Daubechies family of orthogonal filters. However, it is easy to generate orthogonal filters having different discrete moments [54],[43]. The other framework proposed by Elena *et. al.* [56] is not suitable for rationalizing the orthogonal filters as well.

For biorthogonal filters, Abbas *et. al.* [40] use the lifting structures (polyphase framework) which has structural PR but no VM in general except for simple cases with short filters. Even with simple cases it is difficult in general to impose more than one VM with lifting. The method presented here is general and applicable to almost any filter pair as long as there are enough VMs in F_0 (longer filter). Furthermore high VM can be easily achieved.

In [5], Kotteri *et al.* obtained rational biorthogonal filters using the zero compensation method. Only the “9/7” pair was considered in [5] but the method could potentially be used for other biorthogonal pairs. All VMs are preserved for the filters in [5]. However, even though it is stated in [5] that the PR requirement is used to guide the rationalization process, a careful study of the method will reveal that the PR condition (2.1) is only approximated. In [6], all VMs are preserved but the PR condition (2.1) is only approximated for the “9/7” filter. In our method the PR condition (2.1) is exactly satisfied. The sacrifice is the reduction of VMs in the longer filter. No sacrifice is needed however for the shorter filter. There is still a sufficient number of VMs to ensure that the regularity is not reduced substantially. The coding gain and other filter characteristics are almost similar to that of the original irrational coefficients filter.

The idea of reducing the number of VMs is similar to the work in [57] but there are fundamental differences. In [57] only a minimum reduction of two VMs is considered and the method does not generalize for an arbitrary biorthogonal pair. Closed form algebraic solution for the coefficients were obtained for the ‘9/7’ and ‘6/10’ pairs, the latter however being a simple variant (through re-factorization) of the former. For the ‘9/11’ pair closed form solution was not possible as the equations are nonlinear and

the rational solution obtained in [57] serendipitously turned out to be a good solution. The rationalization method proposed here ensures the equations to be solved are always linear and this allows the method to be generic. As explained earlier the key to ensuring linear equations is that the reduction of the VMs occurs only in one filter (F_0) and not the other (H_0).

Finally consider the class of polyphase structures in [58],[59] which can be used for either orthogonal and biorthogonal filter banks. Conditions for one and two VMs were derived in [58],[59] for these structures and is quite simple for the one VM case. Rational coefficients filter banks were designed in [60] using these structures. However these structures are meant for cases when the number of channels M is even and $M \geq 4$. A trivial class of filters consisting of two non-zero coefficients are obtained if the formulas in [58],[59] are used with $M = 2$ for the orthogonal case. The structures in [58],[59] therefore cannot be used to rationalize the 2-channel orthogonal filters considered in this work.

2.6 Conclusion

This chapter has presented techniques to rationalize orthogonal and biorthogonal filter banks with perfect reconstruction preserved. It is much harder to preserve vanishing moments (VM) for orthogonal filters than for biorthogonal filters. Our technique has been able to preserve at least one VM for orthogonal filters and achieve an approximate second VM. An efficient way to implement the rational orthogonal filter coefficient based on lattice structure is also presented. For biorthogonal filters most of the VMs are preserved. The techniques are simple yet general enough to be applied to almost any filter bank. The examples presented show that the rationalized filters have characteristics and performance measures that are close to the original irrational filters.

3 Design of Almost Symmetric Orthogonal Wavelet Filter Bank via Direct Optimisation

It is a well known fact that (compact support) dyadic wavelets (based on the two channel filter banks) cannot be simultaneously orthogonal and symmetric. Even though orthogonal wavelets have the energy preservation property, biorthogonal wavelets are preferred in image processing applications because of their symmetric property. In this chapter a novel method is presented for the design of almost symmetric orthogonal wavelet filter bank. Orthogonality is structurally imposed by using the unnormalised lattice structure and this leads to an objective function which is relatively simple to optimize. The designed filters have good frequency response, flat group delay, almost symmetric filter coefficients and symmetric wavelet function. The designed filters have advantages of both biorthogonal and orthogonal wavelets. The designed almost symmetric orthogonal filters perform on par with the popular 9/7 biorthogonal filter in image coding applications.

3.1 Introduction

Orthogonal (or more strictly orthonormal) wavelets forms a tight Riesz basis and the corresponding transform have the l^2 norm preserving property. In applications the orthogonality property has several advantages such as noise decorrelation in denoising, simple bit-allocation algorithm in compression and more generally energy preservation in the transform coefficients. However one of the major drawback with dyadic orthogonal wavelets based on real coefficient FIR filters is that it cannot be exactly symmetric [8] (except for the simplest Haar wavelets). Orthogonal wavelets based on IIR filters can however be exactly symmetric [61],[62]. In image processing applications symmetry (which manifest as phase linearity in the filters) is particularly important as lines and

edges, which are salient features of most images, are particularly susceptible to non-linear phase distortion. This is possibly the main reason biorthogonal wavelets, where symmetry is possible, are preferred in image processing. Biorthogonal transforms are however not l^2 norm preserving and do not have the advantages mentioned above. In time series analysis orthogonality is important for the analysis of variance [63, chapter 8] and symmetry has the advantage of allowing alignment of the wavelet coefficients [63, chapter 4].

The desire for both orthogonality and symmetry has led several researchers to design orthogonal FB having approximately linear phase [11],[64],[65],[42],[10],[9]. Although the ultimate aim is the same (orthogonality and symmetry) the design strategies reported are different. The original orthogonal wavelets of Daubechies have maximum vanishing wavelet moments and are highly asymmetric. The corresponding filters are obtained from the minimum phase spectral factor of the maximally flat product filter. Symmlets are a variation and are obtained from the same product filter but with a spectral factor that has approximate linear phase. The main idea behind Coiflets (and their generalization) is the reduction of the number of vanishing wavelet moments so that the available degrees of freedom can be used for achieving vanishing scaling function moments. Imposing vanishing scaling function moments has the indirect effect of giving approximately linear phase filters and increasing the symmetry of the scaling and wavelet functions. In [65] and [42] the strategy is to reduce the deviation of the filters' phase response from the linear response. In [65] a specified degree of flatness in the group delay is imposed at DC and the DC group delay is allowed to be a non-integer. In [42] non-centered (wavelet and scaling function) vanishing moments are used and this introduces one free parameter which can be optimized with respect to the phase distortion. In [64] partial symmetry is imposed on some of the filter coefficients and the coefficients value are obtained by imposing the vanishing wavelet moments and orthogonality conditions. The non-symmetric coefficients are ideally small in value but there is no direct control over their values in [64]. The main purpose of these non-symmetric coefficients is to ensure the orthogonality condition is satisfied. In [10] strict symmetry is imposed on the filter coefficients but the orthogonality condition is approximated by minimizing the reconstruction error using optimisation techniques.

For M-D (multidimensional) signal the 1-D filters are applied separably (along each dimensions independently) to give an equivalent separable M-D wavelet system but separable orthogonal FIR filters cannot be exactly symmetric. It is also possible to use non-separable orthogonal M-D FIR filters which can be exactly symmetric and the de-

sign of non-separable symmetric orthogonal wavelets were presented in [66],[67],[68]. The design of non-separable filters are however more difficult than 1-D filters. Imposing a higher number of vanishing moments is more complicated in the non-separable case. The main disadvantage of non-separable filters however is that M-D convolution operations are required in their implementation and this is significantly more intensive computationally than the implementation of separable filters (requiring only 1-D convolutions). In many image processing applications, eg. JPEG2000 compression, separable filters are used.

A novel method is presented in this chapter for the design of almost symmetric orthogonal wavelet filter banks. Unlike the previous methods discussed above which are essentially indirect, the method here is a direct minimization of the asymmetry of the filter coefficients with structural orthogonality and an imposed number of vanishing wavelet moments. The chapter is outlined as follows. The review of the design of coiflets and symmlets is presented in Section 3.2. The new approach to design symmetric orthogonal FB is presented in Section 3.4. Design examples are presented in Section 3.5 and an application to image compression is presented in Section 3.6.3. The chapter concludes in Section 3.7.

3.2 Wavelet Discrete Moments and Coiflets

Let the low pass analysis filter $H_0(z)$ be defined as $H_0(z) \equiv \sum_{n=0}^{2L-1} h_0(n) z^{-n}$. The degrees of freedom available to design $h_0(n)$ is $2L$. The PR condition (2.1) takes half of the degrees of freedom. To impose VMs and other conditions, the remaining L degrees of freedom are utilised. As detailed in the Section 2.2, Daubechies designed orthogonal FB having maximum VMs i.e., all the remaining L degrees of the freedom are used to impose VMs on the orthogonal filter. The rationale behind having the maximum number of VMs are

- To have a very smooth wavelet function
- To have a simple design methodology

However some degrees of freedom can be utilised to tune other characteristics of the wavelet filter such as achieving symmetry of the wavelet function. The symmetry of the wavelet function plays a vital role in the image processing which is the motivational factor behind designing a symmetric wavelet function. It has been found in the literature[43],[11],[69] that setting a few scaling moment of the filter to zero will result

in an almost symmetric wavelet function . The k^{th} scaling moments of the filter $h_0(n)$ is defined as

$$\mu(k) = \sum_n n^k h_0(n) \quad for \quad k = 1, 2, ..L - 1 \quad (3.1)$$

Some degrees of freedom are utilised to set the scaling moment to zero. There is a relationship among scaling moments [70],[55] and it is given by

$$\mu(k) = \frac{1}{2\sqrt{2}} \sum_{l=1}^{k-1} \binom{k}{l} (-1)^l \mu(l) \mu(k-l) \quad (3.2)$$

where $k = 2, 4, ..2K - 2$. A few derivation from the equation (3.2) shows that

$$\begin{aligned} \mu(2) &= -\frac{1}{\sqrt{2}} \mu^2(1) \\ \mu(4) &= \frac{1}{2\sqrt{2}} [8\mu(1)\mu(3) - 3\mu^4(1)] \\ &\dots \end{aligned} \quad (3.3)$$

From the equation (3.3), if $\mu(1)$ is set to zero, then $\mu(2)$ is set to zero automatically. In the Coiflets design, some degrees of freedom are utilised to impose the VMs and the remaining degrees of freedom are utilised to impose the scaling moments. Even though Coiflets filters have symmetric wavelet function, an indirect method is used to obtain a symmetric wavelet. In the Coiflet design, there is no control over the symmetry of the wavelets and it is not clear how many scaling moments are required to control the symmetry of the wavelet. The Coiflets filters have approximately linear phase characteristics.

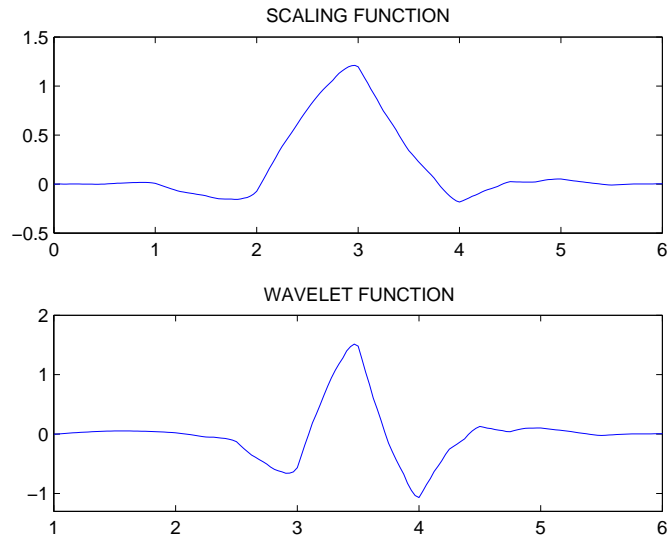
3.3 Symmlets

The Symmlets are designed by Daubechies [7],[8] to have approximately linear phase and approximately symmetric wavelet function. The design of Symmelet is very simple and does not involve setting some scaling moments of the filter (3.1) to zero. The design of Daubechies minimum phase filters are detailed in the Section 2.2.2.1. There are several different distributions of the roots possible with the given product filter $P(z)$. Daubechies choose the roots such that it gives an approximate linear phase filters [8]. The Symmlets are the *least asymmetric* Daubechies wavelet filters.

Table 3.1: Coefficients of Symmlets orthogonal filters. $2L$: Filter Length. p : Number of VMs.

$2L$	p	Filter Coefficients
8	4	-0.07576571,-0.02963553,0.49761867,0.80373875, 0.29785780,-0.09921954,-0.01260397,0.03222310
12	6	0.01540411,0.00349071,-0.11799011,-0.04831174,0.49105594,0.78764114, 0.33792942,-0.07263752,-0.02106029,0.04472490,0.00176771,-0.00780071

Example I: The Symmlet filter of length $2L = 8$ having 4 VMs is designed. The wavelet function in Figure 3.1 shows that it is approximately symmetric. The filter coefficients are shown in Table 3.1.

**Figure 3.1:** Scaling and wavelet function of the length-6 Coiflet filter with two VMs

Example II: The Symmlet filter of length $2L = 12$ having 6 VMs is designed. The wavelet function in Figure 3.2 shows that it is approximately symmetric. The filter coefficients are shown in Table 3.1.

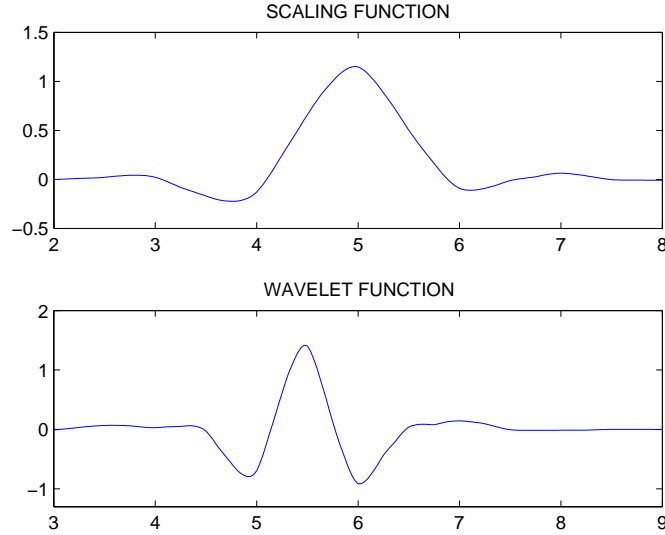


Figure 3.2: Scaling and wavelet function of the length-6 Coiflet filter with two VMs

Symmlets are easy to design as it is based on spectral factorisation and it has maximum VMs. Symmetlet filters of lower length produce asymmetric wavelets and higher order Symmlets can produce least asymmetric wavelets. The higher order Symmlets are difficult to design because of unreliability of the spectral factorisation algorithm.

3.4 Asymmetry Minimization

For symmetric scaling and wavelet functions the filter coefficient $h_0(n)$ must be symmetric and the filter has linear phase response. However orthogonal filters cannot be exactly symmetric except for the simplest two taps filter which corresponds to the Haar wavelet [8]. The goal is therefore to minimize the asymmetry and this require some objective measure of asymmetry to be defined.

3.4.1 Asymmetry Measure

Symmetry is naturally defined in the time (or spatial) domain but exhibits as phase linearity or constant group delay in the frequency domain. In [64] a measure based on group delay $\tau(\omega) \equiv -\frac{d}{d\omega} \angle H_0(e^{j\omega})$ is defined as

$$E_{grp} \equiv \frac{1}{2N} \sum_{n=0}^{N-1} \left| \tau\left(\frac{\pi n}{2N}\right) - \tau_0 \right| \quad (3.4)$$

where there are N points equally distributed over $[0, \frac{\pi}{2}]$ and the mean value is defined as $\tau_0 \equiv \frac{1}{2N} \sum_{n=0}^{N-1} \tau(\frac{\pi n}{2N})$. The value of E_{grp} will be closer to zero if the filter have symmetric coefficients. A similar symmetry measure based of phase distortion is used in [42]. However these frequency domain measures are only proxies. Here we propose a direct measure to minimise the symmetry of the filter. Now the filter $H_0(e^{j\omega})$ length is even ($2L$) and it should have a low-pass characteristics. Therefore if the filter could hypothetically be symmetric it should be a Type 2 FIR system:

$$h_0(n) = h_0(2L - 1 - n) \quad \forall n$$

i.e. the left-half coefficients are mirror image of the right-half coefficients. The deviation from this condition is $(h_0(n) - h_0(2L - 1 - n))$ which leads to the following asymmetry measure

$$E_{sym} \equiv \sum_{n=0}^{L-1} (h_0(n) - h_0(2L - 1 - n))^2 \quad (3.5)$$

The square of the deviation (l^2 norm) instead of the absolute deviation (l^1 norm) is used as it leads to an objective function that is easier to differentiate and has continuous derivative. This measure can also be related to a frequency domain measure as follows. The non-symmetric filter $H_0(e^{j\omega})$ can be decomposed into

$$H_0(e^{j\omega}) = H_{even}(e^{j\omega}) + H_{odd}(e^{j\omega})$$

where the coefficients of H_{even} and H_{odd} have even and odd symmetry respectively:

$$\begin{aligned} h_{even}(n) &\equiv \frac{1}{2}(h_0(n) + h_0(2L - 1 - n)) = h_{even}(2L - 1 - n) \\ h_{odd}(n) &\equiv \frac{1}{2}(h_0(n) - h_0(2L - 1 - n)) = -h_{odd}(2L - 1 - n) \end{aligned}$$

Now E_{sym} is the (scaled) L^2 norm of $H_{odd}(e^{j\omega})$, i.e. $E_{sym} = 4\|H_{odd}(e^{j\omega})\|_2^2$. Minimizing E_{sym} is therefore equivalent to minimizing the energy of the odd part of the filter $H_0(e^{j\omega})$. In the ideal case when a filter is exactly symmetric it will have linear phase and both the E_{grp} and E_{sym} measures will be exactly zero. Filters with near symmetry should have relatively low E_{grp} and E_{sym} values compared to filter without near symmetry. Both E_{grp} and E_{sym} are therefore measure of deviation from symmetry but there is no explicit mathematical relationship between E_{grp} and E_{sym} . It is generally accepted that the human visual system (HVS) is more tolerant to symmetric errors than asymmetric

ones [1],[66]. The HVS perceives an image in the spatial domain and therefore it can be argued that it is more natural to measure asymmetry in the spatial rather than the frequency domain. From an optimisation perspective E_{sym} is a simpler objective function (less non-linear) in the filter coefficients compared to E_{grp} (involves the derivative of the arctangent function). More comparison between E_{grp} and E_{sym} will be made later in the sections 3.5 and 3.6.3.

3.4.2 Optimisation algorithm

Using the lattice parametrization the un-normalized filter coefficients $\hat{h}_0(n)$ ($\equiv \sqrt{K}h_0(n)$) can be expressed as multilinear functions of the lattice parameters. For example the length 8 ($L = 4$) filter coefficients are given by

$$\{\hat{h}_0(0), \dots, \hat{h}_0(7)\} = \{1, -\alpha_1, -\alpha_1\alpha_2 - \alpha_2\alpha_3 - \alpha_3\alpha_4, -\alpha_2 + \alpha_1\alpha_2\alpha_3 + \alpha_1\alpha_3\alpha_4, \\ -\alpha_1\alpha_3 - \alpha_2\alpha_4 + \alpha_1\alpha_2\alpha_3\alpha_4, -\alpha_3 + \alpha_1\alpha_2\alpha_4 + \alpha_2\alpha_3\alpha_4, -\alpha_1\alpha_4, -\alpha_4\}$$

Imposing the sum rule (2.3) results in a multilinear constraint equation in the lattice parameters. For example with the length 8 filter with $k = 0$ the constraint equation is

$$1 + \alpha_1 + \alpha_2 + \alpha_3 - \alpha_1\alpha_2 - \alpha_1\alpha_3 - \alpha_2\alpha_3 - \alpha_1\alpha_2\alpha_3 = 0.$$

The measure in (3.5) can be expressed as a ratio of two multiquadratic functions of the lattice parameters as follows:

$$\begin{aligned} E_{sym} &\equiv \sum_n (h_0(n) - h_0(2L - 1 - n))^2 \\ &= \sum_n (\hat{h}_0(n)/\sqrt{K} - \hat{h}_0(2L - 1 - n)/\sqrt{K})^2 \\ &= (\sum_n (\hat{h}(n) - \hat{h}(2L - 1 - n))^2)/K \equiv \hat{E}_{sym}/K \end{aligned}$$

Now \hat{E}_{sym} is quadratic in $\hat{h}(n)$ and

$$K \equiv \prod_{l=1}^L (1 + \alpha_l^2) > 0$$

The design goal is then to minimize E_{sym} in (3.5) subject to the p VM constraints in (2.3). This requires the use of the Lagrange multiplier method. Note that both the objective function and constraints are non-convex, i.e. non-convex optimisation.

For convenience eqn. (2.3) is scaled by $1/K$ (> 0) before it is incorporated into the Lagrangian function that is given by:

$$H = \frac{\hat{E}_{sym}}{K} + \frac{1}{K} \sum_{k=0}^{p-1} \lambda_k \left(\sum_n (-1)^n n^k \hat{h}_0(n) \right) \equiv \frac{\tilde{E}_{sym}}{K}$$

Now \tilde{E}_{sym} is multiquadratic in α_l 's and linear in λ_k (the Lagrange multipliers). Setting the derivative of H w.r.t. α_l to zero gives

$$\frac{\partial H}{\partial \alpha_l} \equiv H_{\alpha_l} = \frac{K \tilde{E}_{sym, \alpha_l} - \tilde{E}_{sym} K_{\alpha_l}}{K^2} = 0. \quad (3.6)$$

where

$$\tilde{E}_{sym, \alpha_l} \equiv \frac{\partial \tilde{E}_{sym}}{\partial \alpha_l}$$

and

$$K_{sym, \alpha_l} \equiv \frac{\partial K_{sym}}{\partial \alpha_l}$$

It is easy to show that the greatest common factor $\text{gcf}(K, K_{\alpha_l}) = \prod_{k \neq l} (1 + \alpha_k^2)$ and $K_{\alpha_l}/K = 2\alpha_l/(1 + \alpha_l^2)$. Equation (3.6) can then be simplified to

$$\tilde{E}_{sym, \alpha_l} (1 + \alpha_l^2) - \tilde{E}_{sym} 2\alpha_l = 0 \quad (3.7)$$

The equation above is a multivariate polynomial equation and is cubic in α_l , quadratic in all other α 's and linear in the Lagrange multipliers. The optimisation process therefore requires the solution to the set on simultaneous polynomial equations (3.7) for $l = 1, \dots, L$ and (2.3) for $k = 0, \dots, p - 1$. There are a plethora of methods for the solution of simultaneous non-linear equations but a relatively straightforward method is the multivariate version of the classical Newton-Raphson method [71].

Choice of initial values: Iterative methods for solving non-linear equations such the Newton-Raphson method require the specification of the initial guess values which needs to be reasonably close to the final solution. Since the optimisation problem here is non-convex a particular solution may only be a local optimum. To ensure a solution that gives good filter is obtained multiple (instead of one) sets of initial values are tried. Note that only real-valued solutions are of interest here. As discussed in [71] insight or additional information of the particular problem is needed for the iterative methods to work well. Consider now the case with maximum VM, i.e. $p = L$, and there are no degrees of freedom left that can be used to minimize E_{sym} . The lattice parameters values are the solutions to the set of multilinear equations (2.3) for $k = 0, \dots, L - 1$

and correspond to filters that are spectral factors of the maximally flat product filter $P(z)$. Each unique solution set correspond to a unique spectral factor and the set of lattice parameters value can be obtained by applying the lattice factorization algorithm [1] on that spectral factor, i.e. there is no need to explicitly solve the set of multilinear equations. If the number of VM is reduced $p < L$ some of the multilinear equations would still apply but there are now some degrees of freedom available to reduce E_{sym} . This can be viewed as a process of perturbing the maximally flat solution. Therefore the lattice parameters value obtained from the spectral factors of the maximally flat product filter are suitable choices for initial values. Since half of the spectral factors of a given product filter are time-reverse versions ($H_0(z) \rightarrow z^{-(2L-1)}H_0(z^{-1})$) of the other half, only half of the spectral factors need to be considered (note that E_{sym} is the same for two spectral factors that are time reversed version of each other).

A summary of the optimisation algorithm is as follows:

1. Specify the filter length $2L$ and the number of VMs p .
2. Obtain all distinct spectral factors (exclude time-reverse versions) of the maximally flat product filter of length $4L - 1$.
3. Obtain the sets of lattice parameters value corresponding to the distinct spectral factors by using the lattice factorization algorithm [1].
4. For each set of lattice parameters value as initial values, apply the Newton-Raphson (or any other suitable) method to solve the equations (3.7) and (2.3).
5. Choose the solution that gives the lowest E_{sym} measure.

The algorithm was tested on a quad-core PC (Intel i7 2.66GHz) running Matlab (7.9.0.529 (R2009b)) for filters with length up to 40 without any problems.

3.5 Design Examples

Example III: The filter length is $2L = 10$ and in the first instance the number of VMs is set to 3. i.e. $p = 3$. The corresponding scaling and wavelet functions are shown in Figure 3.3. The corresponding symmlet functions (with the same filter length) is also shown (dotted line) for comparison. It can be observed from that the scaling and wavelet functions designed using the proposed technique is more symmetric compared to the symmlet functions.

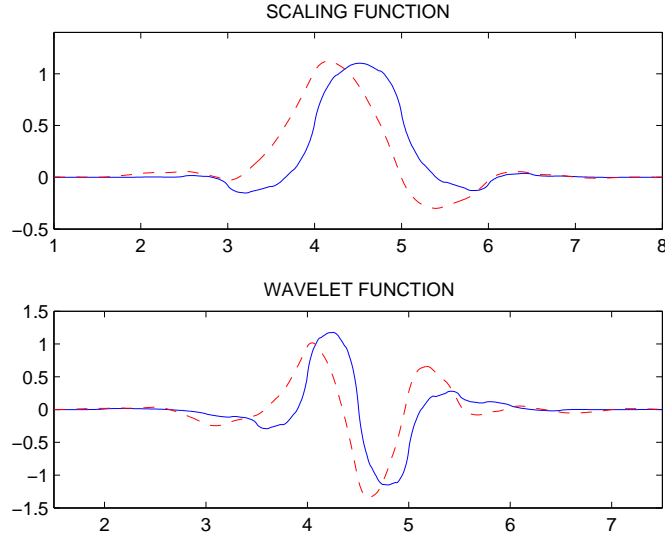


Figure 3.3: Scaling and wavelet function of length 10 filter with 3 VMs. Solid line: Almost symmetric filter. Dotted line: Symmlets

The impulse response and group delay response are shown in Figure 3.4. It can be observed that the impulse response of the filter is symmetric and the filter looks like a Type 2 filter. The group delay response shown in Figure 3.4 (bottom) is virtually flat which also confirms that the filter has linear phase characteristics. The asymmetry measures are

$$(E_{sym}, E_{grp}) = (3.08 \times 10^{-4}, 0.0186)$$

for this example and is lower when compared to $(E_{sym}, E_{grp}) = (0.0626, 0.1453)$ for the symmlet. If the VMs is reduced by one ($p = 2$) the asymmetry measures are

$$(E_{sym}, E_{grp}) = (2.59 \times 10^{-4}, 0.0197)$$

i.e. increased symmetry at the expense of reduced VMs. The filter coefficients values for both the 3 VMs and 2 VMs cases are shown in Table 3.2. The zoomed in zero plot of the designed filter having 3 VMs is shown in Figure 3.5 showing 3 zeros at $z = -1$. The sum rules (2.3) are of order of 10^{-16} indicating the VM constraints are satisfied to within the numerical precision.

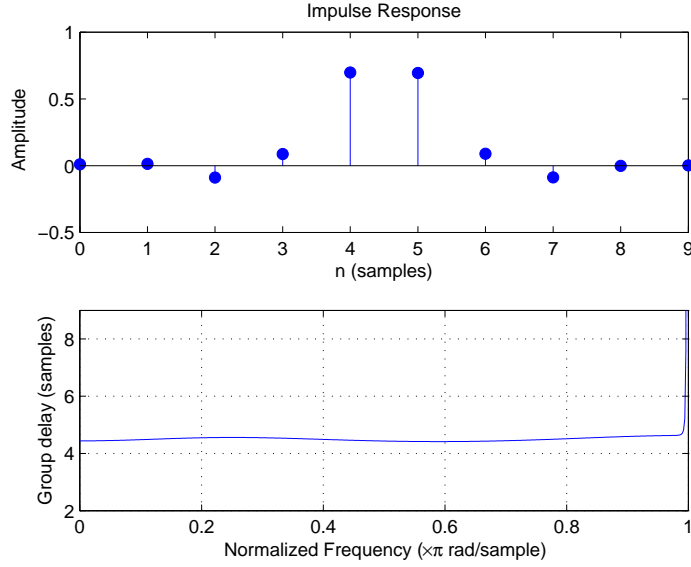


Figure 3.4: Impulse response and group delay response of length 10 filter with 3 VMs.

Table 3.2: Coefficients of almost symmetric orthogonal filters. $2L$: Filter Length. p : Number of VMs.

$2L$	p	Filter Coefficients
10	3	0.00990261, 0.01289124, -0.08868831, 0.08710378, 0.69798784, 0.69379808, 0.08949212, -0.08790576, -0.00158748, 0.00121945
10	2	0.01182899, 0.01068742, -0.08873840, 0.08881929, 0.69550569, 0.69624669, 0.08797808, -0.08805734, 0.00053242, -0.00058929
12	5	0.01123325, 0.00792041, -0.09472487, -0.07758217, 0.40738677, 0.79695609, 0.41944629, -0.05946826, -0.04250054, 0.04816740, 0.00626588, -0.00888668
12	4	-0.00726021, 0.02753967, 0.02907041, -0.11110287, 0.10320477, 0.69967915, 0.67890365, 0.11646589, -0.10273642, -0.02703694, 0.00592457, 0.00156188
12	3	0.00124265, 0.00528768, 0.00621915, -0.08565105, 0.08554397, 0.69632692, 0.69698767, 0.08508043, -0.08557914, 0.00669556, 0.00269248, -0.00063276
20	5	0.00043266, 0.00022687, -0.00160659, -0.00204645, -0.00134142, 0.02040479, -0.00238632, -0.11123623, 0.11472244, 0.68901444, 0.68781713, 0.11551674, -0.11108108, -0.00311168, 0.02226677, -0.00256801, -0.00195077, 0.00135246, 0.00023395, -0.00044617

Example IV: The filter length is $2L = 12$ and several cases with different number of VMs p are considered. Comparisons are also made with other reported works and the

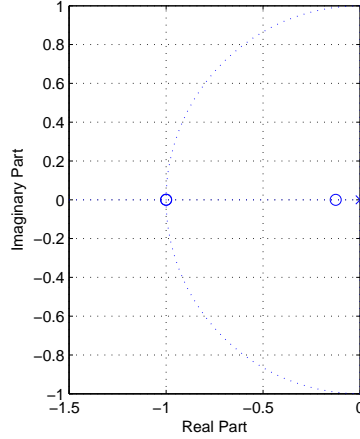


Figure 3.5: Zero plot of length 10 filter having 3 VMs.

Table 3.3: Asymmetry measures for length 12 filter. Comparison made with other methods.

Method	p	E_{grp}	E_{sym}	s_c
Symlets	6	0.0741	0.5478	2.388
optimisation	5	0.0668	0.3825	2.324
optimisation	4	0.0556	0.0044	1.939
Abdelnour [64]		0.0784	0.0075	2
Coiflets		0.0203	1.1427	1.836
Wei [42]		0.0259	1.1433	1.833
optimisation	3	0.0045	1.11×10^{-5}	1.465
Abdelnour[64]		0.014	1.1211	1.843
optimisation	2	0.0047	1.03×10^{-5}	1.464
Abdelnour[64]		9.8×10^{-5}	0.4336	1.037

results are summarized in Table 3.3. As the number of VMs p is reduced E_{sym} (E_{grp}) is also reduced, i.e. a trade-off in VMs for increased symmetry. Reducing p below 3 however does not improve the symmetry significantly as the scaling and wavelet functions with $p = 3$ are already virtually symmetric as can be seen in Figure 3.6 (the corresponding symlets (in dotted line) is also shown for comparison). The impulse response and group delay response are shown in Figure 3.7. It can be observed that the impulse response of the filter is symmetric and the filter looks like a Type 2 filter. The group delay is approximately flat over the passband as shown in Figure 3.7 (bottom). The filter coefficients values are given in Table 3.2. The zoomed in zero plot of the designed filter having 4 VMs is shown in Figure 3.8 showing 4 zeros at $z = -1$. The sum rules (2.3)

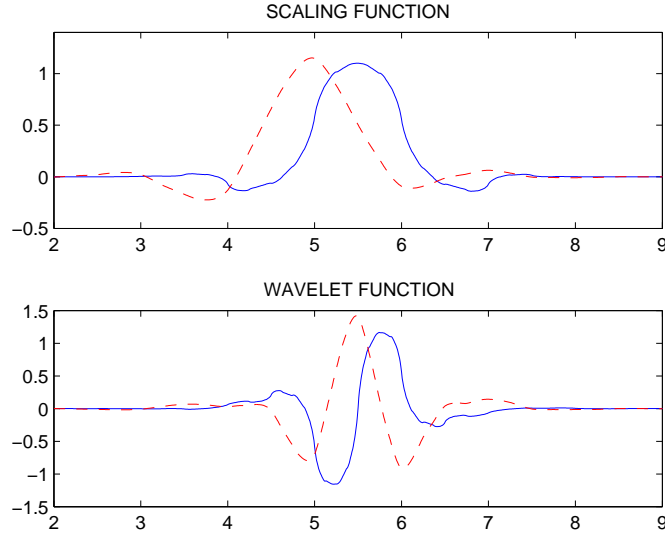


Figure 3.6: Scaling and wavelet function of length 12 filter having 3 VMs. Solid line: Almost symmetric filter. Dotted line: Symmlets

are of order of 10^{-12} indicating the VM constraints are satisfied to within the numerical precision.

Our design is superior in terms of the E_{sym} measure compared with earlier reported works. The E_{grp} measure in our designs is small but is not necessarily the lowest compared to other reported works. Note however in the $p = 4$ case the filters with the lower E_{grp} value (Coifets and Wei [42]) are also the filter with the higher E_{sym} value. The filter with $p = 2$ by Abdelnour [64] has very small E_{grp} value but quite large E_{sym} value. These observations suggest that minimizing E_{grp} may not lead to filters with high symmetry. On the other hand the filters in this work which is optimized w.r.t. to E_{sym} all have reasonably small E_{grp} values.

Example V: The filter length is $2L = 20$ and the number of VMs is $p = 5$. The filter coefficients are given in Table 3.2. The asymmetry measures are

$$(E_{sym}, E_{grp}) = (1.712 \times 10^{-5}, 0.005)$$

for this example and is significantly lower when compared to

$$(E_{sym}, E_{grp}) = (0.456, 0.1324)$$

for the corresponding symmlet. The scaling and wavelet functions are shown in Figure

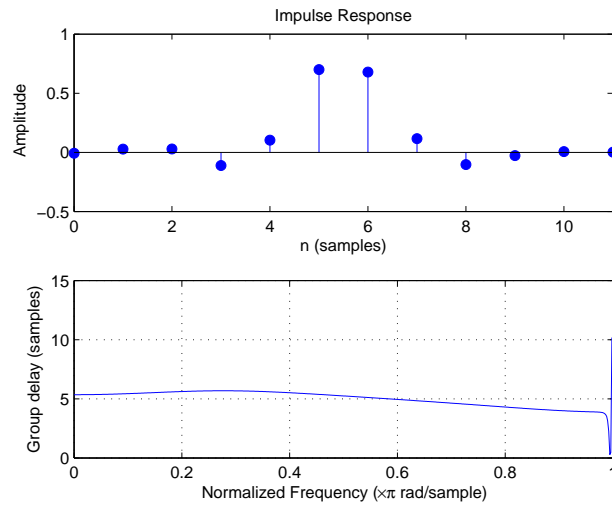


Figure 3.7: Impulse response and group delay response of length 12 filter with 4 VMs.

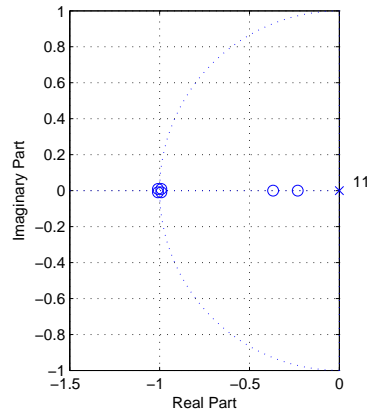


Figure 3.8: Zero plot of length 12 filter having 4 VMs.

3.9 where the corresponding symmlets (in dotted line) is also shown for comparison. The sum rules (2.3) are of order of 10^{-10} indicating the VM constraints are satisfied to within the numerical precision.

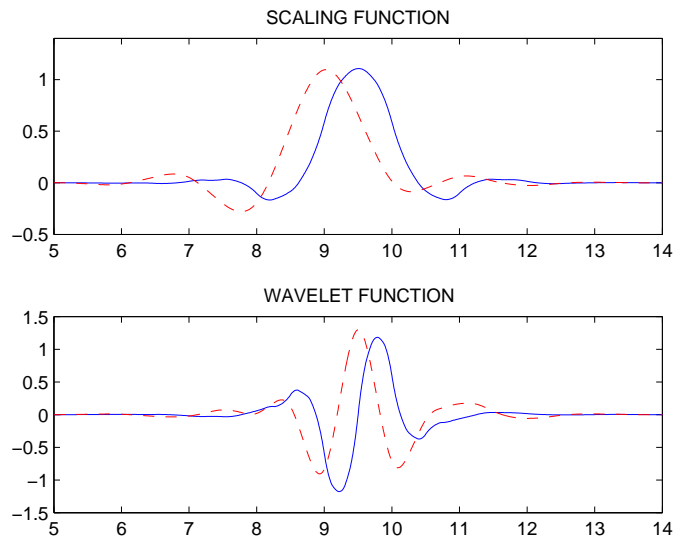


Figure 3.9: Scaling and wavelet function of length 20 filter having 5 VMs. Solid line: Almost symmetric filter. Dotted line: Symmlets

Example VI: The filter length $2L = 40$ having 5 VMs is designed to show the versatility of the proposed technique. The asymmetry measures are

$$(E_{sym}, E_{grp}) = (1.852 \times 10^{-5}, 0.006)$$

for this example. The scaling and wavelet functions are shown in Figure 3.10 where the corresponding symmlets (in dotted line) is also shown for comparison. The impulse response and group delay response are shown in Figure 3.11. The sum rules (2.3) are of order of 10^{-12} indicating the VM constraints are satisfied to within the numerical precision.

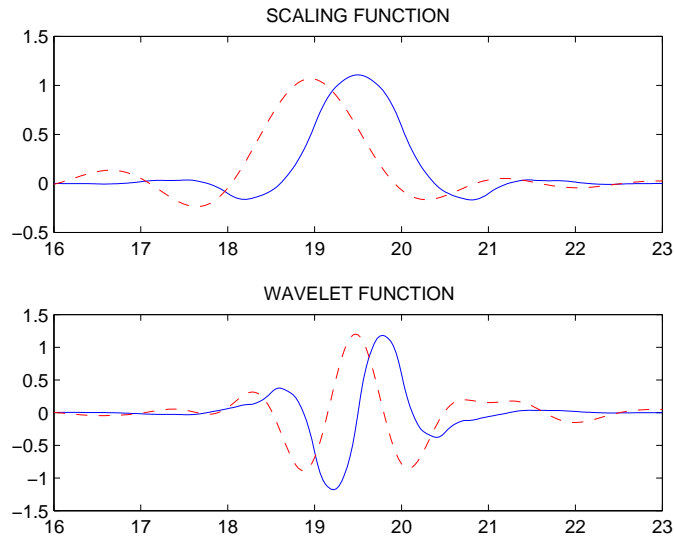


Figure 3.10: Scaling and wavelet function of length 40 filter having 5 VMs. Solid line: Almost symmetric filter. Dotted line: Symmlets

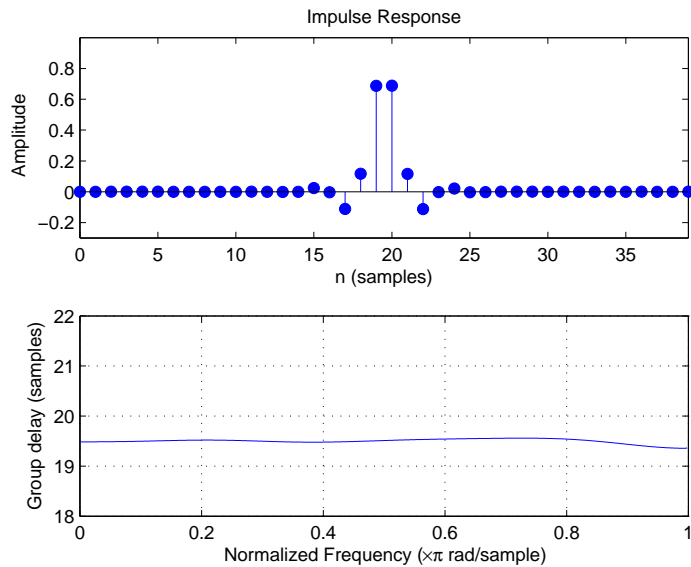


Figure 3.11: Impulse response and group delay response of length 40 filter with 5 VMs.

From all the design examples, it has been proved that the designed filters offer high level of symmetry compared to other methods reported in the literature. Desired number of VMs can be imposed on the filter. Instead of using the Lagrange multiplier, a versatile non-linear optimiser based on interior point method [72] can also be used.

3.6 Application in image compression

In this Section, we will perform image compression using the designed filter, Daubechies filter, Symmlets and Coiflets and compare all the filter performance.

3.6.1 SPIHT

The Set Partitioning In Hierarchical Trees (SPIHT) algorithm is widely used for efficiently compression of images. It is a highly refined version of Embedded Zerotree Wavelet (EZW) algorithm. It was introduced in [73] by Said and Pearlman. The SPIHT algorithm reduces the number of bits needed for encoding compared to EZW algorithm and it favours the progressive transmission. The SPIHT algorithm gives better compression rate and image quality at low bit rates. After the sub-band decomposition of the image, the wavelet coefficients are grouped into sets known as spatial-orientation trees. The coefficients in each spatial orientation are coded from Most Significant Bit-planes (MSB) to Least Significant Bit-planes (LSB). Energy is concentrated in the parent coefficients (coefficients at coarser level). The SPIHT algorithm leverages on the fact that wavelet coefficient values decrease in magnitude from parent to the child. The List of Insignificant Pixels (LIP) contains the individual coefficients that have magnitude values smaller than the threshold. The List of Significant Pixels (LSP) contains the individual coefficients that have magnitude values exceeds or equals the threshold. The List of Insignificant Sets (LIS) contains set of wavelet coefficients at the node in the spatial-orientation tree. The LIS can be one of two types of sets. A type A LIS is a set of four subtrees of pixels where all of the four subtree roots share the same parent and the pixels in the subtrees rooted by those four pixels are all insignificant, including the four subtree root pixels themselves. A type B insignificant set is a set of 16 subtrees of pixels where all of the 16 subtree roots share the same grandparent and the pixels in the 16 subtrees are all insignificant, including the subtree roots. Let $D(i, j)$ be the set of coordinates of all descendants of the node (i, j) . Let $O(i, j)$ be the set of coordinates of all offspring of the node (i, j) . Let H be the set of all spatial orientation tree roots. Let $L(i, j) = D(i, j) - O(i, j)$ and

$$S_n(i, j) = \begin{cases} 1 & \max_{(i,j)} \{|c_{i,j}|\} \geq 2^n \\ 0 & \text{otherwise} \end{cases}$$

where $c_{i,j}$ represents the $(i, j)^{th}$ wavelet coefficient. The SPIHT algorithm [73] is given in Algorithm 3.1 :

Algorithm 3.1 SPIHT Algorithm

1. Initialisation: Output $n = \text{floor}(\log_2(\max_{(i,j)} \{|c_{i,j}|\}))$
 Set the LSP as an empty list and add the coordinates $(i, j) \in H$ to the LIP and descendants to the LIS
 2. Sorting Pass:
 - a) For each entry (i, j) in the LIP do:
 - i. Output $S_n(i, j)$
 - ii. If $S_n(i, j) = 1$ then move (i, j) to the LSP and output the sign of $c_{i,j}$
 - b) For each entry (i, j) in the LIS do:
 - i. If the entry is of type A then
 - A. Output $S_n(D(i, j))$
 - B. If $S_n(D(i, j)) = 1$ then
 For each $(k, l) \in O(i, j)$ do:
 Output $S_n(k, l)$
 If $S_n(k, l) = 1$ then add (k, l) to the LSP and output the sign of $c_{i,j}$
 If $S_n(k, l) = 0$ then add (k, l) to the end of LIP
 if $L(i, j) \neq 0$ then move (i, j) to the end of the LIS as an entry of type B and then go to Step iii; otherwise remove entry (i, j) from the LIS
 - ii. If the entry is of type B then
 - A. Output $S_n(L(i, j))$
 - B. If $S_n(L(i, j)) = 1$ then
 add each $(k, l) \in O(i, j)$ to the end of the LIS as an entry of type A
 remove (i, j) from the LIS
 3. Refinement Pass: for each entry (i, j) in the LSP, except those included in the last sorting pass, output the n th most significant bit of $|c_{i,j}|$
 4. Quantisation Step: Decrement n by 1 and go to step 2
-

3.6.2 Performance measures

3.6.2.1 MSE, PSNR

The Mean Square Error (MSE) between two images $I_1(m, n)$ and $I_2(m, n)$ is given by

$$MSE = \frac{\sum_{M,N}[I_1(m, n) - I_2(m, n)]}{M \times N}$$

The lower the value of MSE, the lower the error between two images. The Peak Signal to Noise Ratio (PSNR) is computed using the equation:

$$PSNR = 10 \times \log_{10} \left(\frac{255^2}{MSE} \right)$$

The value of PSNR is expressed in terms of decibels (dB). The higher the value of PSNR, the better the image quality.

3.6.2.2 SSIM

The MSE and PSNR measures do not capture the perceived visual quality of the image. The Structural SIMilarity (SSIM) index [74] is a method for measuring the similarity between two images. Even though SSIM measure is different from PSNR, there is some analytical relationship between PSNR and SSIM [75]. The SSIM compares the structural similarity between the original image and the synthesised image. The basic measurements involved in computing SSIM are

1. Luminance measurement
2. Contract measurement
3. Structural measurement

The SSIM index can be computed using the formula

$$SSIM(x, y) = \frac{(2\mu_x\mu_y + C_1)(2\sigma_{xy} + C_2)}{(\mu_x^2 + \mu_y^2 + C_1)(\sigma_x^2 + \sigma_y^2 + C_2)}$$

where μ_x and μ_y are the mean intensity of image x and y respectively. The value σ_x and σ_y are the standard deviation of image x and y respectively. The σ_{xy} is the correlation between two images x and y . For a gray scale image, the value of the constant C_1 and C_2 are taken to be 6.5025 and 58.5225. A circular symmetric Gaussian window of size 11×11 is used to compute the local measure such as σ_x , σ_y and σ_{xy} . The Gaussian

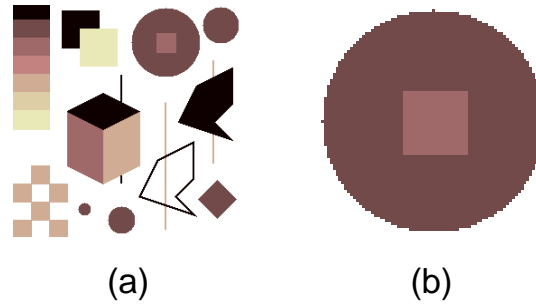


Figure 3.12: (a) Original Image. (b) zoomed in image.

window has a standard deviation of 1.5 samples and it is normalised to unity sum. We use the mean value of SSIM to evaluate the overall image quality

$$MSSIM = \frac{1}{W_n} \sum_{j=1}^{W_n} SSIM(x_j, y_j)$$

where W_n is the number of local windows of the image.

3.6.3 Image Compression Experiment 1

The test image of size 256×256 pixels shown in Figure 3.12 contains a lot of sharp edges. The SPIHT [73] algorithm with 4 levels of wavelet decomposition is applied to compress the image with a target bit-rate of 0.5 bits-per-pixel. Three length 10 orthogonal filters and one biorthogonal filter pair are considered for the wavelet decomposition:

- (i) Daubechies minimum phase D10
- (ii) Symmlets SY10
- (iii) Almost Symmetric optimized AS10
- iv) Daubechies D9/7 (used in JPEG2000).

The reconstructed images are shown in Figure 3.13(a)-(d). Both the PSNR and SSIM index (Structural Similarity Index introduced in [74] as a perceptual measure) of the decompressed images are computed and are shown in Table 3.4. The PSNR with the D9/7 is the highest but the SSIM index is approximately the same with the AS10 pair. However the D9/7 pair does not have the energy preservation of the AS10 pair. The PSNR and SSIM with the D10 is the lowest compared to other filters. The decompressed image with the AS10 and D9/7 have the best overall image quality. The zoomed in portion of the images (on the circular shape with a square inset) are shown in Figure

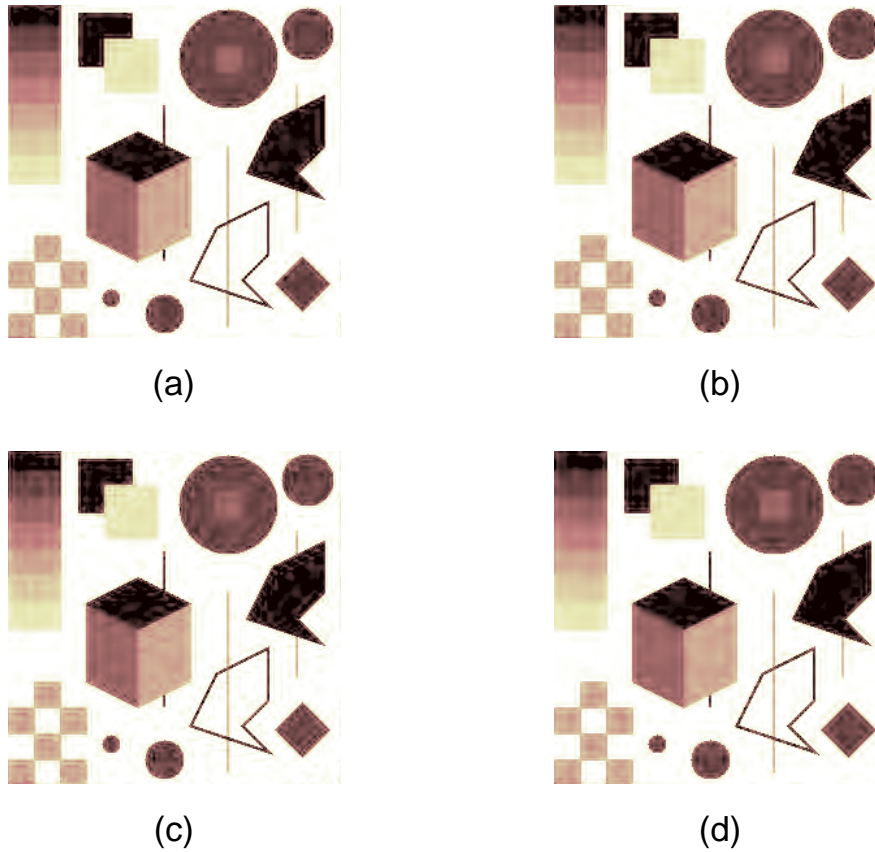


Figure 3.13: SPIHT compressed image at 0.5 bpp using length 10 filters. (a) Using almost symmetric filter. (b) Using Symmlets. (c) Using Daubechies minimum phase. (d) Using Daubechies 9/7 filter.

3.14 and all show distortions due to compression. Visually the worst reconstructed image is with the D10 filter where the edges of the square shape are almost indistinguishable. The best visually is with the AS10 filter where the edges of the square shape are still quite distinguishable. The AS10 filter performs the best at preserving the edges as it is a virtually symmetric even length filter. It was found in [76] that symmetric even length filters have significantly less shift variance and performs better in preserving the location, shape and intensity of impulses compared to symmetric odd length filters (eg. D9/7). Since the AS10 is orthogonal, the task of optimal quantization and bit allocation is much easier [77].

The Sobolev regularity of analysis filter of the D9/7 and the AS10 are 1.41 and 1.51 respectively. The analysis wavelet of the AS10 is more smoother than the D9/7 wavelet. However the synthesis wavelet of D9/7 is smoother than the AS10. The AS10 filter

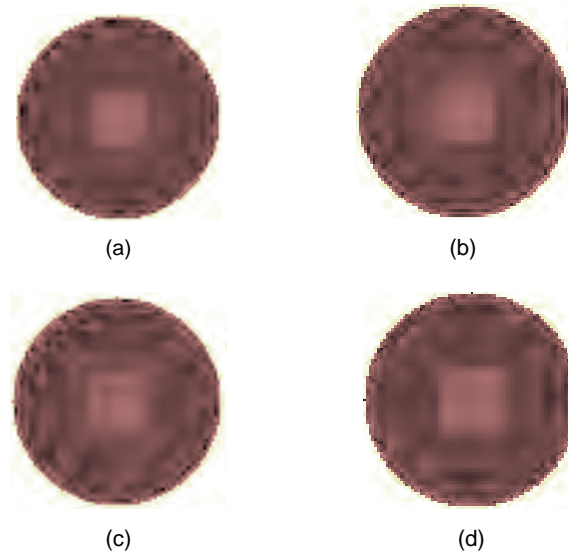


Figure 3.14: Zoomed in image. (a) Using almost symmetric filter. (b) Using Symmlets. (c) Using Daubechies minimum phase. (d) Using Daubechies 9/7 filter.

Table 3.4: PSNR and SSIM for various filters

Filter	PSNR	SSIM
AS10	24.91 dB	0.832
D10	24.35 dB	0.785
SY10	24.93 dB	0.829
Daubechies 9/7	25.38 dB	0.837

having more VMs can be designed easily by the proposed technique described in the Section 3.4.

3.6.4 Image Compression Experiment 2

The length 12 filter by Wei [42] (W12) is designed by minimizing the phase distortion and has lower E_{grp} compared to the length 12 designed here (AS12) - see table 3.3 for $p = 4$ (VMs). However E_{sym} is significantly larger for W12 - see table 3.3 for $p = 4$ (VMs). The SPIHT [73] algorithm with 4 levels of wavelet decomposition is applied to compress the test image shown in Figure 3.12 with a target bit-rate of 0.5 bits-per-pixel. The PSNR and SSIM using AS12 and W12 are (25.08 dB, 0.823) and (24.07, dB, 0.811) respectively. The AS12 has the highest value of PSNR and SSIM values compared to the W12 filter. The edges of the decompressed image shown in Figure 3.15 (b) using W12 were more blurred. This further strengthens the argument of using the spatial domain

measure of asymmetry.

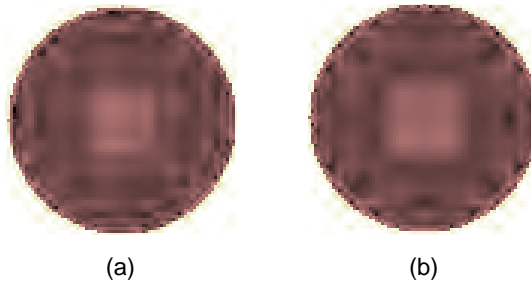


Figure 3.15: Zoomed in image. (a) Using AS12. (b) Using W12

3.6.5 Image Compression Experiment 3

The test image of size 1024×1024 pixels shown in Figure 3.16 (a) contains a lot of horizontal lines, vertical lines and sharp edges. The SPIHT [73] algorithm with 5 levels of wavelet decomposition is applied to compress the image with a target bit-rate of 0.5 bits-per-pixel. Three length 12 orthogonal filters are considered for the wavelet decomposition:

Table 3.5: PSNR and SSIM for various filters

Filter	PSNR	SSIM
AS12	27.23 dB	0.9251
D12	24.44 dB	0.8235
SY12	24.22 dB	0.7951

- (i) Daubechies minimum phase D12
- (ii) Symmlets SY12
- (iii) Almost Symmetric optimized AS12

The reconstructed images are shown in Figure 3.16(b)-(d). Both the PSNR and SSIM index are shown in the Table 3.5. The AS12 filter outperforms the D12 and SY12 filter interms of both PSNR and SSIM. The zoomed in portion of the images are shown in Figure 3.17. The sharp edges are distorted in the decompressed image using D12 and SY12 filters. The best overall image quality is obtained from using AS12 filter.

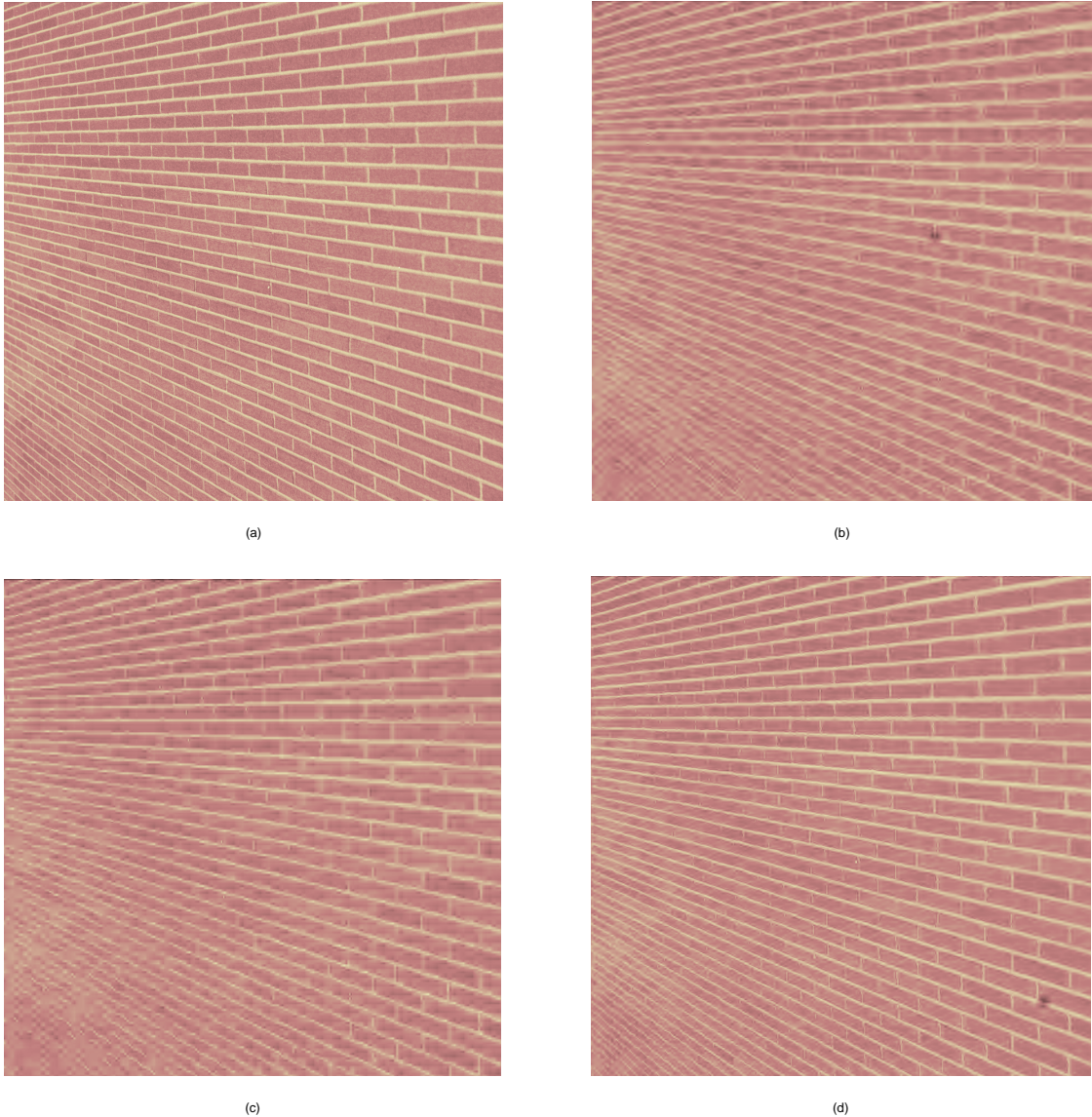


Figure 3.16: (a) Original Image. SPIHT compressed image at 0.5 bpp using length 12 filters. (b) Using Daubechies minimum phase.(c) Using Symmlets. (d) Using almost symmetric filter.

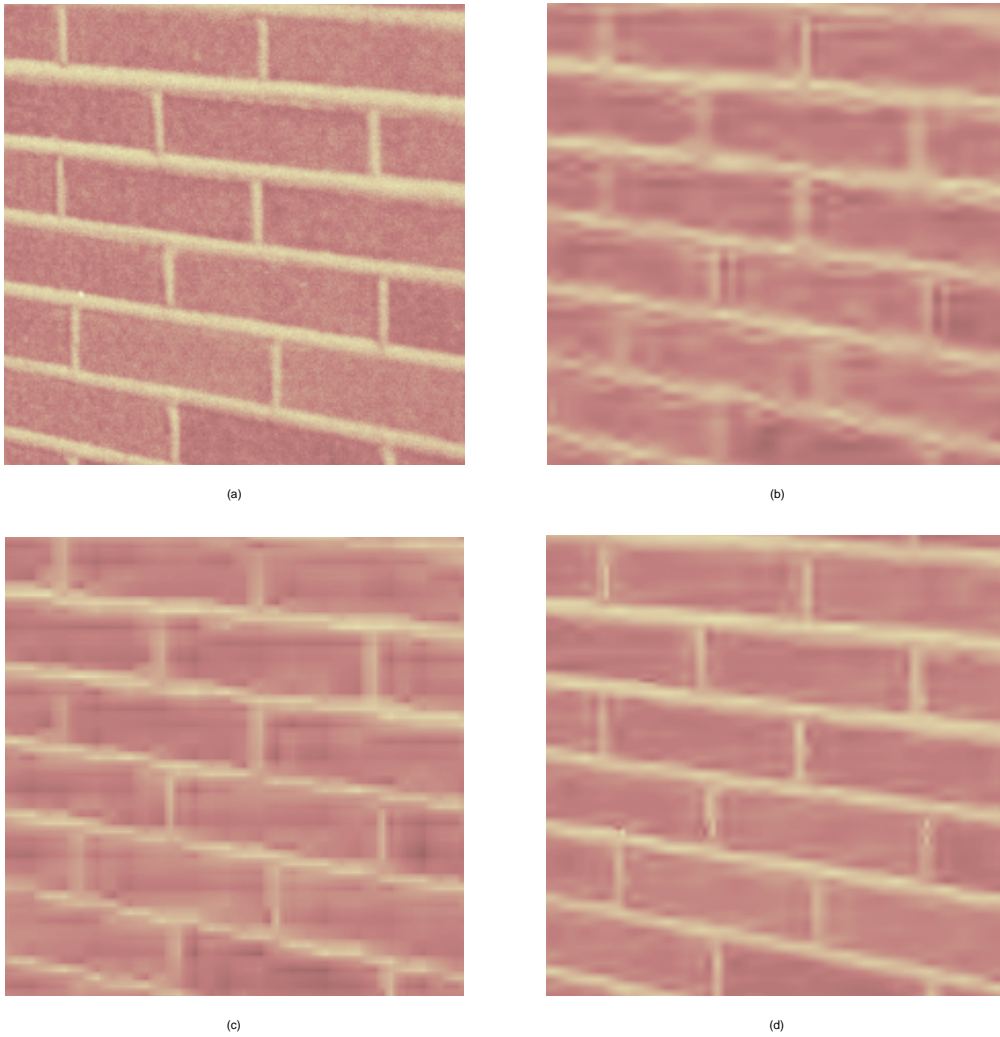


Figure 3.17: Zoomed in image. (a) Original Image. (b) Using Daubechies minimum phase. (c) Using Symmlets. (d) Using almost symmetric filter.

3.7 Conclusion

This chapter has presented a novel optimisation technique for designing almost symmetric orthogonal wavelet filter banks. The technique is simple and can be applied to design relatively long filters. The main advantage of this technique is the structural orthogonality which is achieved by using the lattice parametrization. The required number of vanishing moment are imposed as constraints. The remaining degrees of freedom are then utilised to minimize the objective function which measures directly the degree of asymmetry of the filter. Design examples were presented to show the superiority of the

results compared to previous works. The application of the designed filters to the image compression was also presented. The best overall image quality in image compression application was obtained using the designed almost symmetric orthogonal filters.

4 Design of Almost Symmetric Orthonormal Hilbert Pair of Wavelets

The dual-tree complex wavelet transform offers near shift invariance and better directional selectivity compared to the traditional discrete wavelet transforms. A new class of Hilbert-pair of wavelets that can be used in the dual-tree is presented in this chapter. These Hilbert-pairs are exactly orthogonal but are also virtually symmetric thus have the advantages found in both orthogonal and biorthogonal wavelets. Symmetry in the wavelets is of prime importance in many applications as it offers better directional selectivity. An efficient and flexible design technique is proposed for the design of these new Hilbert-pairs in this chapter. The proposed technique readily allows the designer to trade-off between the degree of symmetry and the analytic quality. The designed wavelet filters have good frequency response, flat group delay and achieve a good approximation to the half sample delay condition which is required for good analytic quality.

4.1 Introduction

The Discrete Wavelet Transform (DWT) is an indispensable tool in a wide range of engineering and scientific applications and can be implemented efficiently with filter banks (FB) [2],[1]. However the DWT suffers from some problems

1. Shift variance
2. Lack of directionality
3. Oscillation & Aliasing

The wavelet coefficients oscillate positive and negative around singularities and it complicates the signal modelling. The shift variance is inherent in the DWT and it is

caused by the downsampling operation in the DWT. A small shift of the signal causes greater perturbation of the wavelet coefficient around singularities [27]. To overcome the shift variance of the DWT, the undecimated DWT was proposed in the literature [78],[79],[2],[24]. The undecimated DWT is a redundant transform (over complete transform) and requires more computation compared to the DWT. A new generation of wavelet based transforms have also been proposed to overcome the DWT problems and they are usually overcomplete or redundant [80],[81]. The Dual Tree Complex Wavelet Transform (DTCWT) introduced by Kingsbury has emerged as one of the most popular redundant transforms in a wide variety of applications [82],[27]. The DTCWT has near shift invariance, provides directional selectivity in multidimensions and lower redundancy than the undecimated DWT [27].

The DTCWT is implemented using a pair of two-channel perfect reconstruction (PR) multirate filter banks. The equivalent wavelet function of the two filter banks, $\psi^h(t)$ and $\psi^g(t)$ (with Fourier transform $\Psi^h(\omega)$ and $\Psi^g(\omega)$ respectively) should ideally satisfy the following Hilbert transform relationship

$$\Psi^g(\omega) = \begin{cases} -j\Psi^h(\omega), & \omega > 0 \\ j\Psi^h(\omega), & \omega < 0 \end{cases} \quad (4.1)$$

The wavelets $(\psi^h(t), \psi^g(t))$ form a Hilbert-pair (and the same can be said of the corresponding pair of filter banks) and can be either biorthogonal or orthogonal. The Hilbert transform relationship (4.1) can however only be approximated with practical filter banks and it is tacit that in all practical Hilbert-pairs the relationship is approximate. Reviews of earlier design techniques for Hilbert-pairs are found in [27] and [83]. Some of the more recent techniques are found in [84],[85],[86],[87],[88],[89]. Most techniques proposed are for FIR filters but recently techniques for IIR filters have been proposed in [90].

Biorthogonal wavelets can be exactly symmetric and the design of biorthogonal Hilbert-pairs with symmetric linear phase odd/even length filters (Type I/II filters) can be found in [91],[92],[93]. Symmetry is particularly important in image processing as salient features such as lines and edges are particularly susceptible to nonlinear distortions. In time series analysis, symmetry allows for the alignment of wavelet coefficients [63, chapter 4]. Biorthogonal transforms however are not l^2 norm preserving. Orthogonal (strictly orthonormal) transforms are l^2 norm preserving and have the advantage of noise decorrelation (in denoising), simple bit allocation (in compression), and more generally, energy preservation in the transform coefficients. However dyadic orthogonal wavelets based

on a real coefficient finite-impulse-response (FIR) filter cannot be exactly symmetric [8] (except for the simplest Haar wavelets). Orthogonal wavelets based on infinite-impulse-response (IIR) or complex coefficient filters can be symmetric but require more complex implementation.

The two most common types of orthogonal Hilbert-pairs are

(i) those based on the common factor technique [14],[88],[89]

(ii) those based on Symmetric-Self-Hilbertian (SSH) filters [15] (which includes the Q-shift filters [16]).

All orthogonal Hilbert-pairs reported so far do not have the symmetry of the biorthogonal Hilbert-pairs. The symmetry of the wavelets $\psi^h(t)$ and $\psi^g(t)$ is important for directional selectivity [14].

In this chapter we present the design of a new class of Hilbert-pairs that have the advantages of both biorthogonal and orthogonal wavelets. The wavelets are exactly orthogonal but are also almost symmetric. The corresponding filters are almost like the Type I/II filters but are exactly orthogonal and therefore l^2 norm preserving. The phase response is approximately linear and the impulse response is approximately symmetric. The overview of the chapter is as follows. Section 4.2 briefly reviews Hilbert pair fundamentals and the common factor technique that is used to design orthogonal Hilbert pair of wavelets. The design of Hilbert pair based on almost symmetric filters is presented in Section 4.3. Techniques to improve the analyticity of Hilbert pair are presented in Section 4.4. This chapter concludes in Section 4.7.

4.2 Preliminaries

A. Dual-Tree Filter Bank

The dual-tree complex wavelet transform is based on a pair of filter banks. The upper and lower tree filters are denoted by superscripts h and g respectively. It is proven in [12] that equation (4.1) will hold if the low-pass filters of the filter banks, $H_0^h(z)$ and $H_0^g(z)$ satisfy

$$H_0^g(\omega) = e^{-j\omega/2} H_0^h(\omega) \quad \text{for} \quad -\pi \leq \omega \leq \pi \quad (4.2)$$

(Note the slight abuse of notation, ie. $H_0^g(\omega) \equiv H_0^g(e^{j\omega})$). Since condition (4.2) can only be approximated with FIR filters (due to the half sample delay term), the Hilbert transform relationship (4.1) is only approximate. Measures of the degree of approximation based on the complex wavelet spectrum $\Psi^C(\omega) = \Psi^h(\omega) + j\Psi^g(\omega)$ are defined in (2.10)

and (2.11).

B. Common Factor Technique

Selesnick proposed a common factor technique to design orthonormal Hilbert pair of wavelets [14]. The scaling low pass filters $H_0^h(z)$ and $H_0^g(z)$ are constructed by

$$\begin{aligned} H_0^h(z) &= F(z) D(z) \\ H_0^g(z) &= F(z) z^{-L_p} D(z^{-1}) \end{aligned}$$

where $F(z)$ is the common factor, $D(z)$ is the phase factor and L_p is the degree of the phase factor. The phase factor is given by

$$D(z) = 1 + \sum_{n=1}^{L_p} d(n) z^{-n}$$

By defining the all pass filter $A(z)$ as

$$A(z) = \frac{z^{-L_p} D(z^{-1})}{D(z)}$$

it can be shown that

$$H_0^g(z) = F(z) A(z)$$

The filter $A(z)$ approximates the half sample delay. Firstly $A(z)$ is designed and then $F(z)$ is designed to have K vanishing moments

$$F(z) = Q(z) (1 + z^{-1})^K$$

Then we have

$$\begin{aligned} H_0^h(z) &= Q(z) (1 + z^{-1})^K D(z) \\ H_0^g(z) &= Q(z) (1 + z^{-1})^K z^{-L_p} D(z^{-1}) \end{aligned}$$

The product filter of the CQFs are given by

$$\begin{aligned}
P(z) &= H_0^h(z) H_0^h(z^{-1}) \\
&= H_0^g(z) H_0^g(z^{-1}) \\
&= Q(z) Q(z^{-1}) (z + 2 + z^{-1})^K D(z) D(z^{-1}) \\
&= R(z) (z + 2 + z^{-1})^K D(z) D(z^{-1})
\end{aligned}$$

where $R(z) = Q(z) Q(z^{-1}) = \sum_n r(n) z^{-n}$. The coefficients of $r(n)$ is obtained using the halfband condition (2.2). The factor $Q(z)$ is then obtained from the spectral factorisation of $R(z)$. Even though the common factor is an easy method to design orthonormal Hilbert pair of wavelets, the Hilbert pair of wavelets are not symmetric. The design procedure has no control over the symmetry of the wavelets. The complex wavelet $\psi^C(t)$ is symmetric. The spectral factorisation of $Q(z)$ can be done in different ways. The mid-phase factorisation gives least asymmetric wavelets compared to minimum phase factorisation. It has been shown in [14] that mid-phase spectral factorisation leads to better directional selectivity compared to minimum phase spectral factorisation. Zhang *et. al* [89] improved the common factor technique to design Hilbert pair with good analytic quality. Tay *et. al* [88] improvised the frequency selectivity of the Hilbert pair of filters. The common factor technique produces Hilbert pair of filters that does not have approximately linear phase. In some cases (for short filters) the mid-phase spectral factorisation produces nearly linear phase response. Thus the common factor technique is not suitable to design a symmetric Hilbert pair of wavelets. A Hilbert pair of filters is constructed using the common factor technique with $K = 4$ and $L_p = 2$. The complex wavelet and complex spectrum are shown in Figure 4.1 . The wavelets ($\psi^h(t)$, $\psi^g(t)$) are not symmetric as shown in Figure 4.1 (top). However the complex wavelet $\psi^C(t)$ is approximately symmetric. The analytic quality measures are $E_1 = 1.83\%$ and $E_2 = 0.04\%$.

C. Symmetric-Self-Hilbertian (SSH) filters

Tay *et. al* [15] constructed Hilbert pair of wavelets where wavelets in g tree is a mirror image of wavelet in h tree. i.e.

$$\psi^g(t) = \psi^h(T - t) \quad (4.3)$$

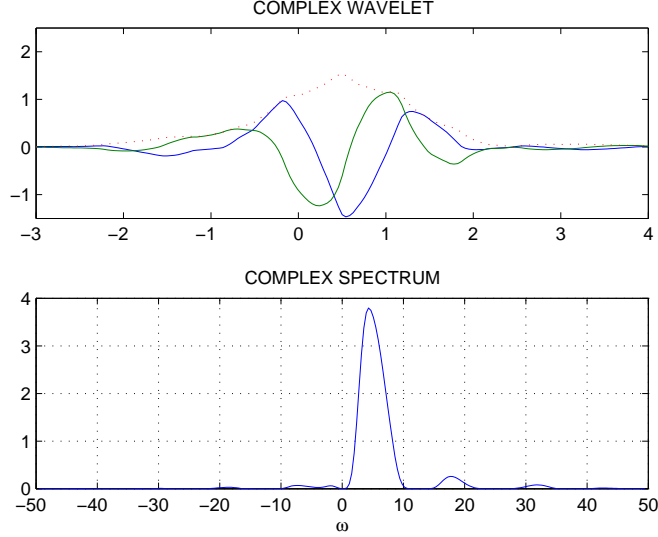


Figure 4.1: Impulse Response of Length 12 filters with 2 VMs Top: AES filter Bottom: AOS filter

where T is a constant and the resulting filters are called SSH filters [15],[94]. Bernstein polynomial was used to construct the product filter and it is given by

$$B_N(x; \kappa) = \sum_{i=0}^{N_b} f(i) \binom{N_b}{i} x^i (1-x)^{N_b-i} \quad (4.4)$$

and $f(i)$ is given by

$$f(i) = \begin{cases} 1 - \kappa_i & 0 \leq i \leq \frac{1}{2}(N_b - 1) \\ \kappa_{N_b-i} & \frac{1}{2}(N_b + 1) \leq i \leq N_b \end{cases}$$

where N_b is odd, $[\kappa \dots \kappa_{(N_b-1)/2}]^T$ are the Bernstein parameters. The equation (4.4) can be transformed into a z -transform filter by using the transformation

$$x = \frac{-1}{4} z (1 - z^{-1})^2 = \sin^2\left(\frac{\omega}{2}\right)$$

and it satisfies the half band filter condition (2.2). The desired number of VMs are imposed on the filters by setting the appropriate Bernstein parameters to zero. Some degrees of freedom can be made available by not setting few Bernstein parameters to zero. In [15], one degree of freedom was utilised to design SSH filters. In [85], two degrees of freedom was utilised to design SSH filters. A more versatile technique to design

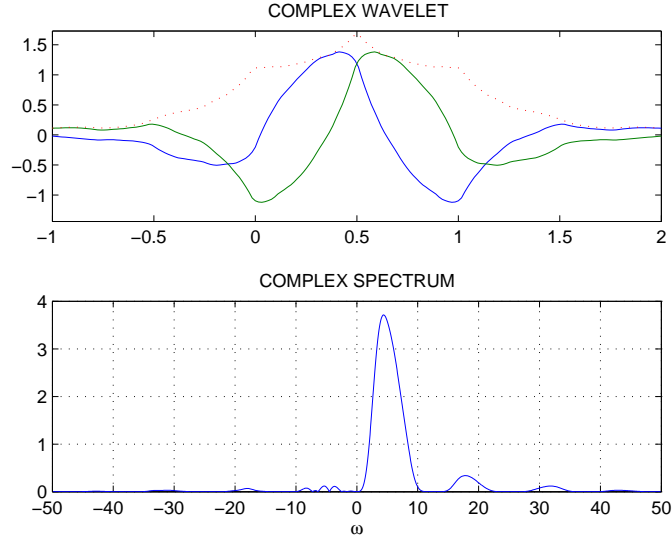


Figure 4.2: Impulse Response of Length 12 filters with 2 VMs Top: AES filter Bottom: AOS filter

SSH filters was proposed in [94] using lattice parameterisation. All of the design techniques [15],[85],[94] produced symmetric complex wavelet $\psi^C(t)$. However the individual wavelets $\psi^h(t)$ and $\psi^g(t)$ are not symmetric. It is difficult to design symmetric wavelets ($\psi^h(t)$, $\psi^g(t)$) because of tight coupling between the SSH filters to satisfy (4.2) and (4.3). A SSH filter of length 8 with 3 VMs is designed. The complex wavelet and complex spectrum are shown in Figure 4.2. The wavelets ($\psi^h(t)$, $\psi^g(t)$) are not symmetric as shown in Figure 4.2 (top). However the complex wavelet $\psi^C(t)$ is symmetric. The analytic quality measures are $E_1 = 3.06\%$ and $E_2 = 0.08\%$. The Q-shift filters [95],[16] are approximately linear phase filters but the filters' impulse response is not symmetric. In [16], a linearisation procedure was adopted to solve the constraints and the resulting filters approximately satisfy the PR condition. Both in [95] and [16] only simple VMs are imposed on the Q-shift filters. In [90], an iterative procedure is implemented to impose orthogonality with a tunable flat group delay response. However the Hilbert pair of wavelets have poor analytic quality.

4.3 Hilbert pair based on Almost Symmetric Filters

Filter symmetry is not a necessary requirement for constructing a Hilbert-pair. Symmetry is however a desirable property in many applications and we will show how to construct orthogonal Hilbert pairs using almost symmetric orthogonal filters. Concep-

tually the construction of a Hilbert pair can be viewed as the process of finding two filter banks that match each other through equation (4.2). The main idea behind the construction here is to match a filter having Type I characteristics (symmetric odd length) with a filter having Type II characteristics (symmetric even length). The details of how this is achieved will be described in this section.

To construct a Hilbert-pair of wavelets, we need two filters which satisfy the half sample delay condition (4.2). The complex valued equation (4.2) can be separated into magnitude and phase parts as follows:

$$|H_0^g(\omega)| = |H_0^h(\omega)| \quad (4.5)$$

$$\angle H_0^g(\omega) = -(\omega/2) + \angle H_0^h(\omega) \quad (4.6)$$

It is possible to satisfy either (4.5) or (4.6) exactly but not both simultaneously. With most of the reported orthogonal Hilbert-pair, e.g. common factor or SSH solution, (4.5) is exact and (4.6) is approximated. With the symmetric biorthogonal Hilbert-pair designed using the matching technique [91],[92],[93] (4.6) is exact and (4.5) is approximated. For these biorthogonal pairs bank h comprise of odd-length linear phase filters (Type I) and bank g comprise of even-length linear phase filters (Type II):

$$H_0^h(\omega) = h_0(0) + 2 \sum_{n \neq 0} h_0^h(n) \cos(n\omega) \quad (4.7)$$

$$H_0^g(\omega) = e^{-j\omega/2} H_{0,R}^g(\omega) \quad (4.8)$$

where $H_{0,R}^g(\omega) \equiv 2 \sum_n h_0^g(n) \cos((n - \frac{1}{2})\omega)$. Without any design effort equation (4.6) is exact due to the presence of the $e^{-j\omega/2}$ factor in $H_0^g(\omega)$ (inherent half-sample delay). The design effort is then to achieve $H_{0,R}^g(\omega) \approx H_0^h(\omega)$ to approximate (4.5). In the spatial domain equations (4.7) and (4.8) respectively imply the following relationships:

$$h_0^h(n) = h_0^h(-n)$$

and

$$h_0^g(n) = h_0^g(1 - n)$$

The center of symmetry is at $n = 0$ and $n = 1/2$ respectively.

Firstly, we address the phase requirement (4.6) because the phase approximation is more important than the magnitude approximation (4.5) as observed in [96]. Now a CQF $H_0(\omega)$ cannot be exactly symmetric except for the simple two coefficients filter

(corresponding to the Haar wavelet) [8]. However a CQF can be designed to have approximate symmetry (Refer Chapter 3) . As argued in the Chapter 3, since the CQF length is even ($L_f = 2L$), if the filter could hypothetically be symmetric, then it should be a Type II filter, i.e. $h_0(n) = h_0(1-n)$, where the left-half coefficients are mirror image of the right-half. A natural measure of deviation from this condition is $(h_0(n) - h_0(1-n))$ and the following asymmetry measure

$$E_{AES} \equiv \sum_{n=1}^L (h_0(n) - h_0(1-n))^2$$

was proposed in the Chapter 3. The design of CQFs approximating Type II filters in the Chapter 3 is achieved by minimizing E_{AES} subject to the VM constraints (2.3). These CQFs will also be referred to as AES (Almost-Even-Symmetric) filters and an example of AES impulse response is shown in Figure 4.3. What is now required to form an orthogonal Hilbert-pair is a CQF approximating a type I filter. This may seem rather counter-intuitive as the CQF is of even length and a type I filter is of odd length. To make an even length CQF filter look like a type I filter, the following points should be considered:

1. The first or last coefficient value ($h_0(-(L-1))$ or $h_0(L)$) should be close to zero (but cannot be exactly zero as this will violate the orthogonality condition). This makes the CQF look like an odd length filter. For convenience we choose the last coefficient, i.e. $h_0(L) \approx 0$.
2. The center of symmetry is then at $n = 0$ and the coefficient value $h_0(0)$ will not affect symmetry.
3. The coefficients to the left of $h_0(0)$ should ideally be mirror image of the coefficients to the right of $h_0(0)$. A natural deviation measure is then $(h_0(n) - h_0(-n))$ for $n = 1, \dots, (L-1)$.

These considerations lead to another asymmetry measure

$$E_{AOS} \equiv \sum_{n=1}^{L-1} (h_0(n) - h_0(-n))^2 + (h_0(L))^2$$

The design of CQFs approximating Type I filter, which will also be referred to as AOS (Almost-Odd-Symmetric) filters, can therefore be achieved by minimizing E_{AOS} subject to the VM constraints (2.3). There are also other methods for designing almost sym-

metric CQFs reported in the literature but they are indirect methods and are reviewed in the Chapter 3. The design of AES filter is detailed in the Chapter 3 of this thesis.

A pair of (AOS, AES) CQFs will therefore approximate the phase condition (4.6). However for a Hilbert-pair there is still the magnitude condition (4.5) to consider. Tay *et al.* [96] observed that the phase approximation is more crucial than the magnitude approximation for Hilbert-pairs. Serendipitiously it turns out that AES and AOS CQFs of the same length and having the same number of VMs have magnitude response that are reasonably close to each other. *In summary a reasonably good quality almost symmetric orthogonal Hilbert-pair can be obtained by designing a pair of (AOS, AES) CQFs with equal length and equal number of VMs.*

4.3.1 Optimisation Algorithm

The optimisation problem for the AOS filter is similar to that of the AES filter. The objective function E_{AOS} has a form similar to that in E_{AES} as both are quadratic in the filter coefficients $h_0(n)$. As shown in the Chapter 3 the objective function is algebraic and can be expressed as a ratio of multiquadratic functions of the lattice parameters. The constraint equations for VMs are multilinear in the lattice parameters as shown in (2.3). In Chapter 3 the Lagrange multiplier method was used and this required solving simultaneous multivariate polynomial equations. In this chapter a versatile non-linear optimizer based on the interior point method [72] is used instead (this algorithm is also used for further optimisation of the filters described in the next section). Matlab R2011b has an in-built function *fmincon* to implement the interior point algorithm that is used in this work. As argued in the Chapter 3 a suitable set of initial values are the lattice parameters derived from all the distinct spectral factors [1] of the maximum VM product filter. The best result is then taken as the final solution.

4.3.2 Design Examples

Example 1: Length $L_f = 12$ ($L = 6$) AES and AOS filter having 2 VMs each. The asymmetry measures of the AOS filter is $E_{AOS} = 1.2708 \times 10^{-8}$. The asymmetry measures of AES filter is $E_{AES} = 1.038 \times 10^{-5}$. The group delay measure (3.4) of the AES and AOS filter are 0.0047 and 9.06×10^{-5} respectively and they confirm that both the filters have approximately flat group delay responses. The impulse response of the AES and AOS filters are shown in Figure 4.3 and look virtually like Type II and I filters respectively. The magnitude response and phase difference of the filters shown in Fig-

Figure 4.4 confirms that the magnitude responses are approximately equal and the phase difference is approximately -0.5ω . Figure 4.5 (top) shows the plot of $\psi^h(t)$, $\psi^g(t)$ and complex envelope that are virtually symmetric. The complex wavelet spectrum shown in Figure 4.5 (bottom) is approximately analytic with quality measures $E_1 = 4.28\%$ and $E_2 = 0.26\%$. The filter coefficients are given in Table 4.1.

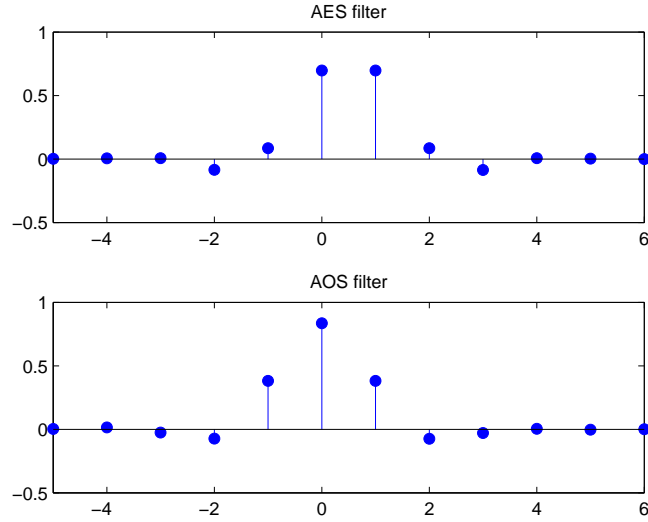


Figure 4.3: Impulse Response of Length 12 filters with 2 VMs Top: AES filter Bottom: AOS filter

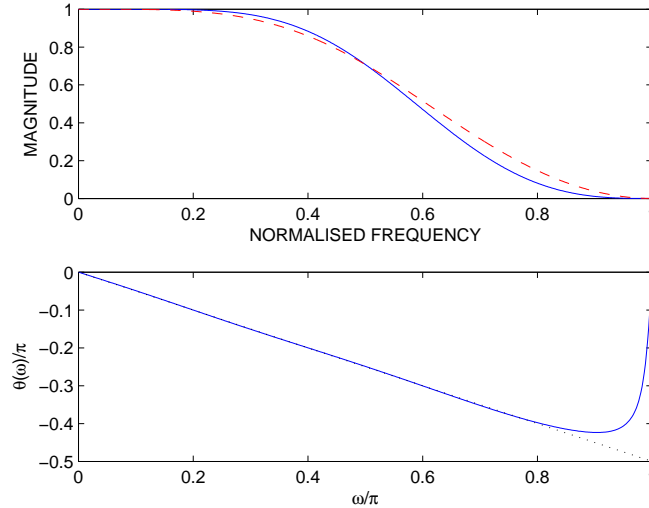


Figure 4.4: Top: Magnitude response of the length 12 filters having 2 VMs. Solid line: AES filter. Dotted line: AOS filter. Bottom: Phase difference between filters

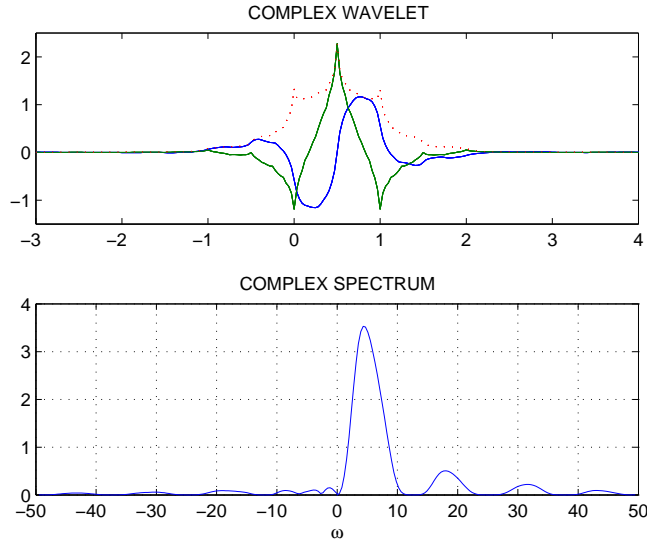


Figure 4.5: Top: Wavelet functions $\psi^h(t)$, $\psi^g(t)$ and $|\psi^C(t)|$. Bottom: Spectrum of complex wavelet

Example 2: Length $L_f = 16$ ($L = 8$) AES and AOS filter having 4 VMs each. The asymmetry measures of the AOS filter is $E_{AOS} = 1.5573 \times 10^{-6}$. The asymmetry measures of AES filter is $E_{AES} = 2.97 \times 10^{-4}$. The group delay measure (3.4) of the AES and AOS filter are 0.0240 and 0.0017 respectively and they confirm that both the filters have approximately flat group delay responses.

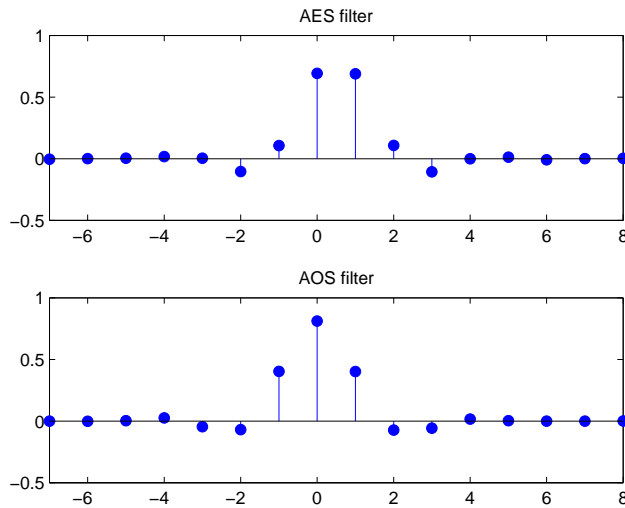


Figure 4.6: Impulse Response of Length 16 filters with 4 VMs Top: AES filter Bottom: AOS filter

The impulse response of the AES and AOS filters are shown in Figure 4.6 and look virtually like Type II and I filters respectively. The magnitude response and phase difference of the filters shown in Figure 4.7 confirms that the magnitude responses are approximately equal and the phase difference is approximately -0.5ω . Figure 4.8 (top) shows the plot of $\psi^h(t)$, $\psi^g(t)$ and complex envelope that are virtually symmetric. The complex wavelet spectrum shown in Figure 4.8 (bottom) is approximately analytic with quality measures $E_1 = 3.20\%$ and $E_2 = 0.06\%$. The filter coefficients are given in Table 4.1.

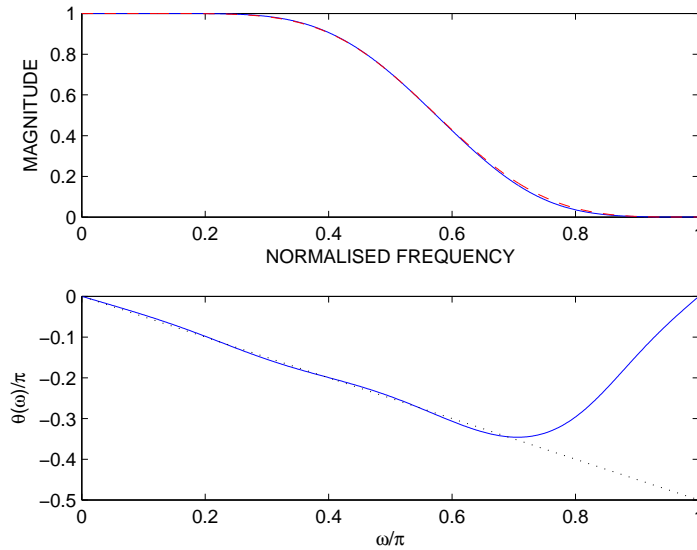


Figure 4.7: Top: Magnitude response of the length 16 filters having 4 VMs. Solid line: AES filter. Dotted line: AOS filter. Bottom: Phase difference between filters

We have demonstrated that reasonable analytic quality Hilbert pairs can be achieved by designing AES and AOS filters independently. There is a natural matching between an AES filter and an AOS filter *with the same length and number of VMs*. Good approximation to the phase condition (4.6) is achieved between the AES and AOS filters but no effort is expended to address the magnitude condition (4.5). Both AES and AOS filters generate virtually symmetric wavelets and have approximate linear phase characteristics. In the next section, we will show how to achieve a better analytic quality without sacrificing the symmetry of the constituent wavelets.

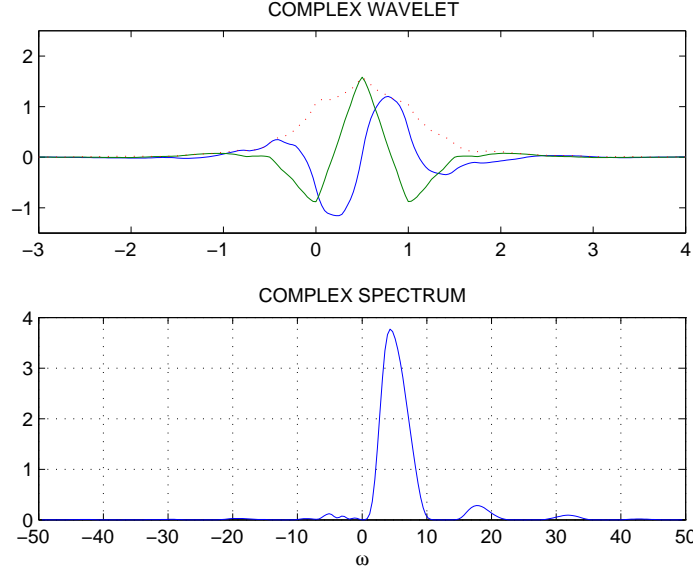


Figure 4.8: Top: Wavelet functions $\psi^h(t)$, $\psi^g(t)$ and $|\psi^C(t)|$. Bottom: Spectrum of complex wavelet

Table 4.1: Filter Coefficients

$2L$	p	filters	Filter Coefficients
12	2	H_0^h	0.00160560,0.00493665,0.00635809,-0.08554776, 0.08525574,0.69674039,0.69655625,0.08544623, -0.08575320,0.00653442,0.00308431,-0.00100314
		H_0^g	0.00012419,0.00144803,-0.01093270,-0.07322610, 0.36435607,0.85060655,0.36434595,-0.07320559, -0.01096065,0.00149880,0.00017391,-0.00001492
16	4	H_0^h	-0.00361061,0.00042545,0.00465890,0.01704841, 0.00436633,-0.10378041,0.10600279,0.69252738, 0.68916438,0.10772591,-0.10610459,-0.00040167, 0.01230589,-0.00918527,0.00032368,0.00274698
		H_0^g	-0.00064071,-0.00143886,0.00303102,0.02040218, -0.05102552,-0.07205762,0.40181545,0.81275607, 0.40190044,-0.07220073,-0.05087235,0.02033099, 0.00304235,-0.00074932,-0.00014389,0.00006407

4.4 Improved Analyticity Design

In section 4.3 the AES and AOS filters are designed independently. No attention was paid to the magnitude condition (4.5) and all effort was used to make the phase condition

(4.6) to be as close as possible. The analytic quality however depends on both the degree of magnitude and phase approximations, although the latter condition is more crucial as observed in [96]. By relaxing the phase approximation, a better magnitude approximation can be achieved. By allowing the trade-off between magnitude and phase approximations there is the possibility of achieving a better overall result in terms of analytic quality.

A. Design via successive re-optimisation

Suppose we have designed a pair of AES and AOS filters using the technique described in section 4.3. We fix the AES filter and re-optimize the AOS filter using the procedure described next. Define the magnitude error measure as

$$G = \int_0^\pi (|H_0^h(\omega)| - |H_0^g(\omega)|)^2 d\omega$$

The optimisation problem is

O_1 : minimize G subject to equality constraints (2.3) and inequality constraint

$$E_{AOS} \leq E_{tol} \tag{4.9}$$

where the parameter E_{tol} determines the degree of asymmetry (compared to a Type I filter) tolerable and implicitly determines the degree of approximation to the phase condition (4.6). The value E_{tol} cannot be too small or else O_1 is infeasible. The smallest possible tolerance $E_{tol,min}$ is the E_{AOS} value of the filter designed using the optimisation described in section 4.3. When $E_{tol} = E_{tol,min}$, the solution to O_1 is the same as that obtained in section 4.3 which has the best phase approximation. As E_{tol} is progressively increased the optimizer has more freedom to reduce the magnitude error measure G . In the other extreme case when (4.9) is not imposed (or when E_{tol} is sufficiently large), the optimizer will give a solution with the best magnitude approximation (smallest possible G). Somewhere between these two extremes will be a solution with the lowest E_1 (or E_2) value. O_1 is effectively magnitude matching, but unlike the matching technique in [92],[91], there is the constraint (4.9) in the former (that controls the degree of asymmetry) and there is no constraint in the latter (as the filters have structural symmetry (Type I/II)).

The design procedure is then as follows:

1. Generate a sufficiently fine grid of E_{tol} values $\{E_{tol,m} : m = 1, \dots\}$ over the range $[E_{tol,min}, E_{tol,max}]$. The $E_{tol,max}$ is the E_{AOS} value using the solution to O_1 without (4.9).
2. Use the lattice coefficients of the AOS filter from section 4.3 (least asymmetric) as the initial solution α^0 . Set $m = 1$.
3. Solve O_1 with $E_{tol} = E_{tol,m}$ to give the solution α^m .
4. Increase m by 1 and repeat the previous step with the latest solution as the initial point.
5. Choose the solution which gives the lowest E_1 measure (best analytic quality).

The interior point algorithm implemented in the Matlab R2011b *fmincon* function is used here to solve O_1 . Each O_1 optimisation in step 3 converges quickly because the initial point used is close to the optimal solution (for that particular iterate) since the increment in E_{tol} is small. In effect we are slowly allowing the magnitudes to match by allowing the filter to be less symmetric, i.e. relaxation. In all our simulations it was observed that $E_{AOS} = E_{tol}$ at the optimal solution for each O_1 , i.e. the optimizer yields a solution that is at the upper bound of (4.9).

In our design procedure described above one filter (AES) is fixed while the other (AOS) is re-optimized. It could be argued that if both filters are re-optimized simultaneously a better analytic quality could be achieved. There are two reasons for not adopting this approach here. They are

1. The design process would be more complex and computationally intensive.
2. The resulting filter pair may end up not have the Type I/II symmetry properties (symmetry is not a necessary condition for analyticity).

If both filters are allowed to change (through re-optimisation) there will be a drift away from symmetry to achieve higher analytic quality. Achieving symmetry however is one of the main aim of this work. Fixing one filter with a high degree of symmetry is like having an anchor that will prevent the other filter from drifting too far from symmetry. The approach adopted here gave high analytic quality filters with good symmetry as the next examples will show.

If the symmetry of the filters are not important both the AES and AOS filters can be re-optimised to get a better analytic quality but the resulting filters will not be symmetric. The below are the design examples where the optimisation technique O_1 is deployed.

Example 3: Length $L_f = 12$ ($L = 6$) AES and AOS filter having 2 VMs each from example 1. The AOS filter is re-optimized using the procedure described above with $[E_{tol,min}, E_{tol,max}] = [1.2708 \times 10^{-8}, 0.2382]$. The plot of G vs E_{tol} and E_1 vs E_{tol} are shown in Figure 4.9, top and bottom, respectively.

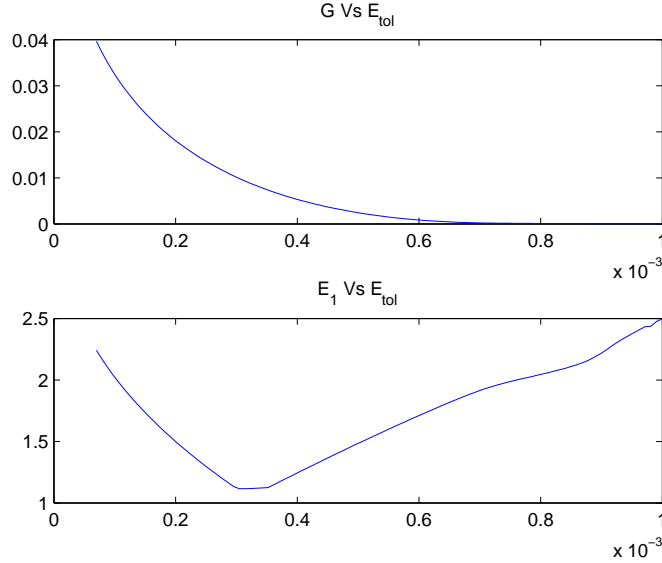


Figure 4.9: Top: Plot of G Vs E_{tol} . Bottom: Plot of E_1 Vs E_{tol} .

The top figure shows that better matching of magnitude is achieved at the expense of greater asymmetry. i.e. The magnitude error G decreases when E_{tol} is increased. The bottom figure shows that there is a point of optimal trade-off between magnitude and phase where the analytic quality measure E_1 is the lowest. The optimal trade-off between magnitude and phase is when $E_{AOS} = E_{tol} = 3.058 \times 10^{-4}$ and the corresponding filter impulse and magnitude response (AES filter also shown) is shown in Figure 4.10. Though more asymmetric than example 1, the impulse response is still very close to a Type I filter and the magnitude is now more closely matched (compared with Figure 4.4 in *Example 1*). The analytic quality measures are $E_1 = 1.11\%$ and $E_2 = 0.02\%$ and are much lower than in example 1 ($E_1 = 4.28\%$ and $E_2 = 0.26\%$). The designed filter coefficients are given in Table 4.2. The computation time for successive re-optimisation is 96.2 seconds.

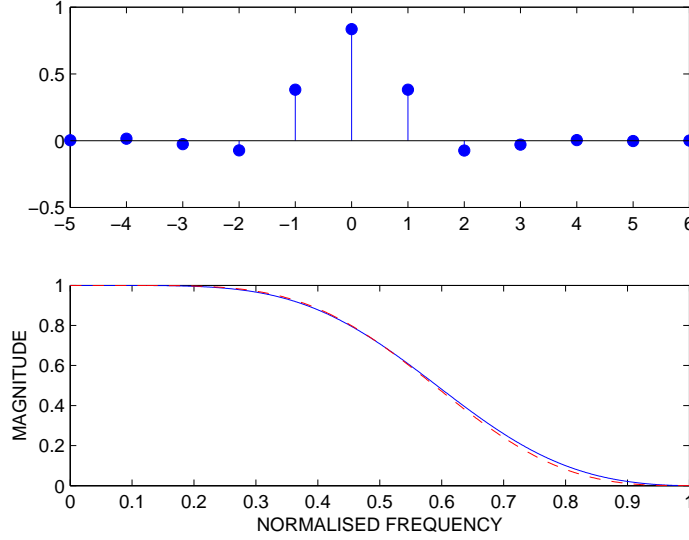


Figure 4.10: Top: Impulse response of the designed AOS filter. Bottom: Magnitude response of the filters. Solid line: AES filter. Dotted line: Designed AOS filter.

Example 4: Length $L_f = 16$ ($L = 8$) AES and AOS filter having 2 VMs each from example 2. The AOS filter is re-optimized using the procedure described above with $[E_{tol,min}, E_{tol,max}] = [1.5573 \times 10^{-6}, 0.0215]$. The plot of G vs E_{tol} and E_1 vs E_{tol} are shown in Figure 4.11, top and bottom, respectively. Again we see that better magnitude matching is achieved at the expense of greater asymmetry. The optimal trade-off between magnitude and phase is when $E_{AOS} = E_{tol} = 5.09 \times 10^{-4}$. The corresponding filter impulse and magnitude response (AES filter also shown) is shown in Figure 4.12. The impulse response is still very close to a Type I filter. The analytic quality measures are $E_1 = 0.989\%$ and $E_2 = 0.0112\%$ and are much lower than in *Example 2* ($E_1 = 3.20\%$ and $E_2 = 0.06\%$). The designed filter coefficients are given in Table 4.2. The computation time for successive re-optimisation is 62.8 seconds.

Table 4.2: Filter Coefficients

$2L$	p	filters	Filter Coefficients
12	2	H_0^g	0.00303403,0.01451398,-0.02592825,-0.07299089, 0.38113782,0.83474245,0.38122497,-0.07400154, -0.02974712,0.00429620,-0.00261467,0.00054658
16	4	H_0^g	-0.00045952,-0.00216164,0.00350992,0.02585192, -0.04632786,-0.07013765,0.40344306,0.81170503, 0.40193836,-0.07365016,-0.05808553,0.01591663, 0.00334873,-0.00047269,-0.00026038,0.00005535

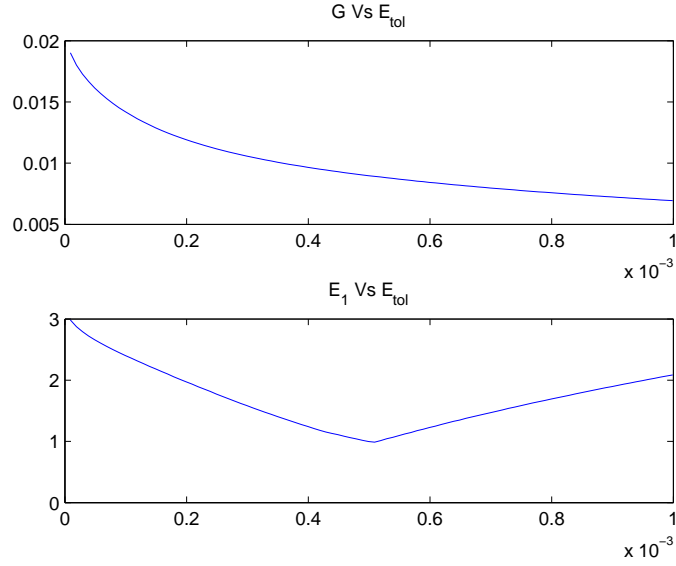


Figure 4.11: Top: Plot of G Vs E_{tol} . Bottom: Plot of E_1 Vs E_{tol} .

B. Fine tuning optimisation

The optimisation procedure described in section 4.4.A gives filters with good analytic quality but does not directly minimize the E_1 (or E_2) measure. A further re-optimisation with respect to E_1 can improve the analyticity. The optimisation problem is

$$O_2: \text{minimize } E_1 \text{ subject to equality constraints (2.3)}$$

using the lattice coefficients from the procedure in section 4.4.A as the initial solution. This optimisation can be considered as a fine tuning of the solution from O_1 and is similar in principle to the two stage optimisation strategy proposed in [94] for SSH filters. In the first stage the optimisation is with respect a measure that is based on the half-sample-delay condition (4.2). In the second stage the optimisation is with respect to the E_1 measure which is based on the Hilbert transform relationship (4.1). Convergence is fast as the initial point is already close to the optimal point. The interior point algorithm implemented in the Matlab R2011b *fmincon* function is used as the solver here.

In summary the design procedure consist of the following steps:

1. Choose the length L_f and number of VMs p of the filter. Design a pair of (AES, AOS) filters using the procedure described in section 4.3.
2. Re-optimisation of the AOS filter through a sequence of O_1 as described in section 4.4.

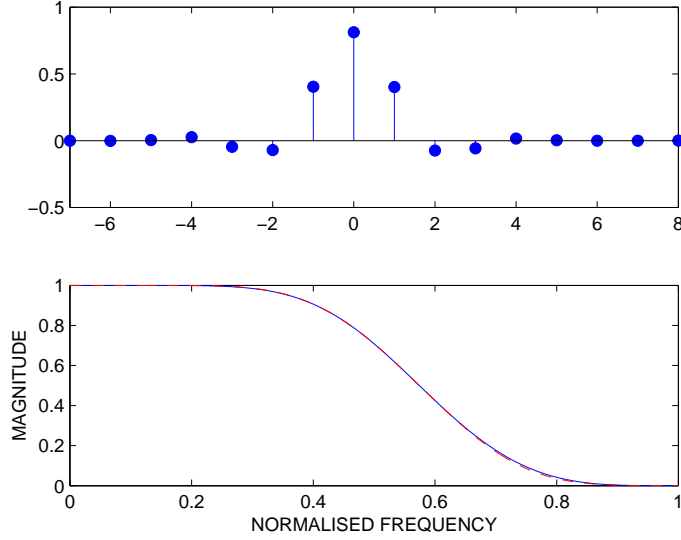


Figure 4.12: Top: Impulse response of the designed AOS filter. Bottom: Magnitude response of the filters. Solid line: AES filter. Dotted line: Designed AOS filter.

3. Fine tune the solution using O_2 described above.

Step 2 (Step 3) is optional if one is satisfied with the analytic quality of the filter from step 1 (step 2). Steps 2 and 3 can be performed on the AES filter instead of the AOS filter.

Even though there are several steps in the design procedure the whole process is quite efficient computationally as each re-optimisation converges quickly. This is because the initial point used is close to the optimal solution. The algorithms were tested on a quad-core personal computer (Intel i7 2.66 GHz) running MATLAB [7.9.0.529 (R2009b)] for filters with length up to 40 without any problems.

In the next two examples all three steps are performed and the analytic quality from steps 2 and 3 are compared.

Example 5: Length $L_f = 14$ ($L = 7$) AES and AOS filter having 3 VMs each. After step 2 the analytic quality measures are $E_1 = 2.33\%$ and $E_2 = 0.08\%$. After step 3, the analytic quality improved with $E_1 = 1.70\%$ and $E_2 = 0.04\%$. The filter coefficients are given in Table 4.3. The plot of the wavelet functions and spectra is shown in Figure 4.13. The computation time for optimisation, successive re-optimisation and fine tuning optimisation are 1.4 seconds, 68.2 seconds and 1.2 seconds respectively. The total time taken is 70.5 seconds.

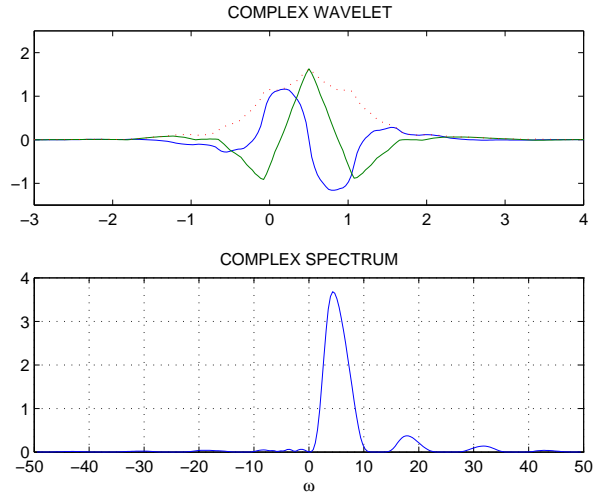


Figure 4.13: Top: Wavelet functions $\psi^h(t)$, $\psi^g(t)$ and $|\psi^C(t)|$. Bottom: Spectrum of complex wavelet

Example 6: Length $L_f = 20$ ($L = 10$) AES and AOS filter having 6 VMs each. After step 2 the analytic quality measures are $E_1 = 2.42\%$ and $E_2 = 0.06\%$. After step 3, the analytic quality improved with $E_1 = 1.21\%$ and $E_2 = 0.01\%$. The filter coefficients are given in Table 4.3. The plot of the wavelet functions and spectra is shown in Figure 4.14. The computation time for optimisation, successive re-optimisation and for fine tuning optimisation are 10.1 seconds, 3.8 minutes and 2.4 seconds respectively. The total time taken is 4 minutes.

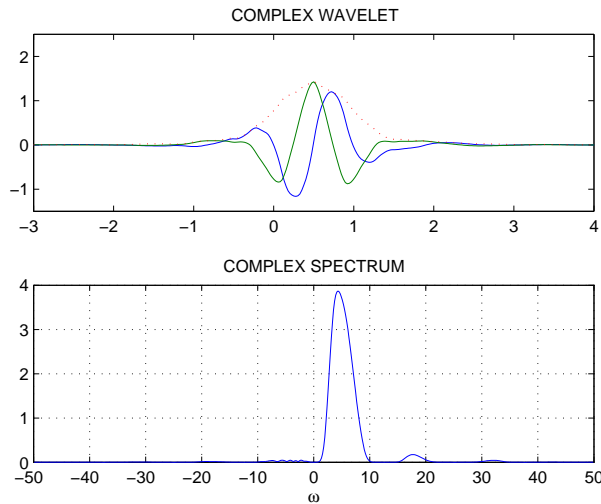


Figure 4.14: Top: Wavelet functions $\psi^h(t)$, $\psi^g(t)$ and $|\psi^C(t)|$. Bottom: Spectrum of complex wavelet

Table 4.3: Filter Coefficients (optimised w.r.t E_1)

$2L$	p	filters	Filter Coefficients
14	3	H_0^h	-0.00034319,0.00034828,0.00589591,0.00539939, -0.08765245,0.08777421,0.69588721,0.69634686, 0.08746862,-0.08764890,0.00582341,0.00486007, 0.00002727,0.00002687
		H_0^g	-0.00077112,-0.00278968,0.01022038,-0.05386629, -0.06878604,0.41331752,0.81716199,0.38179201, -0.07760906,-0.03471922,0.02569016,0.00370428, 0.00120048,-0.00033184
20	6	H_0^h	0.00156092,-0.00051647,-0.00508258,-0.00158263, 0.00175643,0.02742896,0.00220967,-0.11308369, 0.12019887,0.68855283,0.68485517,0.11984911, -0.11780121,-0.00856934,0.02032843,-0.00916655, -0.00055393,0.00529762,-0.00036497,-0.0011030
		H_0^g	0.00018093,0.00045517,-0.00204006,-0.00965610, 0.01007714,0.03818336,-0.06044400,-0.06411582, 0.41387464,0.79552855,0.41720583,-0.07095943, -0.08274220,0.01931267,0.01008973,-0.00162496, 0.00099157,-0.00005117,-0.00008681,0.00003451

A high degree of symmetry is still observed in the wavelets even after re-optimisation. It can be inferred from the Example 5 and Example 6 that the fine tuning optimisation takes only few seconds because the initial point supplied to the optimisation routine O_2 is very close to the optimal solution.

4.5 Hilbert pair of wavelet with different VMs

In this section we construct the Hilbert pair of wavelets with different number of VMs. The AES filter and AOS filter will have same length but have different number of VMs. Firstly the AES filter having desired VMs is designed using the procedure described in Chapter 3. We then design the AOS filter (having one VMs less than the AES filters) using the procedure described in the Section 4.3. Because the AOS and AES filter have different number of VMs, their frequency response will be different. In this scenario, the optimisation sequence O_1 is performed. Because the AOS filter has one VM less than the AES filter, there is one more degree of freedom available to match the frequency response of the AOS filter with the AES filter.

Firstly we will design the AES and AOS filter having same number of VMs first and

then we will re-optimize the AOS filter. During the re-optimization process, we impose one less VM compared to the AES filter. We will then compare the analytic measure and filter symmetry.

Step 1: Length $L_f = 12$ ($L = 6$) AES and AOS filter having 3 VMs each. After the O_1 optimization, the asymmetry measures of the AOS filter and the AES filter are $E_{AOS} = 7.182 \times 10^{-4}$ and $E_{AES} = 1.113 \times 10^{-5}$ respectively. The analytic measure after O_1 optimization is $E_1 = 3.67\%$ and $E_2 = 0.10\%$ respectively. The plot of the wavelet functions and spectra is shown in Figure 4.15.

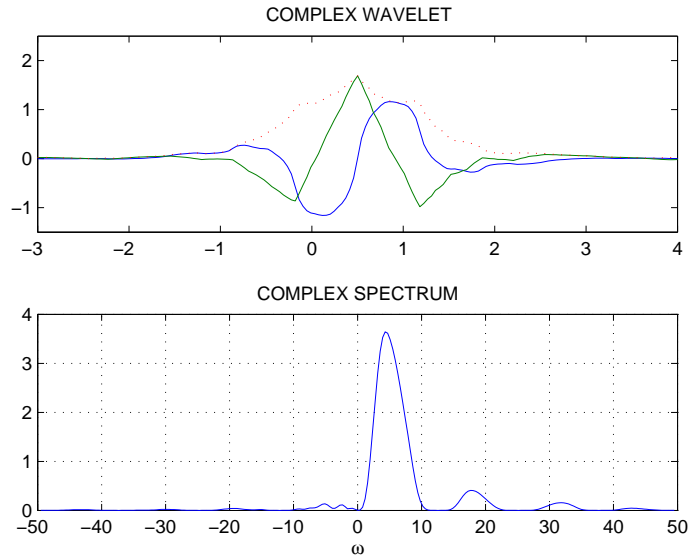


Figure 4.15: Top: Wavelet functions $\psi^h(t)$, $\psi^g(t)$ and $|\psi^C(t)|$. Bottom: Spectrum of complex wavelet

After O_2 fine tuning optimization, the analytic quality improved with $E_1 = 1.35\%$ and $E_2 = 0.03\%$.

Step 2: The AES filter (having 3 VMs) is fixed while AOS filter is constrained to have only 2 VMs during the O_1 optimization. After the O_1 optimization, the asymmetry measures of the AOS filter and the AES filter are $E_{AOS} = 3.182 \times 10^{-4}$ and $E_{AES} = 1.113 \times 10^{-5}$ respectively. The analytic measure after O_1 optimization is $E_1 = 1.10\%$ and $E_2 = 0.02\%$ respectively. The plot of the wavelet functions and spectra is shown in Figure 4.16.

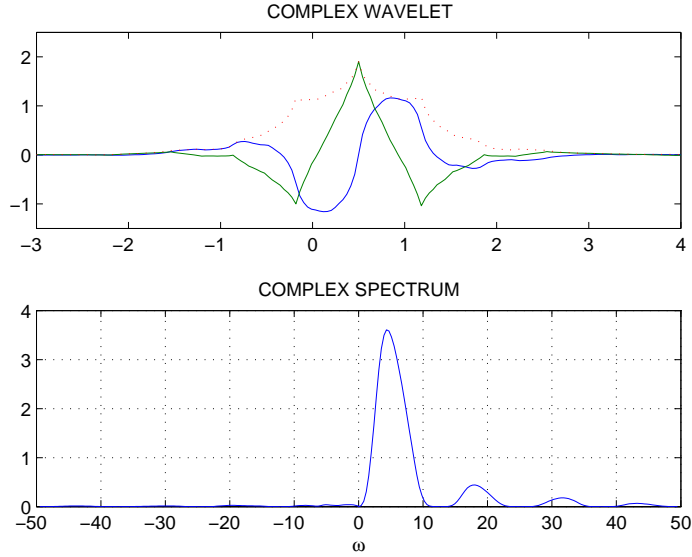


Figure 4.16: Top: Wavelet functions $\psi^h(t)$, $\psi^g(t)$ and $|\psi^C(t)|$. Bottom: Spectrum of complex wavelet

After O_2 fine tuning optimisation, the analytic quality improved with $E_1 = 0.51\%$ and $E_2 = 0.006\%$.

Comparison of step 1 and step 2: The E_{AOS} measure of the filter in step 2 is smaller compared to step 1. The additional degree of freedom available in step 2 (because of reduction of 1 VM) improved the symmetry of the filter of the AOS filter. The analytic measures in step 2 are the best compared to step 1.

4.6 Discussion and Comparison

In the signal processing literature linear phase response in the frequency domain is usually taken to imply symmetry in the time (or spatial) domain and vice versa. This however needs to be carefully examined in the context of digital filters. The impulse response symmetry in Type I/II filters is given by $h_0(n) = h_0(M - n)$ where M must be an integer [1] (there is no such restriction however for analog continuous time filters). The group delay is $M/2$ must either be an integer or integer plus half. Digital filters can have approximately linear phase but with a group delay that is *NOT* approximately an integer or integer plus half and therefore do not have approximate symmetry.

With the SSH (and Q-shift) filters $H_0(e^{j\omega}) \approx A(\omega)e^{j\omega(d-1/4)}$ (d integer and $A(\omega)$ the real valued amplitude function) and the group delay is an integer plus one quarter

[97]. Therefore, even though the SSH filter has approximately linear phase response, the impulse response $h_0(n)$ (and hence the wavelet function) is not approximately symmetric. The equivalent SSH complex wavelet

$$\psi^C(t) \equiv \psi^h(t) + j\psi^g(t)$$

envelope is however symmetric, i.e. $|\psi^C(t)| = |\psi^C(T - t)|$ (T constant). With the new class of Hilbert-pairs the constituent wavelets and envelope are approximately symmetric, i.e.

$$\psi^h(t) \approx \pm\psi^h(T - t)$$

$$\psi^g(t) \approx \mp\psi^g(T - t)$$

and

$$|\psi^C(t)| \approx |\psi^C(T - t)|$$

Symmetric filters (wavelets) imply phase linearity but the converse is not true.

Example 7: The length 14 Q-shift filter having 2 VMs from [95] is compared with the AES/AOS filters with same length and number of VMs. Figure 4.17 show that the AES and AOS filters have significantly more symmetric impulse response than the Q-shift filter.

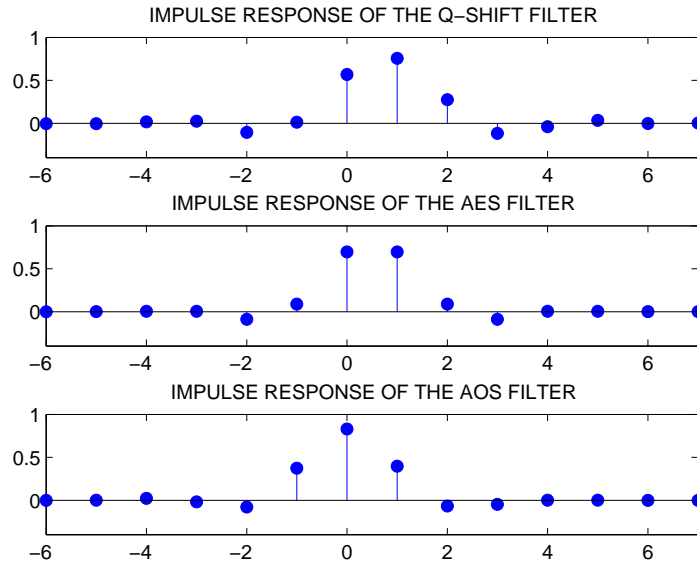


Figure 4.17: Impulse Responses of Length 14 filters having 2 VMs. Top: Q-shift filter. Middle: AES filter Bottom: AOS filter

Figure 4.18 shows the corresponding wavelet functions. If a wavelet function is symmetric, then $\psi(t) = \pm\psi(\Delta - t)$ (+ for even-function and $-$ for odd-function) for an appropriate Δ value. A measure of asymmetry can therefore be defined as

$$\psi_{sym} = \int_{-\infty}^{\infty} |\psi(t) \mp \psi(\Delta - t)| dt$$

where

$$\Delta = \operatorname{argmin}_{\delta} \int_{-\infty}^{\infty} |\psi(t) \mp \psi(\delta - t)| dt$$

The ψ_{sym} value with the AES and AOS filters are 3.13×10^{-4} and 0.0081 respectively compared with the ψ_{sym} value of 0.0512 with the Q-shift filter. The wavelets for the AES/AOS filters are significantly more symmetric than the Q-shift wavelets. The analytic quality measures with the AES/AOS (Q-shift) filter pair are $E_1 = 1.29\%(1.46\%)$ and $E_2 = 0.02\%(0.03\%)$. The analytic quality of the AES/AOS filters is better than Q-shift filters.

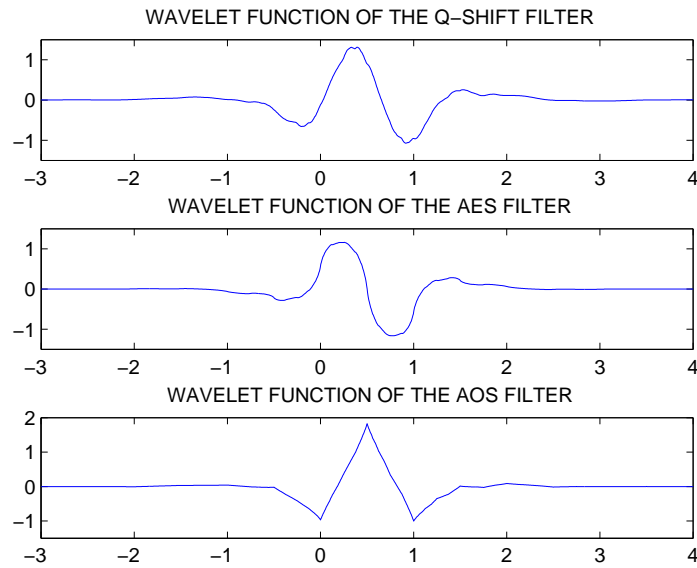


Figure 4.18: Wavelet Function. Top: Q-shift filter. Middle: AES filter. Bottom: AOS filter

Example 8: The length 16 filter having 4 VMs designed using common factor technique [14] is compared with the AES/AOS filters with same length and number of VMs. Figure 4.19 show that the AES and AOS filters have significantly more symmetric impulse response than the Q-shift filter.

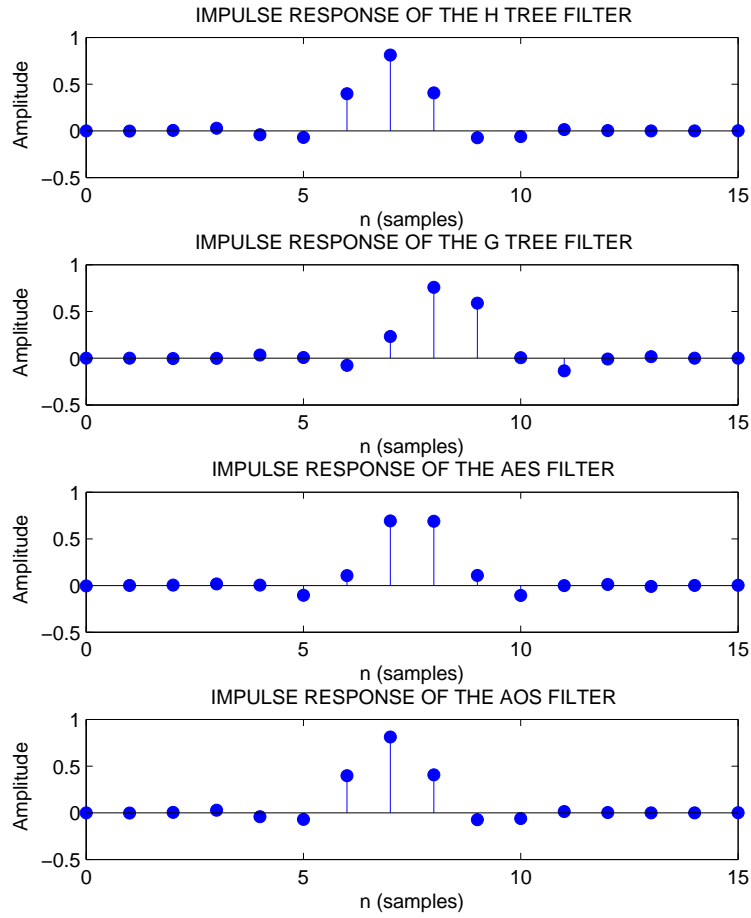


Figure 4.19: Impulse Responses of Length 16 filters having 4 VMs

The ψ_{sym} value with the AES and AOS filters are 0.0104 and 0.0091 respectively compared with the ψ_{sym} value of 0.0504 and 0.0545 with the filters designed using common factor technique. The analytic quality measures with the AES/AOS (filters designed using common factor technique) filter pair are $E_1 = 0.79\%(0.48\%)$ and $E_2 = 0.01\%(0.03\%)$. Figure 4.20 shows that the AES and AOS filters have significantly more symmetric wavelet functions than the filters designed using common factor technique.

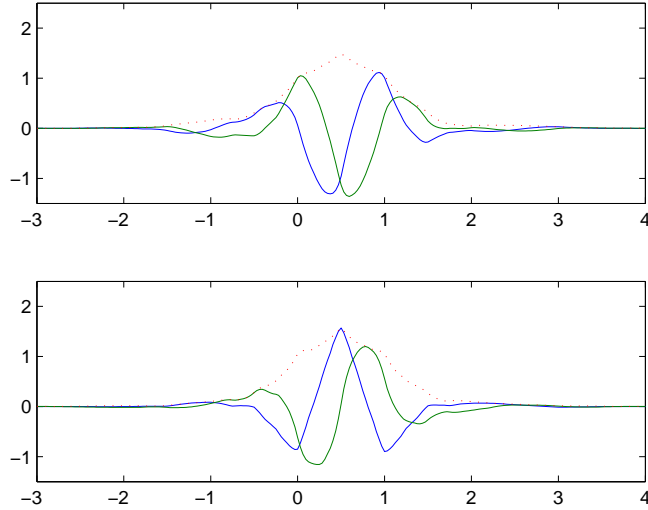


Figure 4.20: Wavelet functions $\psi^h(t)$, $\psi^g(t)$ and $|\psi^C(t)|$. Top: Filters designed using common factor technique. Bottom: filters designed using the optimisation O_2

All the above examples prove that the Hilbert pair of wavelets designed using the proposed technique are more symmetric. The Hilbert pair of filters has approximately linear phase and has flat group delay responses. These filters also have good analytic measures.

4.7 Conclusion

A new class of Hilbert-pair of wavelets that are exactly orthogonal but also virtually symmetric has been presented here. The corresponding filters are almost like Type I/II filters (symmetric linear phase odd/even length filters) and have the advantages of both biorthogonal and orthogonal systems. The direct design of these almost Type I/II filters was first presented which yielded reasonably good quality Hilbert-pairs. We then presented an efficient technique to improve the analyticity of the initial design by successive re-optimisation. The technique simultaneously approximate both the phase and amplitude response requirement of the half-sample-delay relation (4.2). The Hilbert of filters having different VMs can also designed easily using the proposed technique. The design examples show that almost symmetric Hilbert-pair of wavelets with good analytic quality can be designed easily.

5 Application of Hilbert pair of wavelets in denoising

Analysis of Mass Spectroscopy (MS) data provides information about proteins. Efficient identification of proteins enables clinicians to make accurate diagnosis of diseases such as cancer and bio-scientist to develop more targeted drugs. The MS data size is large and it is corrupted by noise. The MS/MS spectrum will reveal the amino acid sequence of the peptide. In this chapter, an efficient algorithm is presented to remove the noise in the MS/MS data and to detect peaks. The Dual Tree Discrete Wavelet Transform (DTCWT) using the almost symmetric filters will be applied to analyse the MS/MS data. The DTCWT is tolerant to shift in the MS/MS data. The algorithms based on the DTCWT performed better compared to the traditional DWT and Stationary Wavelet Transform (SWT). We will also apply the DTCWT to denoise the image. In image processing applications, the almost symmetric Hilbert pair of wavelets preserves salient features in the image as it offer higher directionality.

5.1 Introduction

The DTCWT has been applied extensively in many research fields especially in signal processing. In bioinformatics applications wavelet transform is widely used as it provides sparse representation of signals and has ability to detect specific information from the signal (signal burst). The multiresolution analysis feature of the wavelet transform is one of the main reason for its popularity in bioinformatics applications. The DWT has been applied during the preprocessing stage in proteomics applications [98],[99],[18],[100],[101]. The undecimated DWT is also applied in some proteomics preprocessing stages [18]. However undecimated DWT is not a widely used transform because it requires more computation time compared to the DWT. The alternative to undecimated DWT is the DTCWT. The DTCWT is less redundant compared to undecimated DWT and it is nearly shift invariant. The DTCWT is resilient to the shifts in the signal. In this chap-

ter we apply the DTCWT using the almost symmetric Hilbert pair filters to denoise the MS/MS scans. In the later part of this chapter, we also apply the almost symmetric Hilbert pair of wavelet in image denoising application to demonstrate its higher directionality and robustness in preserving the salient features in the images.

The chapter is outlined as follows. Section 5.2 will introduce to the field of MS based proteomics. Application of the almost symmetric Hilbert pair of wavelets for peptide identification in MS/MS spectrum is presented in Section 5.3. The image denoising application of almost symmetric Hilbert pair of wavelets is presented in Section 5.4. The chapter concludes in Section 5.5.

5.2 Mass Spectroscopy

Proteomics is a study of proteins in the cells and tissues. The proteome gives the sequences of all the proteins in a cell and thus proteomics can be broadly defined as the study of proteins. The main aims of proteomics experiments are

- To study interrelation between protein expressions and certain sample groups
- To study relationships between protein themselves

Proteins are made up of different amino acids. Proteins may contain several thousands of amino acids structure. The amino acids subunits are joined by amide linkages called peptide bonds. A peptide is a compound containing two or more amino acids linked by amide bonds between the amino group of each amino acid and the carboxyl group of the neighboring amino acid. Proteins can be fragmented into peptides and peptides can be fragmented into to amino acids structure. Mass Spectroscopy (MS) is a widely used technique in molecular biology (see [17] for a review) for high throughput identification and sequencing of peptides (and proteins). The basic principle behind MS in proteomics is to fragment complex protein molecules via soft-ionization techniques into smaller molecules such as peptides or amnio acids so they are more readily analyzed. The fragmented ions are separated according to their mass to charge ratio (m/z). There are two main soft-ionization techniques

1. ESI (Electrospray Ionization)
2. MALDI (Matrix-Assisted Laser Desorption/Ionization)

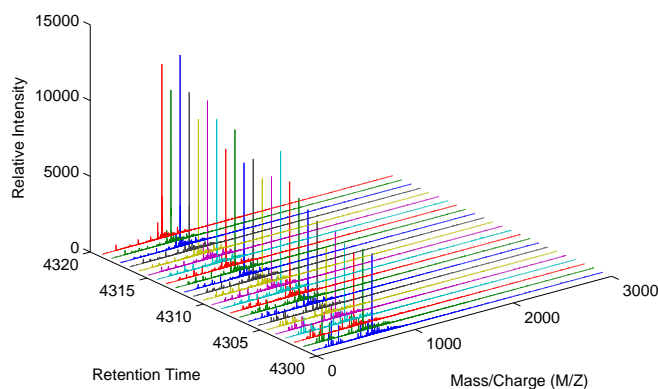


Figure 5.1: Plot of a m/z versus retention time

Peptides with lower molecular mass is favoured by ESI whereas larger molecular weight peptides can be analysed by MALDI. The MALDI process does not favor the identification of hydrophobic peptides. In a typical MS experiment, the protein samples are prepared and they are mixed with an enzyme. The common enzyme that is used in MS process is trypsin. Trypsin digest the proteins into peptides. The protein samples are then injected into Liquid Chromatography (LC) device and peptides with similar amino acids composition will elute at similar retention times. In LC-MS the liquid that elutes from the column is directly introduced into a mass spectrometer and the mass spectral measurements can be obtaining for certain retention time. In the mass spectrometer, the abundance of ions at each m/z value is measured. An example plot of m/z value versus retention time is shown in Figure 5.1. The data generated in a MS experiment is a series of scans where each scan consists of a plot of intensity (representing abundance) versus m/z (mass of molecule to electric charge ratio). An example scan is shown in Figure 5.2. Tandem mass spectrometry is a specialised mass spectrometry technique whereby the sequence of peptides can be determined. Tandem mass spectrometry is also called as MS/MS. In MS/MS technique, peptide ions of interest are first selected in a precursor ion scan. Those ions selection is based on relative abundance. It is also possible to manually program and instruct the mass spectrometer to do MS/MS at a particular value of m/z .

Once the MS procedure for a sample is completed, the post processing of the data generated from the experiment begins. Peptide mass fingerprint is determined by the extraction of the set of measured peptide masses. There are many algorithms developed

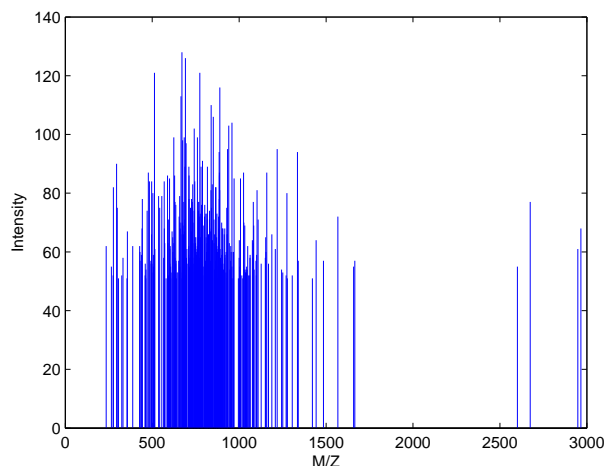


Figure 5.2: Plot of a MS scan

[102],[103] that match the experimental data against the theoretical masses obtained from the in-silico digestion at the same enzyme cleavage sites of all protein amino acid sequences in the database. The proteins in the database are then ranked according to the number of peptide masses matching their sequence within a given mass error tolerance. This whole process is called peptide mass fingerprinting (PMF). Generally peptide mass fingerprinting is used for the rapid identification of a single protein component. There are free protein databases available in the internet. The most famous database is the *SwissProt*. *SwissProt* is a high quality, curated protein database. *SwissProt* is ideal for peptide mass fingerprint searches and MS/MS searches of well characterised organisms. The more comprehensive database is *NCBItr*. In this chapter, we have used *Mascot* search engine that sends query to the *SwissProt* database for effective peptide mass fingerprinting. The direct derivation of peptide sequence from the MS/MS spectrum can be obtained using *de novo sequencing* [104]. The *de novo sequencing* constructs the peptide that maximises the scoring function [104]. Even though *de novo sequencing* does not require any database for protein identification, it requires the correct determination of the ion types. The MS/MS spectrum is corrupted by noise. The post processing of MS/MS produces false peaks and thereby complicates the *de novo sequencing*. For a given value of m/z (of a precursor ion), a database of predicted MS/MS spectra is created for all matching peptides using the rules of peptide fragmentation. The experimental MS/MS spectrum is compared to all predicted spectra and the best matching peptides are determined using a predefined scoring system.

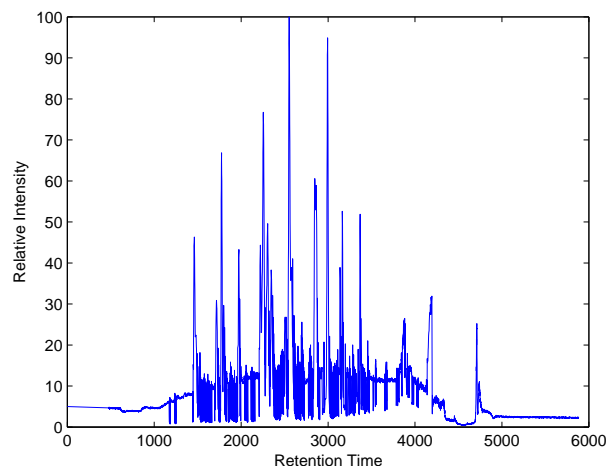


Figure 5.3: Total Ion Chromatogram

Total Ion Chromatogram (TIC) is a surrogate of total amount of protein in the sample that is being measured. Total count of ions of all masses in each scan are summed and they are plotted against the retention time. Thus each peak in the TIC corresponds to one scan. An example of a TIC is shown in Figure 5.3.

All the biological experiments were conducted at LaTrobe Institute of Molecular Science (LIMS). The LIMS has mass spectrometer manufactured by Bruker Daltonics and it supports the ESI technique. The raw spectra obtained from the proteomics experiments are analysed in this chapter.

5.2.1 MS preprocessing

In order to identify and quantify the proteins in the sample, regions of interest (*features*) must be extracted from the raw spectra which is usually corrupted with noise and baseline artifacts. Thus the preprocessing stage plays a vital role in the feature identification stage (post processing). The preprocessing steps involved in MS process is given below (in order)

1. Noise filtering
2. Baseline correction
3. Peak alignment
4. Peak detection

5. Normalisation

The first preprocessing step is noise filtering. The data from MS experiment are corrupted by chemical and instrument noise. Since the volume of MS data is large, noise filtering is essential to clean the data. Some of the noise filtering methods are based on Fourier transform. Recently wavelet based noise filtering is widely applied to denoise the MS data [98],[18],[100]. The hard thresholding of wavelet coefficients is performed after the decomposition of the MS data using DWT. Then the signal is reconstructed by taking inverse DWT. The DWT based denoising is more suitable for MS data as data is non-stationary and the noise is usually modelled as white Gaussian. The baseline artifact is caused due to chemical noise and detector overload in the MS instrument. The baseline is estimated by taking the local minimum of fixed width window. Once the baseline is estimated, it is then subtracted from the spectrum to get the baseline corrected spectrum. The important thing in baseline correction is that it should not remove the peak information from the spectrum. The baseline correction must be performed only after noise filtering step. The peaks in the MS spectrum must be aligned to reference peaks across all the spectra. This step will ensure that peaks appear in the correct m/z value. The peaks misalignment is due to various factors such as equipment calibration procedures, personnel, temperature and sample handling techniques. There are many algorithms available for peak alignment of MS data [105]. Peak detection is the process of distinguishing interesting peaks from noise. Peak detection focuses on scientifically interesting *features* of the MS data. The recent algorithms for peak detection are based on wavelets [99],[106].

The purpose of normalisation is to identify and remove sources of systematic variation between spectra due to varying amounts of protein or degradation over time in the sample or even variation in the instrument detector sensitivity. In MS spectrum, each protein concentration is measured by Area Under the Curve (AUC) of its peak and the natural choice scaling is the average AUC. The average AUC can be obtained from the TIC. The choice of normalisation step alone can greatly affect the post processing stage [107].

5.2.2 MS postprocessing

The post processing process involves quantification of the peaks and searching the protein database to identify the peptides present in the protein sample that is being examined. In all MS based methods, the expression levels of the peptides are measured by observing the signal intensity detected by the mass spectrometer. The peaks can be quantified

either by using the maximum height of a given peak or by calculating the area under the curve representing the peak. In [18],[19] peaks are quantified for each individual spectrum using the maximum log intensity within each peak group. After peak quantification, the peaks (across all the spectra) are written into predefined data format and sent to a search engine for protein identification.

5.3 MS/MS denoising

In this section, we present techniques to preprocess and post process the MS/MS data. Most of the literature concentrates on processing the MS data and this is the first work to concentrate on the MS/MS data. Preprocessing of MS and MS/MS data is vital for efficient post processing tasks such as peak detection and peak quantification. The preprocessing steps begin with denoising followed by baseline correction and normalisation [108]. The post processing begins with peak detection and quantification [18],[19] to produce a reduced dataset that can then be used by peptide identification and/or sequencing software. The MS/MS signal is modelled as following

$$y(t) = s(t) + B(t) + \epsilon(t)$$

where $y(t)$ is the observed signal, $s(t)$ is the original signal, $B(t)$ is the baseline drift and $\epsilon(t)$ is the noise which is modelled as zero mean white Gaussian. The main aim of preprocessing stage is to get $s(t)$ from $y(t)$.

Kwon *et. al* [98] used the undecimated DWT to remove the chemical and instrument noise from MS spectra with the hard thresholding technique. Kwon *et. al* [98] showed that the noise is heterogeneous and it is not uniform in each MS scan. The variation in the noise is due to spatial differences in total protein content and laser inefficiency of the mass spectrometer. In their work, the data is segmented based on the variance change and threshold for each of the segmented data is computed. The noise variance of each segment is estimated using the Median Absolute Deviation [38],[2]. To detect the variance change in the MS spectra, Kwon *et. al* [98] used an iterated cumulative sums of squares algorithm proposed by Gabbanini *et. al* [109]. We observed from all our experiments that the noise in the MS/MS spectra does not show any variance change. Hence the noise is assumed to be uniform over the MS/MS spectra. Li *et.al* [110] showed that wavelet based denoising improved the performance of machine learning methods.

Each peptide will be represented by one or more MS/MS (secondary fragmentation)

scans. The MS/MS scans are used to determine the amino acid sequence of the peptide by matching observed peaks against theoretical peaks in a large database of potential peptides. We have used the Mascot software package (Matrix Science, Ltd., London, United Kingdom) to perform this task. In this work, we apply the DTCWT on MS/MS scans to perform denoising. The procedure is described below.

1. The first step is noise filtering. We apply the DTCWT to decompose the MS/MS spectra. The hard thresholding technique is deployed to reduce the noise. The threshold (T_p) is set to three times the noise variance. The hard thresholding of the wavelet coefficient is defined as

$$\delta_T = \begin{cases} d_{jk} & \text{if } |d_{ij}| > T_p \\ 0 & \text{if } |d_{ij}| \leq T_p \end{cases}$$

where d_{jk} is the wavelet coefficient at the level j at k^{th} index. The noise variance is estimated using the Median Absolute Deviation [111] and it is given by

$$\hat{\sigma} = \frac{\text{median}(d_{11})}{0.6745}$$

where d_{11} is the detail coefficient at the first level.

2. After hard thresholding, we apply the inverse DTCWT to reconstruct the MS/MS signal. The next step is baseline correction. The baseline component is then removed by computing a monotone local minimum curve on the denoised signal. We have used the Matlab function *msbackadj* to correct the baseline and the window width for estimating the local minima is set to 200 separation units.
3. The signal is then normalised using the Matlab command *msnorm*. The function *msnorm* implements the normalisation procedure detailed in the end of the section 5.2.
4. Any local maximum after after denoising, baseline correction and normalisation is assumed to be a peak. Firstly all the local maxima and the associated peak endpoints are computed. Then the signal to noise ratio at each local maxima is calculated. All the local maxima that are greater than a threshold is considered as peaks. The threshold is set at 10% of the maximum signal to noise ratio of that particular scan.

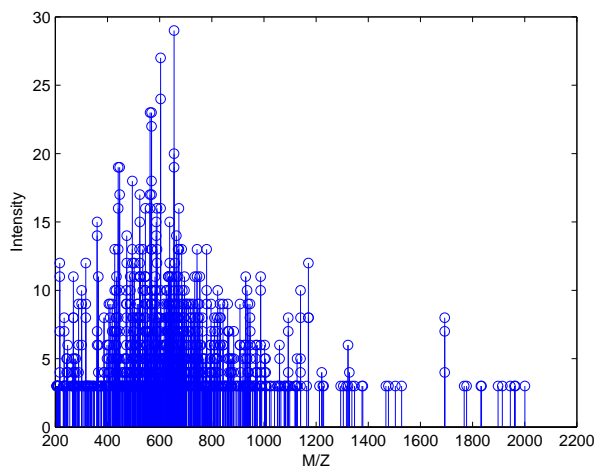


Figure 5.4: Plot of a MS/MS spectra of Dataset 3666

Table 5.1: Peptide count

Dataset	DWT	DTCWT	SWT
3666	59	64	61
3670	59	67	67
3677	63	63	62
3681	62	61	64
3685	47	48	45
3690	65	68	65

5. After peak picking, the peak lists are written into Mascot Generic Format (mgf) format and sent to the Mascot search engine for peptide identification. The schema of the mgf format is available from Matrix Science, Ltd., London, United Kingdom.
6. Raw Mascot search scores are then statistically analysed using Peptide Prophet [112] to produce a confidence level for each.
7. We then count the number of peptides obtained which have more than 95% of confidence level.

The above procedure is applied on six datasets corresponding to biologically independent samples from human cancer cells after enriching for membrane glycoproteins. These data were obtained from the LaTrobe Institute of Molecular Science. Importantly, all samples are relatively complex, containing many different peptides with different abundances. The plot of a MS/MS scan of Dataset 3666 in Figure 5.4 shows that the level of noise is higher in the lower m/z range. Efficient preprocessing of the datasets will improve

quality of MS/MS spectra and it will lead to a great number of identified peptides. We compare the results of DTCWT with other transforms such as DWT and Stationary Wavelet Transform (SWT). The length 12 Hilbert pair of filters having 2 VMs are used in DTCWT. The Daubechies length 12 filter having 6 VMs is used in DWT and SWT. The number of identified peptides are shown in the Table 5.1. In all the cases, the DTCWT performs better than the DWT and has a comparable performance to the SWT. However the computational load of the SWT is higher than the DTCWT.

5.4 Image denoising

We apply the almost symmetric Hilbert pair of wavelets to denoise images. The improvement in directional selectivity of almost symmetric Hilbert filters would preserve prominent features in the images and offer higher performance in denoising application. We compare the performance of three length 14 filters. i.e., Q-shift filter Q14, Almost Symmetric Hilbert filters ASH14 and SSH filter SSH14. A simple hard thresholding is applied after four levels of wavelet decomposition. The Gaussian noise is added to the image and the threshold is set at three times the noise variance (σ). The denoised image is then reconstructed and the performance both in terms of the peak to signal noise ratio (PSNR) [2] and structural similarity index (SSIM) [74] are compared. The test image *Tesmos* and *Lena* is shown in Figure 5.5.

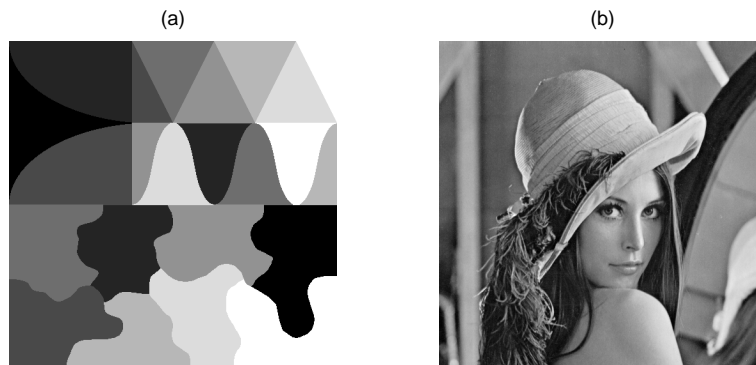


Figure 5.5: Test images: (a) *Tesmos* (b) *Lena*

The test image *Home* is shown in Figure 5.6 (a). Table 5.2 shows the performance measures for the three test images. The ASH14 filter offers better performance compared to filter Q14 and SSH14 for the *Tesmos* and *Home* images where there are many sharp

edges. The *Home image* which is corrupted by noise ($\sigma = 40$) is denoised and the reconstructed images are shown in Figure 5.6 (b)-(d).



Figure 5.6: (a) Original Home image. Image denoising using (b) Q14 (c) ASH14 (d) SSH14

The denoised image using ASH14 has a better visual quality compared to the Q14 and SSH14. The zoomed-in portion of the images (door grill) is shown in Figure 5.7.



Figure 5.7: Zoomed-in image (door grill). (a) Original (b) Q14 (c) ASH14 (d) SSH14

The worst reconstructed image is with the SSH14 where the edges are completely destroyed. The reconstructed image using ASH14 preserved most of the edges and offered the best visual quality. The zoomed-in portion of the images (chimney) is shown in Figure 5.8. The ASH14 filter preserve the sharp edges in the chimney and offer better visual quality. Thus the almost symmetric Hilbert pair of filters would preserve salient features in the image and offer better directional selectivity. The ASH14 filters offers an improvement of about 0.1-0.3dB in *Home* image which contains a lot of directional features.

Table 5.2: Image Denoising

Image	σ	Q14		ASH14		SSH14	
		PSNR	SSIM	PSNR	SSIM	PSNR	SSIM
Lena	10	31.9041	0.9346	31.9867	0.934	32.1665	0.9276
	20	29.0125	0.8773	29.0300	0.8766	28.6539	0.8599
	30	27.3280	0.8261	27.4166	0.8297	26.8455	0.8059
	40	26.3343	0.7923	26.2287	0.7819	25.6394	0.758
	50	25.4451	0.7584	25.4335	0.7479	24.8691	0.7244
Home	10	35.005	0.9466	35.1533	0.9559	35.6935	0.9387
	20	31.2819	0.8862	31.4026	0.9004	30.82	0.865
	30	29.0959	0.8347	29.1363	0.8450	28.4708	0.8028
	40	27.5099	0.7756	27.5938	0.804	27.0532	0.7554
	50	26.4690	0.7364	26.6335	0.7650	26.0677	0.7203
Tesmos	10	35.0781	0.9662	35.7264	0.9806	35.4535	0.961
	20	31.0579	0.9276	31.7131	0.9509	30.8745	0.9149
	30	28.9543	0.8937	29.7136	0.9218	28.6046	0.8771
	40	27.6834	0.8686	28.3317	0.8979	27.191	0.8518
	50	26.622	0.8432	27.2215	0.8747	26.1878	0.8335



Figure 5.8: Zoomed-in image (chimney). (a) Original (b) Q14 (c) ASH14 (d) SSH14

The *Tesmos* image which is corrupted by noise ($\sigma = 50$) is denoised. The noisy *Tesmos* image is shown in Figure 5.9 (a) and the reconstructed images are shown in Figure 5.9 (b)-(d). Once again, the ASH14 filter offered better visual quality compared to other filters.

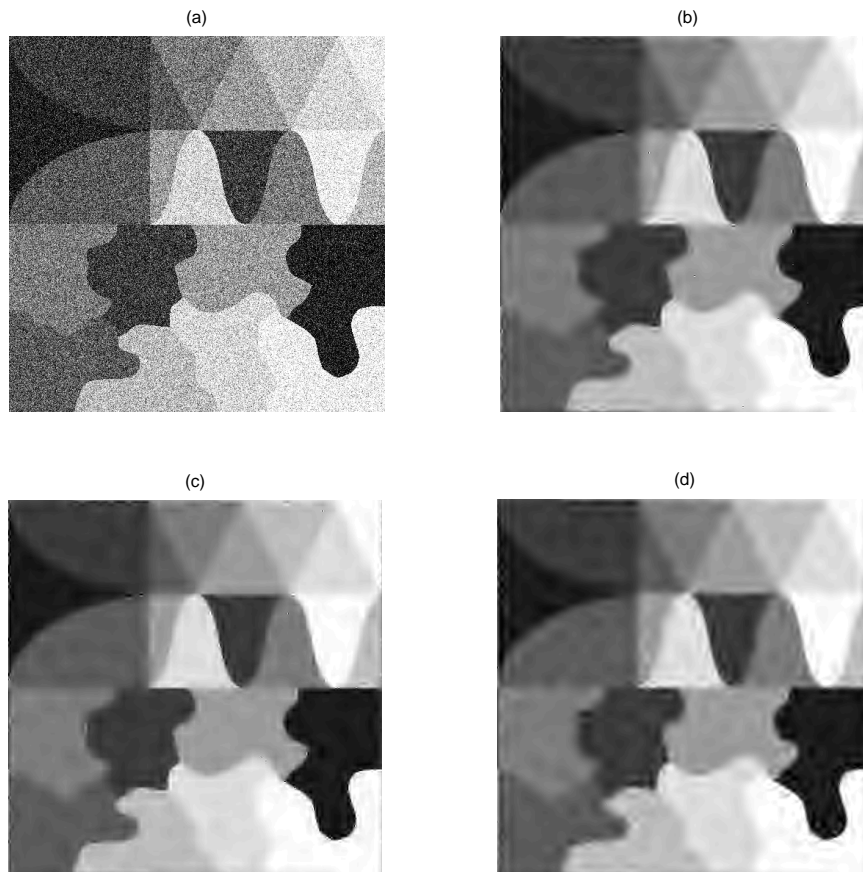


Figure 5.9: (a) Original Home image. Image denoising using (b) Q14 (c) ASH14 (d) SSH14

The better directional selectivity of ASH14 preserved all the salient features such as

edges, contours and lines. The ASH14 filters offers an improvement of about 0.2-0.6dB in *Tesmos* image which contains a lot of directional features. The approximate linear phase characteristics of ASH14 filters is thus suitable for image processing applications.

5.5 Conclusion

We have presented the applications of almost symmetric Hilbert pair of wavelets in proteomics and image processing. In proteomics application of the DTCWT using almost symmetric Hilbert filters performed better compared to DWT and SWT. We have also shown that in image denoising application the almost symmetric Hilbert-pair of wavelets offer better directional selectivity and superior performance compared to other filters.

6 On the Aliasing effect of the Finer Directional Wavelet Transform

The 2D separable wavelet transform offers limited directionality because it can only provide three directional subbands. The finer directional wavelet transform has been proposed to improve the directionality of the 2D separable wavelet transform. The finer directional wavelet transform employs quadrant filters on subband outputs of the 2D separable wavelet transform. It divides the three directional subband of wavelet transform into six finer directional subbands. Even though the finer directional wavelet transform has advantages of being non redundant and has efficient separable implementation, it suffers in performance due to aliasing. The aliasing occurs due to the quadrant filters' inherent frequency response characteristics and thus cannot be eliminated. This chapter addresses the aliasing involved in the implementation of the finer directional wavelet transform and recommends ways to reduce the aliasing. This chapter also shows that using a higher order quadrant filter in finer directional wavelet transform does not eliminate the aliasing completely. This chapter proposes the undecimated finer directional wavelet transform as a way to reduce the aliasing. Application of the proposed transform in image denoising shows performance improvements compared with the original finer directional wavelet transform.

6.1 Introduction

The separable 2D Discrete Wavelet Transform (DWT) is the most commonly used version of wavelet transform in image processing but it provides limited directional information. Directional information is important for image processing applications such as image enhancement [113], [114] denoising [27] and feature extraction [115],[116]. The lack of directional selectivity greatly complicates

- modeling of images

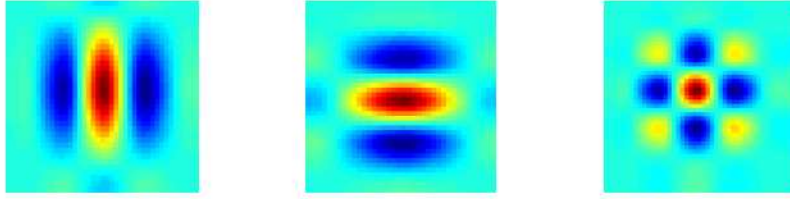


Figure 6.1: Directionality of 2D wavelets: Left: Vertical band Middle: Horizontal band Right: Diagonal band

- processing of geometric features of images such as edges and ridges

The separable 2D DWT provides three directional information. They are

1. Horizontal
2. Vertical
3. Diagonal

The three directional components of the 2D DWT are shown in Figure 6.1 and they are generated from the length 12 Daubechies filter. As observed from Figure 6.1, all of the three wavelets are oriented along several directions and the diagonal band produces checkerboard artifact. The 2D DWT does not provide any information about *phase of the signal* which is essential for signal location information. The phase information of the signal can aid in efficient motion estimation and detection [117]. The desire for more directional features has lead several researchers to proposed other types of transforms [21],[23],[118],[22],[119],[120],[121],[122],[123]. The finer directional wavelet transform (fiDWT) is proposed in [20] as a simple extension to the separable 2D DWT to improve the directionality of the subbands. The fiDWT employs a pair of quadrant filters on the subband outputs of the 2D DWT. The quadrant filters can be used as an “add-on” to an existing separable 2D DWT. In the separable 2D DWT the diagonal band output contains a mixture of the 45^0 and 135^0 orientations. The quadrant filters allow the separation of the 45^0 orientation from the 135^0 orientation. The fiDWT is popular compared to other transforms [21],[23],[118],[121],[122],[123] because it uses the DWT transform as the building block. There are efficient algorithms that facilitates the implementation of DWT [24].

We will show in this chapter that although the fiDWT improves the directionality of separable 2D DWT this comes at a expense of significant aliasing. The aliasing is inherent in the system and is due to a combination of the downsampling operation and the

frequency response characteristics of practical quadrant filters. Aliasing is theoretically zero if the quadrant filter response has an ideal brickwall characteristics. With practical quadrant filters there is a transition band which introduces aliasing. We will show that unlike in the 1D case, with the fiDWT the level of aliasing cannot be easily reduced by using a higher order filter and this is due to the the energies along the edges of the subbands.

The overview of this chapter is as follows. Section 6.2 presents the overview of the directional filter banks. Section 6.3 presents the overview of the fiDWT. The Quadrant filter design technique is reviewed in Section 6.4. Section 6.5 analyzes the aliasing in the subbands of fiDWT and proposes the undecimated finer directional wavelet transform (ufiDWT) as a way to improve the performance. The directionality of the fiDWT and ufiDWT is presented in Section 6.6. Section 6.7 considers an image denoising application with the fiDWT and (ufiDWT). Section 6.8 concludes the chapter.

6.2 Review of directional filter banks

In this section we review some of the filter banks that has been proposed to improve the directionality. Some of the transforms are based on 1D filter banks [27] while others employ non-separable multidimensional filter banks [21],[23],[118],[121],[122],[123]. There are few hybrid transform that combine both 1D and 2D filter banks to provide multiresolution representation of images and offer higher directionality[120],[124],[125],[126].

6.2.1 Dual Tree Complex Wavelet Transform

The Dual Tree Complex Wavelet Transform (DTCWT) was introduced by Kingsbury [27] to address the problems with DWT. The 2D DTCWT is nearly shift invariant and produces six directional subbands. The six directional bands of the 2D DTCWT is shown in Figure 6.2 and they are generated from length 14 Q-shift filter [95],[16]. Comparing with Figure 6.1, it is evident that checkboard artifact is absent in the DTCWT and all the six wavelets have distinct orientation. Each 2D DTCWT six basis function has one phase angle which encodes the 1D shift of image features perpendicular to its orientation and this phase information has been proved useful in many image processing applications [113], [114],[115],[116],[117]. The 2D DTCWT is an overcomplete transform and it is four times redundant than tight frames. The 2D DTCWT is implemented using two filter banks and the two filter banks are related via the Hilbert transform in (4.1).

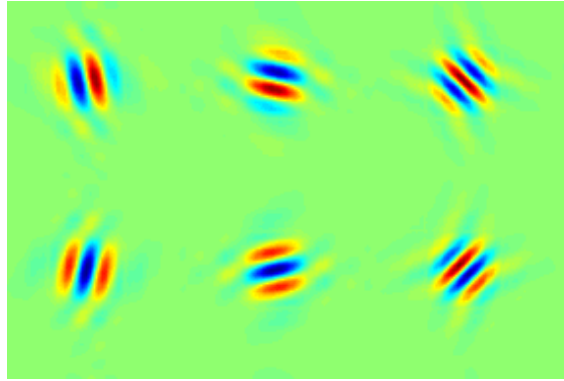


Figure 6.2: Directionality of 2D Dual Tree wavelets

The tight coupling between two filter banks makes the filter design tedious. Despite the tedious design process, the 2D DTCWT has been very popular and widely used in many applications.

6.2.2 Directional filter banks

Bamburger *et. al* [21] introduced critically sampled Directional Filter Bank (DFB) to capture the directional components of images. The DFB is a shift variant transform. The directional partitioning of the 2D spectrum is shown in Figure 6.3. The input image needs to be modulated and the DFB uses diamond subband filters to extract directional information of an image. The attractive feature of DFB is that it is maximally decimated, has high angular resolution for directional subbands and high computation efficiency. The efficient implementation of the DFB is done using the polyphase structures. The DFB suffers from the *frequency scrambling* phenomenon where low frequency regions of the images are geometrically repositioned in the subband image and it causes spatial distortions in the images. Park *et. al* [127] addressed the frequency scrambling problem of the DFB and proposed a new efficient framework. In their new framework, only fan filters were used. Because of the frequency scrambling phenomenon, the DFB has found limited applications [128].

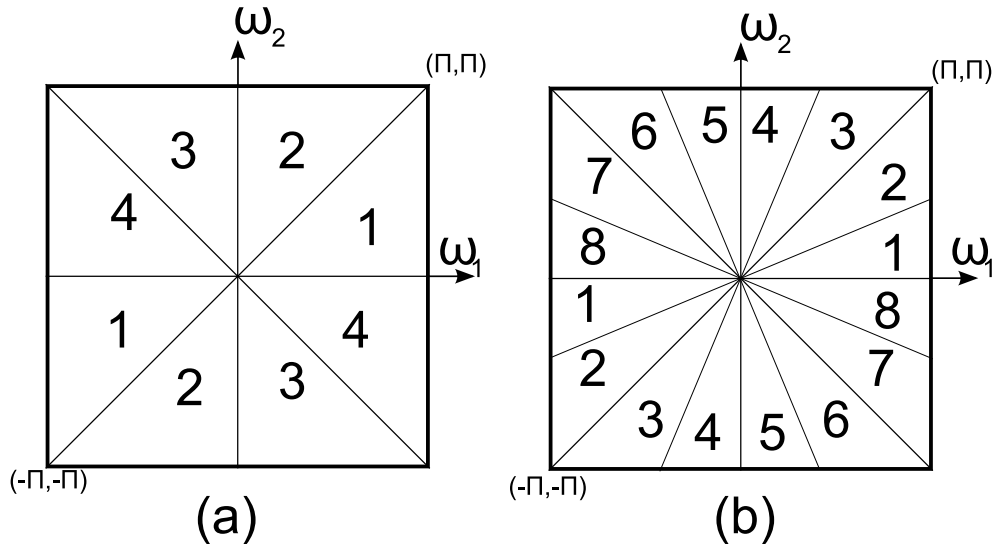


Figure 6.3: Directional partitioning (a) Four band (b) Eight band

6.2.3 Contourlets

Contourlets transform was introduced by Do and Vetterli [23] and it addressed the shortcomings of 2D separable wavelets. The contourlet transform captures the intrinsic geometrical structures in the images while wavelets are only good at isolating the discontinuities at edge points in the images. The contourlets transform provides a multiscale and directional decomposition thus allowing to efficiently approximate smooth contours at multiple resolutions. The contourlet filter bank is a combination of Laplacian pyramid [129] and the conventional DFB [21]. The contourlet transform can be considered as a natural extension of curvelet transform [121],[122] which is implemented in the continuous domain and the critical sampling is difficult to implement. The contourlet transform overcomes the disadvantages of the curvelet transform and it uses pyramidal directional filter bank for its implementation. However designing good filters for pyramidal directional filter bank is a difficult task. A nonsubsampling, shift invariant contourlet transform was proposed by Cunha *et. al* [130] and it is easy to implement using ladder steps. The filter design problem of the nonsubsampling contourlet transform is much simpler than the pyramidal directional filter bank.

6.2.4 Multiresolution Directional Filter Banks

Nguyen *et. al* [118],[22] introduced a class of multiresolution directional filter banks. Those directional filter banks have different frequency partitioning. They are maximally

decimated and have perfect reconstruction property. There is no DC leakage in any directional subbands. All of the multiresolution directional filter banks uses tree structure decomposition. Some filter bank design involves designing two channel parallelogram filter bank while others uses diamond filter bank. The design of parallelogram and diamond shape filter banks can be easily constructed using the transformation of variables technique as detailed in [131]. The multiresolution directional filter bank has been used in many application [118],[22] and can be efficiently implemented using the ladder structure [132]. The complexity of implementing multiresolution directional filter banks is the same as that of the conventional DFB.

6.3 Finer directional wavelet transform

The fiDWT has been proposed in [20] to extract directional information from the images thus providing an efficient multiresolution image representation. The fiDWT employs quadrant filter after the DWT to improve the directionality of the original DWT. The idea of combining 1D and 2D filter banks for multiresolution image representation has been explored in [124],[125],[126]. The merits of hybrid transforms (by combining 1D and 2D filter banks) are efficient implementation and simpler filter design.

The separable 2D DWT frequency partitioning is shown in Figure 6.4(a). The separable 2D DWT produces one low pass subband LL (Low) and three directional subbands namely HL (High-Low), LH (Low-High) and HH (High-High). The HH is the result of high pass filtering the rows and columns. The HL subband is the result of low pass filtering the columns followed by high pass filtering the rows. The LH subband is the resultant of low pass filtering the rows followed by high pass filtering the columns. The problem with the DWT are

1. HH subband mixes the orientation $+45^{\circ}$ with $+135^{\circ}$
2. HL subband mixes the orientation $+15^{\circ}$ with $+105^{\circ}$
3. LH subband mixes the orientation $+75^{\circ}$ with $+165^{\circ}$

The fiDWT subband partitioning is shown in Figure 6.4(b). The HH subband from the separable 2D DWT is decomposed into two smaller subbands labeled 5 and 6. The frequency content of the HH subband is shown in the Figure 6.5(a) and is scrambled after downsampling as shown in Figure 6.5(b). In order to separate the HH band into the bands 5 and 6, quadrant filters are used. One of the quadrant filter has an ideal

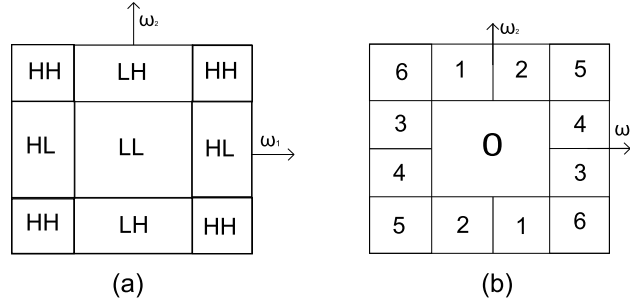


Figure 6.4: Frequency band partitioning of the (a) separable 2D DWT (b) Finer directional wavelet transform

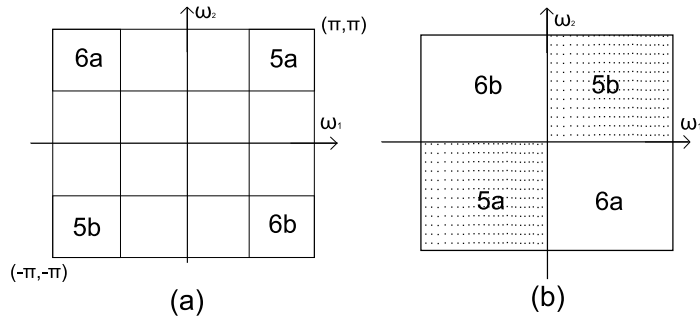


Figure 6.5: (a) Diagonal subband of separable DWT (b) Frequency band of the HH band after downsampling

passband shown as shaded (dotted, regions 5a and 5b) in Figure 6.5(b). The other quadrant is complementary and has an ideal passband shown as unshaded (regions 6a and 6b) in Figure 6.5(b). The same quadrant filters can be used to separate the LH and HL subbands into smaller directional subbands. The analysis filter bank structure to compute the fDWT is shown in Figure 6.6 which consists of the separable 2D DWT filter bank structure and the quadrant filter banks as “add-on”. There is a corresponding synthesis filter bank structure (not shown) that reverses the operations in Figure 6.6 for the inverse transform.

The separable filter bank is obtained from a 1D two channel filter bank with filters $H_0^{1D}(z)$ (analysis low pass), $H_1^{1D}(z)$ (analysis high pass), $F_0^{1D}(z)$ (synthesis low pass) and $F_1^{1D}(z)$ (synthesis high pass). The filters in the filter bank satisfy the following conditions: $H_1^{1D}(z) = z^{-1}F_0^{1D}(-z)$, $F_1^{1D}(z) = zH_0^{1D}(-z)$ and $H_0^{1D}(z)F_0^{1D}(z) + H_1^{1D}(z)F_1^{1D}(z) = 2$ which ensures perfect reconstruction. For orthogonal filter banks there is the extra condition $F_0^{1D}(z) = H_0^{1D}(z^{-1})$ (time reversal relationship).

The quadrant filter bank has 2D filters $H_0^Q(z_1, z_2)$, $H_1^Q(z_1, z_2)$ (complementary analysis) and $F_0^Q(z_1, z_2)$, $F_1^Q(z_1, z_2)$ (complementary synthesis). The downsampling is defined

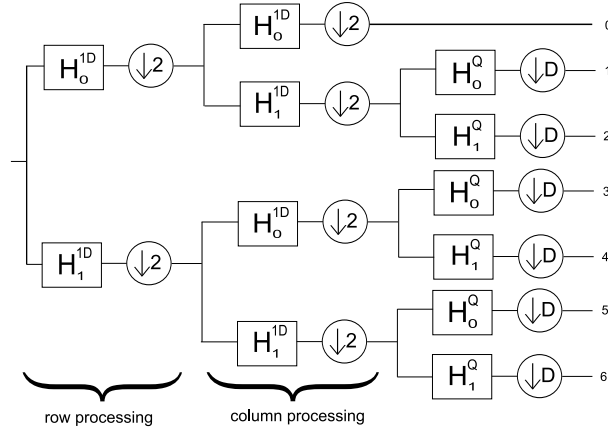


Figure 6.6: Analysis filter banks for the fdWT.

by a diagonal sampling matrix $D = \text{diag}(2, 1)$. For perfect reconstruction the following condition is required for the filters: $H_1^Q(z_1, z_2) = z_1^{-1}F_0^Q(-z_1, z_2)$, $F_1^Q(z_1, z_2) = z_1H_0^Q(-z_1, z_2)$ and

$$H_0^Q(z_1, z_2)F_0^Q(z_1, z_2) + H_1^Q(z_1, z_2)F_1^Q(z_1, z_2) = 2$$

Although the sampling structure for the quadrant filter bank is similar to that in the separable filter bank, the 2D filters are not strictly separable, i.e. $H_0^Q(z_1, z_2) \neq A(z_1)B(z_2)$. However there are design techniques yielding quadrant filters that has some form of generalized separability [131]. The complexity of those quadrant filters is therefore comparable to that of separable filters.

6.4 Quadrant filter design

There are many ways to design a PR quadrant filter [132],[131]. Transformation of variables technique is considered as more generalised mapping technique compared with the McClellan transformation [131],[133],[134]. The McClellan transformation uses the same kernel to transform 1D filters into 2D filters [134]. Phoong's method [132] can also be shown to be a special case of transformation of variables [131]. The transformation of variable technique to design quadrant filter band is detailed below.

Let H_0^{2D} and H_1^{2D} be the 2D analysis low pass and high pass filters respectively. Let F_0^{2D} and F_1^{2D} be the 2D synthesis low pass and high pass filters respectively. The perfect reconstruction (PR) condition of the filter bank is given as

$$H_0^{2D}(z_1, z_2)F_0^{2D}(z_1, z_2) + H_1^{2D}(z_1, z_2)F_1^{2D}(z_1, z_2) = 2$$

The below condition achieves aliasing cancellation

$$\begin{aligned} H_1^{2D}(z_1, z_2) &= z_1^{-k_1} z_2^{-k_2} F_0^{2D}(-z_1, -z_2) \\ F_1^{2D}(z_1, z_2) &= z_1^{k_1} z_2^{k_2} H_0^{2D}(-z_1, -z_2) \end{aligned}$$

where $k_1 + k_2 = \text{odd}$.

Now define the product filter to be $D(z_1, z_2) = H_0^{2D}(z_1, z_2)F_0^{2D}(z_1, z_2)$. Then the PR condition can be given as

$$D(z_1, z_2) + D(-z_1, -z_2) = 2$$

The transformation kernel that facilitates the factorization of the product filter $D(z_1, z_2)$ is given as

$$W = M(z_1, z_2) = \sum_{k_1} \sum_{k_2} m(k_1, k_2) z_1^{k_1} z_2^{k_2}$$

such that

$$M(-z_1, -z_2) = -W$$

The below condition holds based on the definition of the transformation kernel. i.e

$$m(k_1, k_2) = \begin{cases} 0 & \text{for } k_1 + k_2 = \text{even} \\ \text{arbitrary} & \text{for } k_1 + k_2 = \text{odd} \end{cases} \quad (6.1)$$

This transform a 1D polynomial $D_T(W)$ into $D(z_1, z_2)$. $D_T(W)$ is a 1D product filter. The 1D product filter $D_T(W)$ can be factored to give $H_T(W)$ and $F_T(W)$. Thus 2D filter can be obtained by transforming 1D filters using the mapping kernel. The transformation of variable technique can be summarized as below.

1. Design the mapping kernel that approximates the desired frequency response using the condition (6.1)
2. Design the 1D product filter $D_T(W)$ and factorizes them into $H_T(W)$ and $F_T(W)$. The 1D filters can be obtained by factorisation of Lagrange half-band filter [36],[132].

3. The 2D low pass filters can be obtained as $H_0^{2D}(z_1, z_2) = H_T(M(z_1, z_2))$ and $F_0^{2D}(z_1, z_2) = F_T(M(z_1, z_2))$
4. The 2D high pass filters can be obtained using the alias cancellation condition

6.4.1 Quadrant filter mapping kernel

The sampling matrix $D = \text{diag}(2, 1) = \begin{pmatrix} 2 & 0 \\ 0 & 1 \end{pmatrix}$. The ideal subband shape of the quadrant filter is given in Figure 6.5(b). The ideal impulse response for the desired frequency response is calculated using calculus and it is given as

$$h_{ideal}(n_1, n_2) = \text{sinc}(k_1\pi/2)\text{sinc}(k_2\pi/2) \cos((k_1 + k_2)\pi/2)$$

The transformation kernel can be designed as

$$m(k_1, k_2) = m_1(k_1)m(k_2)\cos((k_1 + k_2)\pi/2)$$

where $m_1(k)$ satisfies the condition (2.1). The 1D filters can be obtained by factorizing the Lagrange Half band filter

$$D(z) = z^K \left(\frac{1 + z^{-1}}{2} \right)^{2K} \sum_{n=0}^{K-1} \binom{K+n-1}{n} \left(\frac{2 - (z + z^{-1})}{4} \right)^n$$

The 1D filters $H_T(W)$ and $F_T(W)$ can be obtained by symmetric factorization of the Lagrange product filter with $K = 3$. The transformation kernel is obtained by designing $m_1(k)$. The $m_1(k)$ is a 1D product filter which is obtained using the Lagrange Half band filter with $K = 4$. The frequency response of the quadrant filter $H_0^Q(z_1, z_2)$ is shown in Figure 6.7. The frequency response of the complementary quadrant filter $F_0^Q(z_1, z_2)$ is shown in Figure 6.8.

6.5 Aliasing effect in the subband

In order to study the effect of aliasing in the fiDWT we designed a pair of linear phase complementary quadrant filters $H_0^Q(z_1, z_2)$ and $H_1^Q(z_1, z_2)$ of size 13×13 and 29×29 respectively as detailed in the Section 6.4. Their frequency response of $H_0^Q(z_1, z_2)$ and $H_1^Q(z_1, z_2)$ are shown in the Figure 6.7 and 6.8. For the separable filter bank, we initially considered the 8 tap symmlet filter of Daubechies which has approximate linear phase

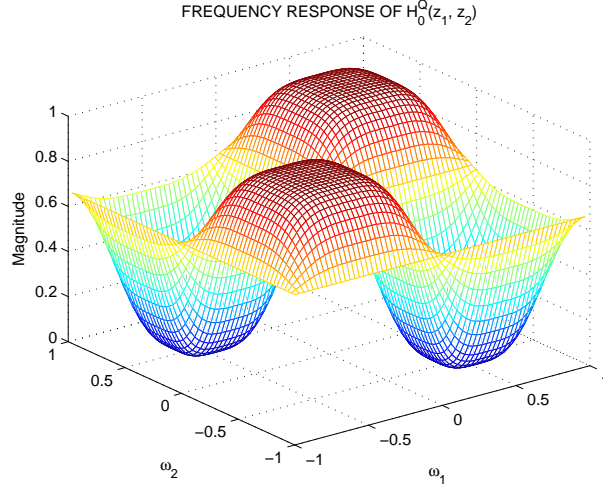


Figure 6.7: Frequency response of $H_0^Q(z_1, z_2)$

characteristics and approximate symmetric wavelet function. Using multirate identities the total effective frequency response of the subband 5 (referring to Figure 6.6) is given by

$$T_5(z_1, z_2) = H_1^{1D}(z_1)H_1^{1D}(z_2)H_0^Q(z_1^2, z_2^2)$$

The ideal frequency band support of $H_0^Q(z_1^2, z_2^2)$ (squeezed version in both axes of Figure 6.5(b)) is shown as the shaded regions in Figure 6.9(a). The ideal frequency band support of $H_1^{1D}(z_1)H_1^{1D}(z_2)$ is shown as the shaded regions in Figure 6.9(b). The ideal frequency band support of $T_5(z_1, z_2)$ is therefore the intersection of the shaded regions of figures 6.9 (a) and (b). Ideally the stopband regions labeled A and B in Figure 6.9(a) is supposed to completely remove the frequency band region labelled 6a and 6b in Figure 6.9(b). However with practical filters there are transition band regions which are shown as encircled regions in Figure 6.9(a) and (b) and they are in the vicinity of the edges. The overlap between the transition bands of $H_0^Q(z_1^2, z_2^2)$ and $H_1^{1D}(z_1)H_1^{1D}(z_2)$ results in aliasing energy which can also be viewed as energy leakage from one band to another. Using the real (practical) filters mentioned above the actual frequency response of subband 5, $|T_5(e^{j\omega_1}, e^{j\omega_2})|$, is shown in Figure 6.10. The aliased components shown as encircled in Figure 6.10 are quite large. A similar frequency domain analysis will reveal that significant aliasing also occur in the other directional subbands 1, 2, ... 4 and this is due to the overlap between the transition bands of the separable and quadrant filter banks. As another example the actual equivalent frequency response of subband 1,

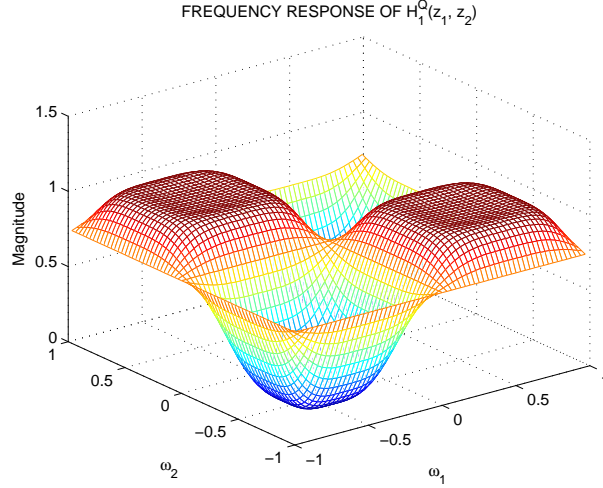


Figure 6.8: Frequency response of $H_1^Q(z_1, z_2)$

$|T_1(e^{j\omega_1}, e^{j\omega_2})|$, is shown in Figure 6.11 with the aliasing component shown as encircled. It is clearly evident from Figure 6.10 and Figure 6.11 that there is a energy leakage occurring along the edges and some regions in the stopband. Increasing the order of the filters can reduce the level of aliasing energy but it is very difficult to achieve a substantial reduction due to the inherent nature of system which has energy leakage distributed along the edges of the frequency band. This aliasing will have negative impact in image processing applications. Even though the fiDWT increases the directionality of the DWT, the aliasing present in the transform makes it less useful in many image processing applications.

If the undecimated version of the fiDWT (ufiDWT) is used, the effective total frequency response of the subband 5 is given by

$$T(z_1, z_2) = H_1(z_1)H_1(z_2)H(z_1, z_2)$$

Using the real (practical) filters mentioned above the actual frequency response of subband 5, $|T_5(e^{j\omega_1}, e^{j\omega_2})|$, is shown in Figure 6.12. which exhibit significant reduction in aliasing compared to Figure 6.10. There are still some aliasing energy present along some of the edges which cannot be completely eliminated because of the inherent frequency characteristics of quadrant filters. An objective measure of the degree of aliasing is defined as the ratio of aliasing energy to the signal energy:

$$E_{AS} \equiv \frac{\int_{Region\ 6} |T_5(\omega_1, \omega_2)|^2 d\omega_1 d\omega_2}{\int_{Region\ 5} |T_5(\omega_1, \omega_2)|^2 d\omega_1 d\omega_2}$$

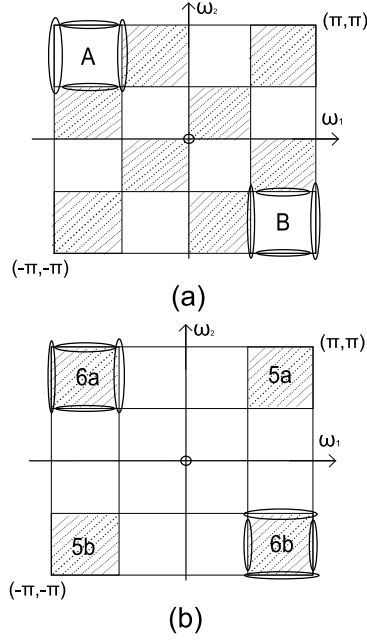


Figure 6.9: Ideal frequency band support of (a) $H_0^Q(z_1^2, z_2^2)$ (b) $H_1^{1D}(z_1)H_1^{1D}(z_2)$. Shaded region: passband. Unshaded region: stopband

Table 6.1: Ratio of aliasing energy to signal energy E_{AS} values.

	H_0^Q order is 13×13		H_0^Q order is 77×77	
	fiDWT	ufiDWT	fiDWT	ufiDWT
Symmlet 8	0.3267	0.1968	0.2399	0.0757
Biorthogonal 9/7	0.2585	0.2083	0.1730	0.0779
Daubechies 8	0.3267	0.1968	0.2399	0.0757
Daubechies 6	0.3593	0.1968	0.2742	0.0757

The E_{AS} measure can also be defined for other subbands as well. In an ideal case where there is no aliasing energy present in the region 6, the E_{AS} value would be zero. Table 6.1 lists the value of E_{AS} using various 1D filters and different order quadrant filters. It is evident from Table 6.1 that ufiDWT has significantly lower aliasing compared to the fiDWT. From Table 6.1, it is also clear that increasing the order of quadrant of filters cannot reduce the aliasing energy substantially. Thus the ufiDWT is more robust than fiDWT.

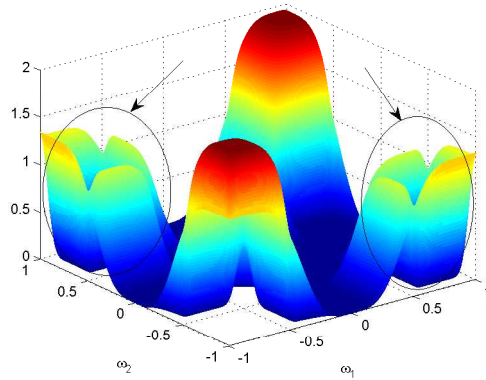


Figure 6.10: Magnitude response of subband 5 in the fdWT. Aliasing components indicated by the arrows.

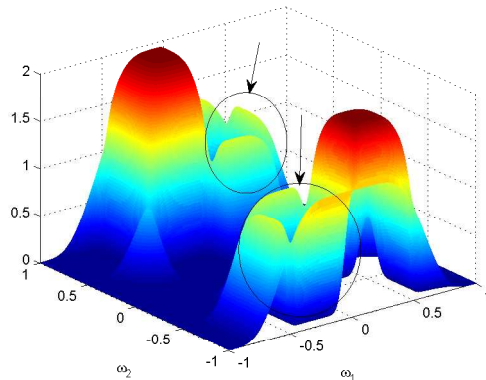


Figure 6.11: Magnitude response of subband 1 in the fdWT. Aliasing components indicated by the arrows.

6.6 Directional Information

The image shown in Figure 6.13(a) which is made up of lines oriented (the normal vector) along the 45° and 135° directions. Using the separable 2D DWT the (zoomed in portion of) image of HH band is shown in Figure 6.13(b) which captures the diagonal information (both the 45° and 135° components). Using the fdWT the (zoomed in portion of) image of band 6 is shown in Figure 6.14(a). A careful examination of Figure 6.14(a) will reveal that it consists mainly of features along the 135° direction but there are also residual features along the 45° direction. Ideally band 6 is suppose to capture features in the 135° direction but because of aliasing some of the features in the 45° direction have 'leaked' into this band. If the ufdWT is used instead the degree of 'leakage' is reduced as seen

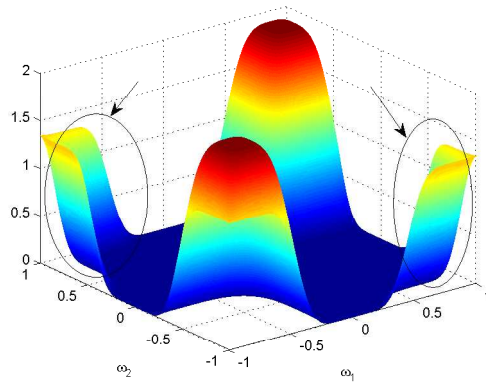


Figure 6.12: Magnitude response of subband 5 in the ufiDWT. Aliasing components indicated by the arrows.

in Figure 6.14(b) with reduced residual features along the 45° direction. The ufiDWT is more robust in extracting the directional information compared to fiDWT. Thus the ufiDWT has a better performance compared to fiDWT. The computational complexity of the ufiDWT is however approximately 10 times that of the fiDWT.

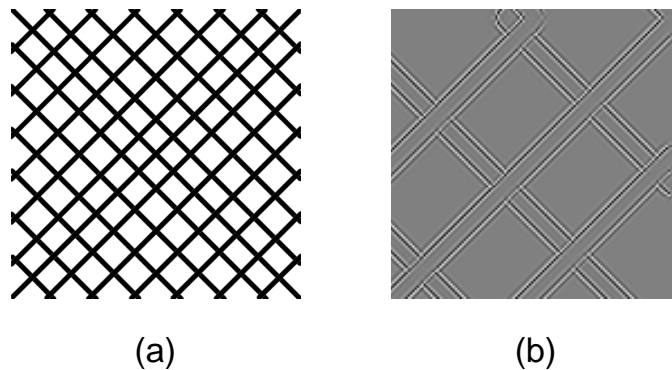
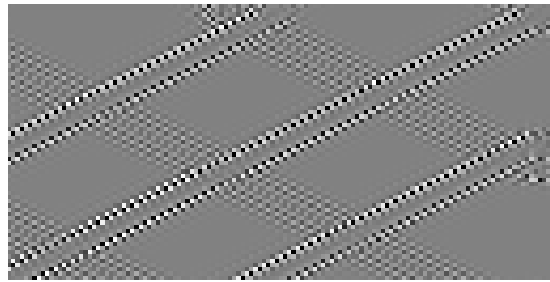


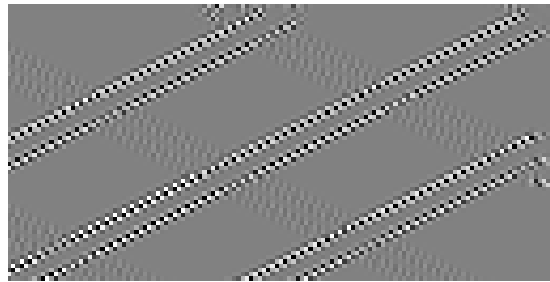
Figure 6.13: (a) Original test image (b) zoomed in image of the HH band

6.7 Applications

The performance of the fiDWT and ufiDWT is compared in image denoising application. A simple soft thresholding technique [111] is employed to denoise the image corrupted by additive Gaussian noise. The procedure of image denoising is as follows.



(a)



(b)

Figure 6.14: zoomed in portion of image in band 6 using (a) fiDWT (b) ufiDWT.

1. The Additive White Gaussian Noise (AWGN) of known variance σ^2 is added to standard test image
2. The noise in the image is estimated using Median Absolute Deviation [111]
3. The noisy image is decomposed into 4 level using forward fiDWT and ufiDWT respectively
4. A soft thresholding is done by having the threshold set to $T = 3\sigma$
5. Image is reconstructed using inverse fiDWT and ufiDWT respectively
6. PSNR is computed for the denoised image and comparison is made between fiDWT and ufiDWT

First, we applied the above denoising process on the standard test image *Lena*. For the case where input PSNR is 24.35 dB, the denoised image using the fiDWT and ufiDWT is shown in Figure 6.15 and Figure 6.16 respectively. Both the output PSNR and visual



Figure 6.15: *Lena* image denoised using fiDWT. Output PSNR: 25.11 dB

quality is substantially superior with the ufiDWT. The Figure 6.17 compares the output PSNR over a range of input PSNR for the ufiDWT, fiDWT and DWT. The ufiDWT is the superior of the three. We carried out the denoising process on the another standard image *Boat*. The Figure 6.18 compares the output PSNR over a range of input PSNR for the ufiDWT, fiDWT and DWT. The ufiDWT is the superior of the three transform in both of test images.



Figure 6.16: *Lena* image denoised using ufiDWT. Output PSNR: 28.11 dB

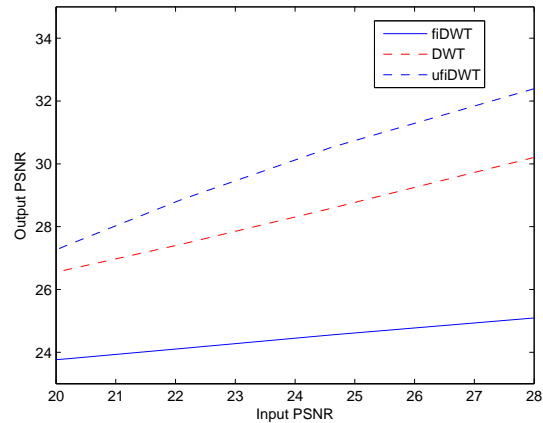


Figure 6.17: PSNR in denoising for *Lena*

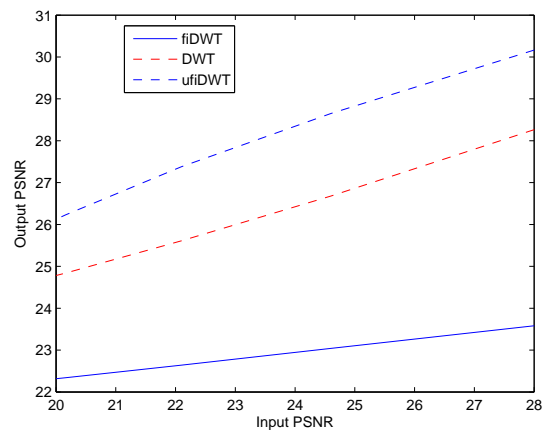


Figure 6.18: PSNR in denoising for *Boat*

6.8 Conclusion

In this chapter, the aliasing phenomena of the finer directional DWT (fiDWT) has been studied. There is a significant level of aliasing in the fiDWT which is inherent in the system and cannot be easily eliminated by using high order filters. The aliasing is due to the overlapping of transition bands resulting in energy leakage from one band to another. The aliasing phenomena is fundamentally different in nature to the 1D case as it involves 2D regions and edges. To reduce the level of aliasing, the undecimated version of the fiDWT has been proposed (ufiDWT) which has a substantially lower level of aliasing energy for a given filter order. We have also showed that the ufiDWT offer

more defined directional information compared to the fiDWT. In the image denoising application the ufiDWT gives substantially superior performance but with increased computational complexity.

7 Conclusion and Future Directions

7.1 Main contributions

The aim of this thesis is the design of new classes of wavelet filters and its applications in the fields such as proteomics and image coding. The main contributions of this thesis can be summarised as follows

1. A new technique is proposed to rationalise the orthogonal and biorthogonal wavelet filter banks. The rational coefficient of orthogonal filter will simplify the implementation in hardware. All the properties of the orthogonal filters are preserved during the rationalisation procedure including the perfect reconstruction, vanishing moments and frequency response. The rationalisation of filter coefficients can be extended to the Hilbertian filters which implement the DTCWT. A generalised technique to rationalise the biorthogonal wavelet filters is also demonstrated.
2. A new technique to design orthogonal almost symmetric wavelet filters has been proposed. The symmetric wavelets are crucial in image processing applications as the image features (edges, lines) are susceptible to non-linear distortions. Haar wavelet is the only wavelet available in the literature which is orthogonal and symmetric. With the proposed technique almost symmetric orthogonal wavelet filters having arbitrary vanishing moments can be designed with ease. The designed wavelet filters perform on par with 9/7 biorthogonal filters in image coding application.
3. A novel technique based on optimisation to design a new class of almost symmetric Hilbert pair of wavelets has been proposed. The symmetry of Hilbert pair of wavelets is important for directional selectivity. The designed Hilbert pair of wavelets is symmetric and offers good directional selectivity. The designed Hilbert pair of wavelets have approximate linear phase and approximately flat group delay.
4. The designed almost symmetric orthonormal hilbert pair of wavelets is applied to Mass Spectroscopy data to denoise the MS/MS spectra. The processed peak list

are searched in Mascot database to identify the peptides. Denoising done using DTCWT with almost symmetric hilbert filters identified more number of peptides compared to DWT and SWT.

5. The finer directional wavelet transform (fiDWT) has been proposed as a simple extension to DWT to increase the directionality of DWT. However, the fiDWT suffers from aliasing which is inherent in its transform. The proposed undecimated finer directional wavelet transform (ufiDWT) reduces the aliasing and gives better performance improvements compared with fiDWT.

7.2 Further Improvements and Future Directions

7.2.1 Rationalising Orthogonal Wavelet Filters

The technique to rationalise orthogonal and biorthogonal wavelet filters has been proposed in Chapter II. Up to two VMs has been imposed on rational orthogonal wavelet filter. Imposition of more than 2 vanishing moments on rational orthogonal filters should be investigated further as it will lead to a smoother wavelet (higher Sobolev regularity). The rational biorthogonal wavelet filters are achieved by reducing VMs from the one of the biorthogonal filter. Since the VMs are reduced on biorthogonal filters, further investigation should be done to know its effect on image coding applications.

7.2.2 Almost Symmetric Orthogonal Wavelet Filters

Design of almost symmetric orthogonal wavelet filters focuses mainly on the symmetry of the wavelet. Symmetric orthogonal filters correspond to approximate linear phase. Symmetric wavelets are crucial in image processing as edges in the images are susceptible to non-linear distortions. However in some applications, frequency selectivity is also important in addition to symmetric wavelets. Design of sharper almost symmetric wavelet filter should be investigated further. If both the symmetry and frequency selectivity are considered, the problem can be formulated as multi-objective function. Genetic algorithm can be used to solve such problems so that an optimal trade-off between wavelet symmetry and filter sharpness is achieved. The time and frequency localisation of almost symmetric orthogonal wavelet should also be studied further. The designed AS10 filter performs on par with the D9/7 filter and mathematical properties of AS10 filters should be studied further [47].

7.2.3 Almost Symmetric Orthogonal Hilbert Pair of Wavelet Filters

Design of almost symmetric Hilbert pair of wavelet filter focuses on symmetry of Hilbert pair of wavelets. At first, the AES and AOS are designed independently. The AES and AOS filters form a Hilbert pair as their phase difference is approximately -0.5ω and their frequency response is approximately equal. To get a better analytic quality, the AES filter is fixed while the AOS filter is re-optimised iteratively. The re-optimisation can also be performed on the AES filters while fixing the AOS and this needs to be further investigated. An iterative re-optimisation of both the AES and AOS filters can be also be done until the best analytic measures are obtained. Will the iterative re-optimisation on both the filters yield better analytic quality? This question is very interesting as a detailed study will throw lot of insight on how the filter characteristics change over each iteration. Designing of sharper almost symmetric orthogonal Hilbert pair of wavelet filters has to be studied. The phase difference between the designed Hilbert pair of filters is -0.5ω . Tay *et. al* [97] showed that Hilbert pair of filters can have an integer plus half sample. A further investigation is needed to design the AOS and AES filters to have an integer plus half sample delay to form a Hilbert pair and they can be further re-optimised to get a better analytic quality.

7.2.4 Applications

The denoising of MS/MS spectra for Mass Spectroscopy using the designed almost symmetric hilbert pair of wavelets (implementing DTCWT) leads to finding more number of peptides compared to other transform such as SWT and DWT. A futher investigation is required in finding new algorithms to detect peaks efficiently. The feature finding in MS data is very challenging due to misalignment in MS data and false peaks. Efficient algorithms need to be developed for better peak detection and feature finding.

Bibliography

- [1] P.P.Vaidyanathan, *Multirate Systems and Filter Banks*, E. Cliffs, Ed. Prentice-Hall, 1992.
- [2] G. Strang and T. Nguyen, *Wavelets and Filter Banks*. Wellesley-Cambridge Press, 1997.
- [3] A. Skodras, C. Christopoulos, and T. Ebrahimi, “The jpeg 2000 still image compression standard,” *IEEE Signal Processing Magazine*, vol. 18, no. 5, pp. 36–58, 2001.
- [4] H. Samueli, “An improved search algorithm for the design of multiplierless FIR filters with powers-of-two coefficients,” *IEEE Transactions on Circuits and Systems*, vol. 36, no. 7, pp. 1044–1047, Jul. 1989.
- [5] K. A. Kotteri, A. E. Bell, and J. E. Carletta, “Design of multiplierless, high-performance, wavelet filter banks with image compression applications,” *IEEE Transactions on Circuits and Systems I: Regular Papers*, vol. 51, no. 3, pp. 483–494, 2004.
- [6] M. Martina and G. Masera, “Low-complexity, efficient 9/7 wavelet filters VLSI implementation,” *IEEE Transactions on Circuits and Systems II: Express Briefs*, vol. 53, no. 11, pp. 1289–1293, 2006.
- [7] I. Daubechies, “Orthonormal bases of compactly supported wavelets,” *Communications on Pure and Applied Mathematics*, vol. 41, no. 7, pp. 909–996, 1988.
- [8] ———, *Ten lectures on wavelets*, ser. CBMS-NSF Regional Conference Series in Applied Mathematics. Philadelphia, PA: Society for Industrial and Applied Mathematics (SIAM), 1992, vol. 61.
- [9] Y. Zhao and M. N. S. Swamy, “Design of least asymmetric compactly supported orthogonal wavelets via optimization,” in *IEEE Canadian Conference on Electrical and Computer Engineering*, vol. 2, 1999, pp. 817–820.

- [10] —, “New technique for designing nearly orthogonal wavelet filter banks with linear phase,” *IEEE Proceedings - Vision, Image and Signal Processing*, vol. 147, no. 6, pp. 527–533, 2000.
- [11] C. Burrus and J. Odegard, “Coiflet systems and zero moments,” *IEEE Transactions on Signal Processing*, vol. 46, no. 3, pp. 761–766, 1998.
- [12] I. W. Selesnick, “Hilbert transform pairs of wavelet bases,” *IEEE Signal Processing Letters*, vol. 8, no. 6, pp. 170–173, 2001.
- [13] R. Yu and H. Ozkaramanli, “Hilbert transform pairs of orthogonal wavelet bases: necessary and sufficient conditions,” *IEEE Transactions on Signal Processing*, vol. 53, no. 12, pp. 4723 – 4725, dec. 2005.
- [14] I. W. Selesnick, “The design of approximate hilbert transform pairs of wavelet bases,” *IEEE Transactions on Signal Processing*, vol. 50, no. 5, pp. 1144–1152, 2002.
- [15] D. B. H. Tay, N. G. Kingsbury, and M. Palaniswami, “Orthonormal hilbert-pair of wavelets with (almost) maximum vanishing moments,” *IEEE Signal Processing Letters*, vol. 13, no. 9, pp. 533–536, 2006.
- [16] N. Kingsbury, “Design of q-shift complex wavelets for image processing using frequency domain energy minimization,” in *Image Processing, 2003. ICIP 2003. Proceedings. 2003 International Conference on*, vol. 1, 2003, pp. I–1013–16 vol.1.
- [17] H. Steen and M. Mann, “The ABC’s (and XYZ’s) of peptide sequencing,” *Nature Reviews Molecular Cell Biology*, vol. 5, pp. 699–711, Sept 2004.
- [18] K. R. Coombes, S. Tsavachidis, J. S. Morris, K. A. Baggerly, M.-C. Hung, and H. M. Kuerer, “Improved peak detection and quantification of mass spectrometry data acquired from surface-enhanced laser desorption and ionization by denoising spectra with the undecimated discrete wavelet transform,” *Proteomics*, vol. 5, no. 16, pp. 4107–4117, 2005.
- [19] J. S. Morris, K. R. Coombes, J. Koomen, K. A. Baggerly, and R. Kobayashi, “Feature extraction and quantification for mass spectrometry in biomedical applications using the mean spectrum,” *Bioinformatics*, vol. 21, no. 9, pp. 1764–1775, 2005.

- [20] L. Yue and M. N. Do, “The finer directional wavelet transform [image processing applications],” in *Proceedings IEEE International Conference on Acoustics, Speech, and Signal Processing*, vol. 4, pp. iv/573–iv/576.
- [21] R. H. Bamberger and M. J. T. Smith, “A filter bank for the directional decomposition of images: theory and design,” *IEEE Transactions on Signal Processing*, vol. 40, no. 4, pp. 882–893, 1992.
- [22] T. N. Truong and O. Soontorn, “A class of multiresolution directional filter banks,” *IEEE Transactions on Signal Processing*, vol. 55, no. 3, pp. 949–961, 2007.
- [23] M. N. Do and M. Vetterli, “The contourlet transform: an efficient directional multiresolution image representation,” *IEEE Transactions on Image Processing*, vol. 14, no. 12, pp. 2091–2106, 2005.
- [24] S. Mallat, *A Wavelet Tour of Signal Processing, Third Edition: The Sparse Way*, 3rd ed. Academic Press, Dec. 2008.
- [25] J. Petukhov, “Best wavelet bases for image compression generated by rational symbols,” *HAIT Journal of Science and Engineering C*, vol. 4, no. 1-2, pp. 763–771, 2007.
- [26] M. Smith and S. Eddins, “Analysis/synthesis techniques for subband image coding,” *IEEE Transactions on Acoustics Speech and Signal Processing*, vol. 38, no. 8, pp. 1446–1456, aug 1990.
- [27] I. W. Selesnick, R. G. Baraniuk, and N. C. Kingsbury, “The dual-tree complex wavelet transform,” *IEEE Signal Processing Magazine*, vol. 22, no. 6, pp. 123–151, 2005.
- [28] N. Kingsbury, “Complex wavelets for shift invariant analysis and filtering of signals,” *Applied and Computational Harmonic Analysis*, vol. 10, no. 3, pp. 234–253, 2001.
- [29] G. Shi, W. Liu, L. Zhang, and F. Li, “An efficient folded architecture for lifting-based discrete wavelet transform,” *IEEE Transactions on Circuits and Systems II: Express Briefs*, vol. 56, no. 4, pp. 290–294, april 2009.
- [30] C. Zhang, C. Wang, and M. Ahmad, “A pipeline VLSI architecture for high-speed computation of the 1-D discrete wavelet transform,” *IEEE Transactions on Circuits and Systems I: Regular Papers*, vol. 57, no. 10, pp. 2729–2740, oct. 2010.

- [31] J. Song and I.-C. Park, "Pipelined discrete wavelet transform architecture scanning dual lines," *IEEE Transactions on Circuits and Systems II: Express Briefs*, vol. 56, no. 12, pp. 916–920, dec. 2009.
- [32] D. Shi and Y. J. Yu, "Design of linear phase FIR filters with high probability of achieving minimum number of adders," *IEEE Transactions on Circuits and Systems I: Regular Papers*, vol. 58, no. 1, pp. 126–136, jan. 2011.
- [33] J.-C. Liu and Y.-L. Tai, "Design of 2-D wideband circularly symmetric FIR filters by multiplierless high-order transformation," *IEEE Transactions on Circuits and Systems I: Regular Papers*, vol. 58, no. 4, pp. 746–754, april 2011.
- [34] M. Lightstone, E. Majani, and S. K. Mitra, "Low bit-rate design considerations for wavelet-based image coding," *Multidimensional Systems and Signal Processing*, vol. 8, no. 1, pp. 111–128, 1997.
- [35] A. Cohen, I. Daubechies, and J.-C. Feauveau, "Biorthogonal bases of compactly supported wavelets," *Communications on Pure and Applied Mathematics*, vol. 45, no. 5, pp. 485–560, 1992.
- [36] R. Ansari, C. Guillemot, and J. F. Kaiser, "Wavelet construction using lagrange halfband filters," *IEEE Transactions on Circuits and Systems*, vol. 38, no. 9, pp. 1116–1118, 1991.
- [37] W. Sweldens, "Lifting scheme: a new philosophy in biorthogonal wavelet constructions," F. L. Andrew and A. U. Michael, Eds., vol. 2569. SPIE, 1995, pp. 68–79.
- [38] P. P. Vaidyanathan and P. Q. Hoang, "Lattice structures for optimal design and robust implementation of two-channel perfect-reconstruction qmf banks," *IEEE Transactions on Acoustics, Speech and Signal Processing*, vol. 36, no. 1, pp. 81–94, 1988.
- [39] K. A. Kotteri, S. Barua, A. E. Bell, and J. E. Carletta, "A comparison of hardware implementations of the biorthogonal 9/7 dwt: convolution versus lifting," *IEEE Transactions on Circuits and Systems II: Express Briefs*, vol. 52, no. 5, pp. 256–260, 2005.

- [40] A. Abbas and T. D. Tran, "Rational coefficient dual-tree complex wavelet transform: Design and implementation," *IEEE Transactions on Signal Processing*, vol. 56, no. 8, pp. 3523–3534, 2008.
- [41] Z. Doganata and P. Vaidyanathan, "On one-multiplier implementations of FIR lattice structures," *IEEE Transactions on Circuits and Systems*, vol. 34, no. 12, pp. 1608 – 1609, Dec. 1987.
- [42] D. Wei and A. Bovik, "Generalized coiflets with nonzero-centered vanishing moments," *IEEE Transactions on Circuits and Systems II: Analog and Digital Signal Processing*, vol. 45, no. 8, pp. 988–1001, 1998.
- [43] C. S. Burrus, R. A. Gopinath, and H. Guo, *Introduction to Wavelets and Wavelet Transforms: A Primer*, 1st ed. Prentice Hall, Aug 1997.
- [44] H. Ojanen, "Orthonormal compactly supported wavelets with optimal sobolev regularity," *Rutgers Univ. Math. Dept*, vol. 10, pp. 93–98, 1998.
- [45] B. Sherlock and D. Monroe, "On the space of orthonormal wavelets," *IEEE Transactions on Signal Processing*, vol. 46, no. 6, pp. 1716 –1720, Jun. 1998.
- [46] M. Parfieniuk and A. Petrovsky, "Quaternion multiplier inspired by the lifting implementation of plane rotations," *IEEE Transactions on Circuits and Systems I: Regular Papers*, vol. 57, no. 10, pp. 2708 –2717, oct. 2010.
- [47] M. Unser and T. Blu, "Mathematical properties of the JPEG 2000 wavelet filters," *IEEE Transactions on Image Processing*, vol. 12, no. 9, pp. 1080–1090, 2003.
- [48] K.-Y. Khoo, A. Kwentus, and J. Willson, A.N., "A programmable fir digital filter using csd coefficients," *IEEE Journal of Solid-State Circuits*, vol. 31, no. 6, pp. 869–874, 1996.
- [49] G. A. Ruiz and M. Granda, "Efficient canonic signed digit recoding," *Microelectronics Journal*, vol. 42, no. 9, pp. 1090 – 1097, 2011.
- [50] M. D. Ercegovic and T. Lang, "Digital arithmetic." San Francisco: Morgan Kaufmann, 2004.
- [51] S.-M. Kim, J.-G. Chung, and K. Parhi, "Low error fixed-width CSD multiplier with efficient sign extension," *IEEE Transactions on Circuits and Systems II: Analog and Digital Signal Processing*, vol. 50, no. 12, pp. 984 – 993, 2003.

- [52] J. Katto and Y. Yasuda, "Performance evaluation of subband coding and optimization of its filter coefficients," T. Kou-Hu and K. Toshio, Eds., vol. 1605. SPIE, 1991, pp. 95–106.
- [53] H. M. Paiva, M. N. Martins, R. Galvao, and J. Paiva, "On the space of orthonormal wavelets: Additional constraints to ensure two vanishing moments," *IEEE Signal Processing Letters*, vol. 16, no. 2, pp. 101–104, 2009.
- [54] G. Regensburger, "Parametrizing compactly supported orthonormal wavelets by discrete moments," *Applicable Algebra in Engineering, Communication and Computing*, vol. 18, no. 6, pp. 583–601, 2007.
- [55] G. Regensburger and O. Scherzer, "Symbolic computation for moments and filter coefficients of scaling functions," *Annals of Combinatorics*, vol. 9, no. 2, pp. 223–243, 2005.
- [56] M. E. Domínguez Jiménez, "A new general expression for 2-channel FIR paraunitary filterbanks," *Signal Process.*, vol. 88, no. 7, pp. 1725–1732, Jul 2008.
- [57] D. B. H. Tay, "Rationalizing the coefficients of popular biorthogonal wavelet filters," *IEEE Transactions on Circuits and Systems for Video Technology*, vol. 10, no. 6, pp. 998–1005, 2000.
- [58] S. Oraintara, T. Tran, and T. Nguyen, "A class of regular biorthogonal linear-phase filterbanks: theory, structure, and application in image coding," *IEEE Transactions on Signal Processing*, vol. 51, no. 12, pp. 3220 – 3235, 2003.
- [59] S. Oraintara, T. Tran, P. Heller, and T. Nguyen, "Lattice structure for regular paraunitary linear-phase filterbanks and M-band orthogonal symmetric wavelets," *IEEE Transactions on Signal Processing*, vol. 49, no. 11, pp. 2659 –2672, Nov. 2001.
- [60] T. Tran, "M-channel linear phase perfect reconstruction filter bank with rational coefficients," *IEEE Transactions on Circuits and Systems I: Fundamental Theory and Applications*, vol. 49, no. 7, pp. 914 –927, Jul. 2002.
- [61] X. Zhang, T. Muguruma, and T. Yoshikawa, "Design of orthonormal symmetric wavelet filters using real allpass filters," *Signal Processing*, vol. 80, no. 8, pp. 1551–1559, 2000.

- [62] X. Zhang, A. Kato, and T. Yoshikawa, “A new class of orthonormal symmetric wavelet bases using a complex allpass filter,” *IEEE Transactions on Signal Processing*, vol. 49, no. 11, pp. 2640–2647, nov 2001.
- [63] D. B. Percival and A. T. Walden, *Wavelet Methods for Time Series Analysis (Cambridge Series in Statistical and Probabilistic Mathematics)*. Cambridge University Press, 2006.
- [64] A. Abdelnour and I. Selesnick, “Design of 2-band orthogonal near-symmetric CQF,” in *Proceedings of IEEE International Conference on Acoustics, Speech, and Signal Processing, 2001*, vol. 6, 2001, pp. 3693–3696.
- [65] I. W. Selesnick, J. E. Odegard, and C. S. Burrus, “Nearly symmetric orthogonal wavelets with non-integer DC group delay,” in *IEEE Digital Signal Processing Workshop Proceedings, 1996*, pp. 431–434.
- [66] D. Stanhill and Y. Zeevi, “Two-dimensional orthogonal filter banks and wavelets with linear phase,” *IEEE Transactions on Signal Processing*, vol. 46, no. 1, pp. 183–190, jan 1998.
- [67] S. Muramatsu, A. Yamada, and H. Kiya, “A design method of multidimensional linear-phase paraunitary filter banks with a lattice structure,” *IEEE Transactions on Signal Processing*, vol. 47, no. 3, pp. 690–700, mar 1999.
- [68] L. Gan and K.-K. Ma, “A simplified lattice factorization for linear-phase perfect reconstruction filter bank,” *IEEE Signal Processing Letters*, vol. 8, no. 7, pp. 207–209, jul 2001.
- [69] D. Cerná, V. Finek, and K. Najzar, “On the exact values of coefficients of coiflets,” *Central European Journal of Mathematics*, vol. 6, no. 1, pp. 159–169, 2008.
- [70] R. Gopinath and C. Burrus, “On the moments of the scaling function ψ_0 ,” in *Proceedings IEEE International Symposium on Circuits and Systems*, vol. 2, 1992, pp. 963–966.
- [71] W. H. Press, B. P. Flannery, S. A. Teukolsky, and W. T. Vetterling, *Numerical Recipes in C: The Art of Scientific Computing, Second Edition*, 2nd ed. Cambridge University Press, 1992.

- [72] R. A. Waltz, J. L. Morales, J. Nocedal, and D. Orban, “An interior algorithm for nonlinear optimization that combines line search and trust region steps,” *Mathematical Programming*, vol. 107, no. 3, pp. 391–408, 2006.
- [73] A. Said and W. Pearlman, “A new, fast, and efficient image codec based on set partitioning in hierarchical trees,” *IEEE Transactions on Circuits and Systems for Video Technology*, vol. 6, no. 3, pp. 243–250, jun 1996.
- [74] Z. Wang, A. Bovik, H. Sheikh, and E. Simoncelli, “Image quality assessment: from error visibility to structural similarity,” *IEEE Transactions on Image Processing*, vol. 13, no. 4, pp. 600–612, april 2004.
- [75] A. Hore and D. Ziou, “Is there a relationship between peak-signal-to-noise ratio and structural similarity index measure?” *IET Image Processing*, vol. 7, no. 1, pp. 12–24, 2013.
- [76] J. D. Villasenor, B. Belzer, and J. Liao, “Wavelet filter evaluation for image compression,” *IEEE Transactions on Image Processing*, vol. 4, no. 8, pp. 1053–1060, 1995.
- [77] P. Moulin, “A multiscale relaxation algorithm for snr maximization in nonorthogonal subband coding,” *IEEE Transactions on Image Processing*, vol. 4, no. 9, pp. 1269–1281, 1995.
- [78] R. R. Coifman and D. L. Donoho, “Translation-invariant de-noising.” Springer-Verlag, 1995, pp. 125–150.
- [79] G. Nason and B. Silverman, “The stationary wavelet transform and some statistical applications,” in *Wavelets and Statistics*, ser. Lecture Notes in Statistics, A. Antoniadis and G. Oppenheim, Eds. Springer New York, 1995, vol. 103, pp. 281–299.
- [80] R. Rubinstein, A. Bruckstein, and M. Elad, “Dictionaries for sparse representation modeling,” *Proceedings of the IEEE*, vol. 98, no. 6, pp. 1045–1057, June 2010.
- [81] R. Gopinath, “The phaselet transform—an integral redundancy nearly shift-invariant wavelet transform,” *IEEE Transactions on Signal Processing*, vol. 51, no. 7, pp. 1792–1805, 2003.

- [82] N. Kingsbury, "Image processing with complex wavelets," *Phil. Trans. Royal Society London A*, vol. 357, pp. 2543–2560, 1997.
- [83] D. B. H. Tay, "Designing hilbert-pair of wavelets: Recent progress and future trends," in *6th International Conference on Information, Communications Signal Processing*, Dec. 2007, pp. 1–5.
- [84] H. Shi, B. Hu, and J. Q. Zhang, "A novel scheme for the design of approximate hilbert transform pairs of orthonormal wavelet bases," *IEEE Transactions on Signal Processing*, vol. 56, no. 6, pp. 2289–2297, June 2008.
- [85] B. Dumitrescu, I. Bayram, and I. Selesnick, "Optimization of symmetric self-hilbertian filters for the dual-tree complex wavelet transform," *IEEE Signal Processing Letters*, vol. 15, pp. 146–149, 2008.
- [86] B. Dumitrescu, "SDP approximation of a fractional delay and the design of dual-tree complex wavelet transform," *IEEE Transactions on Signal Processing*, vol. 56, no. 9, pp. 4255–4262, Sept 2008.
- [87] J. Wang and J. Q. Zhang, "A globally optimal bilinear programming approach to the design of approximate hilbert pairs of orthonormal wavelet bases," *IEEE Transactions on Signal Processing*, vol. 58, no. 1, pp. 233–241, Jan 2010.
- [88] D. Tay, "A new approach to the common-factor design technique for hilbert-pair of wavelets," *IEEE Signal Processing Letters*, vol. 17, no. 11, pp. 969–972, Nov. 2010.
- [89] X. Zhang, "A new phase-factor design method for hilbert-pairs of orthonormal wavelets," *IEEE Signal Processing Letters*, vol. 18, no. 9, pp. 529–532, Sept. 2011.
- [90] D. Wang and X. Zhang, "IIR-based DTCWTs with improved analyticity and frequency selectivity," *IEEE Transactions on Signal Processing*, vol. 60, no. 11, pp. 5764–5774, Nov. 2012.
- [91] D. Tay, "ETHFB: A new class of even-length biorthogonal wavelet filters for hilbert pair design," *IEEE Transactions on Circuits and Systems I: Regular Papers*, vol. 55, no. 6, pp. 1580–1588, July 2008.

- [92] D. Tay and M. Palaniswami, “Design of approximate hilbert transform pair of wavelets with exact symmetry [filter bank design],” in *Proceedings IEEE International Conference on Acoustics, Speech, and Signal Processing, (ICASSP '04), 2004*, vol. 2, May 2004, pp. ii – 921–4 vol.2.
- [93] —, “Hilbert pair of wavelets via the matching design technique [matched filters],” in *IEEE International Symposium on Circuits and Systems, 2005. ISCAS 2005*, vol. 3, May 2005.
- [94] D. Tay, “Symmetric self-hilbertian wavelets via orthogonal lattice optimization,” *IEEE Signal Processing Letters*, vol. 19, no. 7, pp. 387 –390, July 2012.
- [95] N. Kingsbury, “A dual-tree complex wavelet transform with improved orthogonality and symmetry properties,” in *Image Processing, 2000. Proceedings. 2000 International Conference on*, vol. 2, 2000, pp. 375–378 vol.2.
- [96] D. Tay, “Daubechies wavelets as approximate hilbert-pairs?” *IEEE Signal Processing Letters*, vol. 15, pp. 57 –60, 2008.
- [97] —, “Hilbert pair of orthogonal wavelet bases: Revisiting the condition,” *IEEE Transactions on Signal Processing*, vol. 56, no. 4, pp. 1716 –1721, April 2008.
- [98] D. Kwon, M. Vannucci, J. J. Song, J. Jeong, and R. M. Pfeiffer, “A novel wavelet-based thresholding method for the pre-processing of mass spectrometry data that accounts for heterogeneous noise,” *PROTEOMICS*, vol. 8, no. 15, pp. 3019–3029, 2008.
- [99] P. Du, W. A. Kibbe, and S. M. Lin, “Improved peak detection in mass spectrum by incorporating continuous wavelet transform-based pattern matching,” *Bioinformatics*, vol. 22, no. 17, pp. 2059–2065.
- [100] R. Hussong and A. Hildebr, “The isotope wavelet: A signal theoretic framework for analyzing mass spectrometry data,” Eleventh Annual International Conference on Research in Computational Molecular Biology, 2007.
- [101] R. Hussong, B. Gregorius, A. Tholey, and A. Hildebrandt, “Highly accelerated feature detection in proteomics data sets using modern graphics processing units.” *Bioinformatics*, vol. 25, no. 15, pp. 1937–1943, 2009.

- [102] P. H. M. Mann and P. Roepstorff, "Use of mass spectrometric molecular weight information to identify proteins in sequence databases," *Biological mass spectrometry*, vol. 6, no. 22, pp. 338–345, 1993.
- [103] S. J. W. S. G. C. Henzel WJ, Billeci TM and W. C., "Identifying proteins from two-dimensional gels by molecular mass searching of peptide fragments in protein sequence databases." *Proc Natl Acad Sci U S A*, vol. 90, no. 11, pp. 5011–5015, 1993.
- [104] V. Dancik, T. A. Addona, K. R. Clauser, J. E. Vath, and P. A. Pevzner, "De novo peptide sequencing via tandem mass spectrometry: a graph-theoretical approach," in *RECOMB '99: Proceedings of the third annual international conference on Computational molecular biology*. ACM Press, 1999, pp. 135–144.
- [105] N. Jeffries, "Algorithms for alignment of mass spectrometry proteomic data," *Bioinformatics*, vol. 21, no. 14, pp. 3066–3073, 2005.
- [106] A. Antoniadis, J. Bigot, and S. Lambert-Lacroix, "Peaks detection and alignment for mass spectrometry data," *Journal de la Societe Francaise de Statistique*, vol. 151, no. 1, pp. 17–37, 2010.
- [107] M.-C. W. G. J. H. B. M. J. R. Wouter Meuleman, Judith YMN Engwegen and L. F. Wessels, "Comparison of normalisation methods for surface-enhanced laser desorption and ionisation (SELDI) time-of-flight (TOF) mass spectrometry data," *BMC Bioinformatics*, vol. 9, 2008.
- [108] V. A. Emanuele and B. M. Gurbaxani, "Benchmarking currently available SELDI-TOF MS preprocessing techniques," *Proteomics*, vol. 9, no. 7, pp. 1754–1762, 2009.
- [109] F. Gabbanini, M. Vannucci, G. Bartoli, and A. Moro, "Wavelet packet methods for the analysis of variance of time series with application to crack widths on the brunelleschi dome," *Journal of Computational and Graphical Statistics*, vol. 13, no. 3, pp. 639–658, 2004.
- [110] X. Li, J. Li, and X. Yao, "A wavelet-based data pre-processing analysis approach in mass spectrometry." *Comp. in Bio. and Med.*, vol. 37, no. 4, pp. 509–516, 2007.
- [111] D. Donoho, "De-noising by soft-thresholding," *IEEE Transactions on Information Theory*, vol. 41, no. 3, pp. 613–627, 1995.

- [112] A. Keller, A. I. Nesvizhskii, E. Kolker, and R. Aebersold, “Empirical statistical model to estimate the accuracy of peptide identifications made by ms/ms and database search,” *Analytical Chemistry*, vol. 74, no. 20, pp. 5383–5392, 2002.
- [113] C. Shaffrey, N. Kingsbury, and I. Jermyn, “Unsupervised image segmentation via markov trees and complex wavelets,” in *Proceedings. International Conference on Image Processing*, vol. 3, 2002, pp. 801–804.
- [114] J. Romberg, H. Choi, R. Baraniuk, and N. Kingbury, “Multiscale classification using complex wavelets and hidden markov tree models,” in *Proceedings. International Conference on Image Processing*, vol. 2, 2000, pp. 371–374.
- [115] E. Lo, M. Pickering, M. Frater, and J. Arnold, “Scale and rotation invariant texture features from the dual-tree complex wavelet transform,” in *International Conference on Image Processing*, vol. 1, 2004, pp. 227–230.
- [116] M. Kokare, P. Biswas, and B. N. Chatterji, “Rotation invariant texture features using rotated complex wavelet for content based image retrieval,” in *International Conference on Image Processing*, vol. 1, 2004, pp. 393–396.
- [117] J. Magarey and N. Kingsbury, “Motion estimation using a complex-valued wavelet transform,” *IEEE Transactions on Signal Processing*, vol. 46, no. 4, pp. 1069–1084, 1998.
- [118] T. Nguyen and S. Orintara, “Multiresolution direction filterbanks: theory, design, and applications,” *IEEE Transactions on Signal Processing*, vol. 53, no. 10, pp. 3895–3905, 2005.
- [119] G. Shi, L. Liang, and X. Xie, “Design of directional filter banks with arbitrary number of subbands,” *IEEE Transactions on Signal Processing*, vol. 57, no. 12, pp. 4936–4941, 2009.
- [120] V. Velisavljevic, B. Beferull-Lozano, M. Vetterli, and P.-L. Dragotti, “Directionlets: anisotropic multidirectional representation with separable filtering,” *IEEE Transactions on Image Processing*, vol. 15, no. 7, pp. 1916–1933, 2006.
- [121] E. J. Candès and D. L. Donoho, *Ridgelets: A key to higher-dimensional intermittency?* Phil. Trans. R. Soc. Lond. A., 1999.

- [122] ———, *Curvelets – A Surprisingly Effective Nonadaptive Representation For Objects with Edges*. Vanderbilt Univ. Press, 2000.
- [123] E. Simoncelli, W. Freeman, E. Adelson, and D. Heeger, “Shiftable multiscale transforms,” *IEEE Transactions on Information Theory*, vol. 38, no. 2, pp. 587–607, 1992.
- [124] R. Eslami and H. Radha, “A new family of nonredundant transforms using hybrid wavelets and directional filter banks,” *IEEE Transactions on Image Processing*, vol. 16, no. 4, pp. 1152–1167, 2007.
- [125] Y. Tanaka, M. Ikehara, and T. Nguyen, “Multiresolution image representation using combined 2-d and 1-d directional filter banks,” *IEEE Transactions on Image Processing*, vol. 18, no. 2, pp. 269–280, 2009.
- [126] Y. Tanaka, M. Hasegawa, S. Kato, M. Ikehara, and T. Nguyen, “Adaptive directional wavelet transform based on directional prefiltering,” *IEEE Transactions on Image Processing*, vol. 19, no. 4, pp. 934–945, 2010.
- [127] S.-I. Park, M. J. T. Smith, and R. Mersereau, “Improved structures of maximally decimated directional filter banks for spatial image analysis,” *IEEE Transactions on Image Processing*, vol. 13, no. 11, pp. 1424–1431, 2004.
- [128] S. Park, M. J. T. Smith, and R. Mersereau, “A new directional filter bank for image analysis and classification,” in *Proceedings. IEEE International Conference on Acoustics, Speech, and Signal Processing*, vol. 3, 1999, pp. 1417–1420.
- [129] P. Burt and E. Adelson, “The laplacian pyramid as a compact image code,” *IEEE Transactions on Communications*, vol. 31, no. 4, pp. 532–540, 1983.
- [130] A. da Cunha, J. Zhou, and M. Do, “The nonsubsampled contourlet transform: Theory, design, and applications,” *IEEE Transactions on Image Processing*, vol. 15, no. 10, pp. 3089–3101, 2006.
- [131] D. B. H. Tay and N. G. Kingsbury, “Flexible design of multidimensional perfect reconstruction fir 2-band filters using transformations of variables,” *IEEE Transactions on Image Processing*, vol. 2, no. 4, pp. 466–480, 1993.
- [132] P. See-May, C. W. Kim, P. P. Vaidyanathan, and R. Ansari, “A new class of two-channel biorthogonal filter banks and wavelet bases,” *IEEE Transactions on Signal Processing*, vol. 43, no. 3, pp. 649–665, 1995.

- [133] R. Mersereau, W. Mecklenbrauker, and J. Quatieri, T., “McClellan transformations for two-dimensional digital filtering-part i: Design,” *IEEE Transactions on Circuits and Systems*, vol. 23, no. 7, pp. 405–414, 1976.
- [134] J. Shapiro, “Adaptive multidimensional perfect reconstruction filter banks using mccllellan transformations,” in *IEEE International Symposium on Circuits and Systems, 1992. ISCAS '92. Proceedings.*, vol. 2, 1992, pp. 939–942.